CZECH TECHNICAL UNIVERSITY IN PRAGUE

Faculty of Civil Engineering

Department of Concrete and Masonry Structures

Idealisations in the Analysis of Reinforced Concrete Walls under Impact Loading

DOCTORAL THESIS

Ing. Alena Horská

Doctoral study programme: Civil Engineering

Branch of study: Building and Structural Engineering

Doctoral thesis tutor: prof. Ing. Alena Kohoutková, CSc.

Prague, 2022

CZECH TECHNICAL UNIVERSITY IN PRAGUE
Faculty of Civil Engineering
Thákurova 7, 166 29 Praha 6

DECLARATION

Ph.D. student's name: Ing. Alena Horská

Title of the doctoral thesis: Idealisations in the Analysis of Reinforced Concrete Walls under Impact Loading

I hereby declare that this doctoral thesis is my own work and effort written under the guidance of the tutor prof. Ing. Alena Kohoutková, CSc.
All sources and other materials used have been quoted in the list of references.

In Prague on 18.03.2022

signature

Abstrakt

Tato práce se věnuje studiu idealizací implementovaných ve výpočetních modelech železobetonových stěn zatížených nárazem. První část práce poskytuje všeobecný teoretický přehled o zatížení nárazem a odezvě železobetonových konstrukcí na toto zatížení. Jsou v ní zdůrazněná specifika odlišující tyto nárazové jevy od statických jevů. V práci jsou popsány běžné výpočetní postupy a idealizace, které inženýři standardně využívají při tvorbě výpočetních modelů. Jakákoliv idealizace reálného chování konstrukce vnáší do výpočtu potenciální nepřesnosti. Míra nepřesnosti výsledků souvisí s mírou idealizace. Rozdíly mezi reálným chováním konstrukce, chováním mírně idealizovaného modelu a chováním vysoce idealizovaného modelu jsou stěžejním tématem výzkumu v oblasti analýzy konstrukcí.

Druhá část práce se podrobněji zaměřuje na jednu z nejrozšířenějších a také jednu z často chybně aplikovaných idealizací – modelování trojrozměrných konstrukcí dvojrozměrným výpočetním modelem. Rozdíly mezi výsledky silně zjednodušené dvojrozměrné a přesnější trojrozměrné analýzy byly sledovány a vyhodnoceny na případu stěny zatížené koncentrovaným zatížením. Toto zatížení simuluje náraz vozidla a je vyjádřeno ekvivalentní statickou silou. Předmětná stěna byla modelována jako svislá konzola. Veličinou, pomocí níž bylo chování modelů vyhodnoceno a porovnáváno, byl zvolen ohybový moment ve svislém směru, jelikož právě ten určuje míru vyztužení v hlavním nosném směru konstrukce. V rámci výzkumu byl sledován vliv deseti parametrů vstupujících do analýzy na hodnotu maximálního ohybového momentu ve svislém směru. Výsledky byly vyhodnoceny pro dvou- i trojrozměrné modely a tyto byly následně porovnány. Na základě tohoto srovnání byla stanovena nepřesnost idealizace trojrozměrné stěny dvourozměrným modelem. Zjištěná nepřesnost byla vyjádřena zavedením korekčních součinitelů. Použitím korekčních součinitelů na hodnoty ohybových momentů, které byly jednoduše stanoveny na dvourozměrných modelech, lze získat modifikované hodnoty, které svou přesností odpovídají výsledkům trojrozměrné analýzy.

Na základě srovnání výsledků dvou- a trojrozměrné analýzy byl vytvořen praktický výpočetní nástroj Wall-imp. Wall-imp po zadání několika vstupních parametrů vypočítá hodnotu maximálního ohybového momentu ve svislém směru na vetknuté stěně, přičemž kombinuje přesnost trojrozměrné a jednoduchost dvojrozměrné analýzy.

Abstract

The thesis studies structural modelling idealisations of reinforced concrete wall elements subjected to impact loads. Overall background information on impact loads and structural response of reinforced concrete elements is presented in the first part of the thesis to point out the specifics and issues of the phenomenon. Standard engineering approaches of structural modelling are described, emphasising common model idealisations. Every idealisation of reality for the purpose of structural modelling is potential cause of result inaccuracies. The result inaccuracy is linked to the degree of model simplification. The discrepancy between real, moderately idealised, and heavily idealised behaviour of structures is the core research topic in the field of structural engineering.

The second part of this thesis deeply focuses on one of the most common and often wrongly used idealisations – two-dimensional modelling of three-dimensional problems. The differences between the results from heavily simplified two-dimensional models and more accurate tree-dimensional models were quantified and evaluated on the case of a wall subjected to concentrated loads. The load simulates the event of vehicle impact and was expressed as equivalent static force; the wall was modelled as a vertical cantilever. The value of vertical bending moment was chosen to represent the behaviour of the wall, as it governs the design of the main load-bearing reinforcement. Ten variable parameters entering the structural analysis were investigated and their effect on the bending moment peak value was quantified, providing comparison of two- and three-dimensional modelling results. The inaccuracies caused by using two-dimensional models for an analysis of three-dimensional walls were evaluated based on the investigation outcomes. Correction coefficients expressing the differences between two- and three-dimensional models were proposed. When the correction coefficients are applied to the results of a simple two-dimensional analysis, the inaccuracy of results is rectified, and the accuracy of three-dimensional analysis is achieved.

A practical tool Wall-imp was developed for easy peak bending moment calculation based on the findings obtained from comparison of two- and three-dimensional models. Wall-imp computes the value of peak bending moment with accuracy equal to results from three-dimensional models, while the simplicity of its use corresponds to two-dimensional approach.

Acknowledgements

I would like to express my sincere thanks to prof. Ing. Alena Kohoutková, CSc. for her supervision, guidance, and patience throughout this research project. I also wish to thank doc. Ing. Marek Foglar, Ph.D. for his mentorship and enthusiasm I received at the beginning of my studies. My deep gratitude belongs to Ing. Radek Štefan, Ph.D. for all the inspiring discussions and consultations. I very much appreciate the encouragement from Ing. Michal Drahorád, Ph.D., doc. Ing. Josef Fládr, Ph.D. and Ing. Karel Šeps, Ph.D. Thanks belong also to Geotechnics and Tunnels department of Mott MacDonald CZ for providing stimulating environment. I would like to express special thanks to my partner, parents, and family for their unwavering support and care.

https://doi.org/10.14311/dis.fsv.2022.006

Table of Contents

SECTION A – Background to structural design of reinforced concrete structures under impact loads

The issue of idealisation in the analysis of reinforced concrete (RC) structures under impact loads was chosen as the topic of this thesis. Understanding the subject on academic level opens the opportunity to apply theoretical knowledge in practice, and thus, contribute to engineering development. Section A of this thesis aims to give deeper reasoning for the topic choice and provides sufficient theoretical background to the subject of the research. General information on the topic presented in Section A supports subsequent investigation of a practical engineering problem presented in Section B.

Section A is structured as follows:

- **Section 1** presents the importance of the topic and explains author's motivation to explore the field. The objective and scope of the research is defined.
- **Section 2** presents principles of impact loading and describes the behaviour of RC elements under such specific conditions.
- **Section 3** describes various types of idealisations that are used in structural modelling.
- **Section 4** provides review of others' research related to the topic of this thesis.
- **Section 5** summarises standardized design approach commonly used in engineering practice.

1. Introduction to reinforced concrete walls subjected to accidental loading

Many structural engineers design load-bearing structures primarily to withstand the loads that are expected to occur during the lifetime of the structure with high probability of appearance. On an example of a building, it is mainly dead load, service load and climatic load that are typically considered. These types of loading are a sufficient input for the design of structures of low failure consequence, as there is very low probability that any other load type will affect the structure, and, even in the rare case of extreme loading situation, the damage is not extensive.

For structures of high failure consequence, this approach is not sufficient. Failure of such structures may lead to loss of lives, causes financial issues, and may damage cultural heritage. Therefore, it is necessary to anticipate extreme load scenarios that may occur during the lifetime of the structure and mitigate the consequences of its damage.

Extreme loads have many possible causes – both intentional and accidental. The intentional causes include gun fire and blasts, which is a very current topic all over the world today. The accidental causes of extreme loads include blasts due to failure of industrial equipment, vehicle crashes, rock falls, etc. Such load scenarios do not occur on regular basis; nevertheless, they do happen, and the risk is notable. It is obvious from the list of possible extreme load scenarios above that the issue of extreme loads needs to be addressed.

This thesis focuses specifically on RC structures subjected to accidental impact loads or other concentrated loads and idealisations in their modelling. The choice of the topic raises from following:

- The review of research summarised in Section 4 shows that the topic is not new to scientists and plenty of work was done already. However, there are still areas in this field that were not properly researched and deserve attention. This statement is supported by the fact that European standardisation of RC design for impact events is in some of its parts insufficient and inadequate, as several researchers concluded.
- The outcomes of the research in this field bring not only understanding and satisfaction to a scientific mind, but their application finds also practical use in structural engineering. Using deep theoretical knowledge to develop practical engineering tools is the goal of research. This thesis and its topic choice were driven by needs of engineers struggling with design of RC elements under impact loads.

The objective of this thesis is to study behaviour of RC elements under impact loading, and based on the findings, to develop a calculation tool for the analysis of RC cantilever walls subjected to impact loads. The calculation tool is intended to be used by engineers in their practice.

Following steps were taken to fulfil the purpose of the thesis:

1. Study on principles of impact events - understanding the energy balance of the event, defining the loads, analysing the response of RC elements.
2. Reviewing others' research of the field to get familiar with current state of work and detect unresolved issues. Reviewing standards used in practice.
3. Narrowing the focus to the specific problem of cantilever walls under impact loads. Describing common approach to their analysis; defining its issues. Suggesting rectification of incorrect solutions.
4. Development of rectification mechanisms by investigating the effects of various parameters of the structure and load on the results. Finding relationship between inputs and results of the structural analysis.
5. Application of the investigation findings - development of practical tool Wall-imp in spreadsheet environment.
6. Validation of Wall-imp results. Defining its range of applicability.

2. Structural response to impact loading

Theoretical background on behaviour of concrete structures under impact loading is provided by many, e.g. (Daudeville, et al., 2011), (Wright, 2012), (Sangi, 2011), (Baera, et al., 2016), (Kennedy, 1976), (Koechlin, et al., 2009), (Akin, 2015), (Riisgaard, et al., 2007), (Grote, et al., 2001), (Visser, 2017), (Pajak, 2011), (Fujikake, et al., 2009).

Design approach for concrete structures is also standardized in following codes, applicable mainly in Europe: (fib Model Code, 2010), (EN 1991-1-7, 2006), (EN 1992-1-1, 2004).

Following subsections summarise the key points of the phenomenon widely explained in the publications listed above.

a. Basic principles

Structures subjected to impact loading are locally exposed to a short-term dynamic impulse caused by collision of a moving object (striker) and the structure (target). Velocity of the striker corresponds to its kinetic energy. Analysis of the phenomenon respects the principle of energy conservation. Kinetic energy of the striker is conversed to multiple types of energy, involving following:

- Kinetic energy of the target (for targets not rigidly supported)
- Residual kinetic energy of the striker (if the target does not stop the striker entirely)
- Elastic strain energy of the striker in global/local scale (deformation of the striker as a whole and/or local deformation at the contact point)
- Elastic strain energy of the target in global/local scale (deformation of the target as a whole and/or local deformation at the contact point)
- Plastic strain energy of the striker in global/local scale (deformation of the striker as a whole and/or local deformation at the contact point)
- Plastic strain energy of the target in global/local scale (deformation of the target as a whole and/or local deformation at the contact point)
- Fracture energy of the striker (cracking of the striker)
- Fracture energy of the target (cracking of the target)
- Heat generated at the contact point

Quantification of the energy types requires deep knowledge of the mechanical parameters of both striker and target, and in many cases, those parameters reflect the microstructure of the materials involved. For that, it is hardly possible to analytically express the full equation of energy balance. However, implementing several idealisations into the impact event reduces complexity of the problem. Following section describes the idealisations.

b. Load definition

The behaviour of the striker and target may be idealised due to deformability of the objects. Two ultimate states of impact are distinguished – hard and soft impact. According to (Koechlin, et al., 2009), soft impact is defined for situations where stiffness of the striker is much lower compared to the target. The kinetic energy of the striker is completely conversed into strain energy of the striker. The target is considered indefinitely rigid, and therefore, does not receive any energy from the striker. Contrarily, hard impact is defined for the situations where stiffness of the striker is much higher compared to the target. The kinetic energy of the striker is completely conversed into strain energy of the target. The striker is considered indefinitely rigid, and therefore, its kinetic energy is fully received by the target. The nomenclature in definition of soft and hard impact according to (Koechlin, et al., 2009) is derived from the striker perspective. All other types of energy generated during the impact event are neglected.

Contrarily, (EN 1991-1-7, 2006) defines soft and hard impact from the target perspective. That means that the nomenclature of the impact type is in reverse. Soft impact refers to the event where the striker is infinitely rigid, and the target is soft and deformable. Hard impact refers to the event when the target is infinitely rigid, and the striker is soft and deformable. Like in the definition provided by (Koechlin, et al., 2009), all other types of generated energy are neglected.

The dynamic character of the loading may be simplified as an equivalent static force. According to (EN 1991-1-7, 2006), using equivalent static force in structural design is allowed for structures of CC2 (consequence class 2), which corresponds to medium consequence of failure.

(Akin, 2015) explains that the value of equivalent static force needs to induce equal displacement in the structure as would the dynamic force. (EN 1991-1-7, 2006) offers equations to determine the values of equivalent static force for both soft and hard impact and quantifies the values for common design scenarios to be at hand for structural designers. More details on standardized equivalent static force are provided in Section 5.

(Zhao, et al., 2019) proposes a method for calculation of peak impact force based on momentum and energy conservation. Material and geometry of the target structure and velocity, mass and size of the striker are the input to the calculation. Strain rate effects are considered, using formulas presented in (Adhikary, et al., 2012). The method is applicable to simply supported RC beams with impact load acting at its mid-span.

c. Concrete behaviour under high load rates

There are many possible causes of impact loading. Various strain rates $\dot{\varepsilon}$ are induced by the loading depending on the velocity and deformability of both striking object and target structure. Strain rate $\dot{\varepsilon}$ is time derivate of strain, see Equation 1.

$$\dot{\varepsilon} = \frac{d\varepsilon}{dt} \qquad \textit{Equation 1}$$

Table 1 presents selected loading events and corresponding range of strain rates that are induced in structures during the event. The ranges of strain rates are indicative and vary in different sources, e. g. (fib Model Code, 2010), (Pajak, 2011), (Visser, 2017).

Loading event	$\dot{\varepsilon}$ [s^{-1}]
Creep and shrinkage	$< 10^{-5}$
Quasi-static	$10^{-8} – 10^{-4}$
Vehicle impact	$10^{-5} – 10^{-2}$
Earthquake, traffic	$10^{-5} – 10^{2}$
Plane crash, missiles, rock falls	$10^{-2} – 10^{3}$
Blasts	$> 10^{-2}$

Table 1: Strain rate during various loading events

Some material characteristics, such as elastic modulus *E* and compressive and tensile strength $f_{c/t}$, appear to be properties of a constant value, as they are usually used in the analysis of quasi-static load events and for those they are determined. However, these properties are sensitive to strain rates for many materials, including concrete and reinforcement steel. In general, strength of a material increases with increasing strain rate. This phenomenon is known as a strain-rate effect and is quantified by dynamic increase factor (*DIF*), see Equation 2.

$$DIF = \frac{f_d}{f_s}$$ *Equation 2*

where f_d [MPa] is material strength under dynamic loading

f_s [MPa] is material strength under quasi-static loading

DIF dependence on strain rate was widely experimentally researched for concrete. It was observed that strain rate effect affects concrete differently in compression and tension. Very low strain rates at the level of creep effects cause decrease in both compressive and tensile strength compared to quasi-static rates, causing *DIF* drop below the value of 1.0. However, for higher than quasi-static strain rates, *DIF* is significantly larger for elements in tension than compression.

According to data published by (Pajak, 2011), tensile *DIF* is equal to approximately 12.5 at strain rates around 10^2 s^{-1} while compressive *DIF* is equal to approximately 1.5 at the same rates. (Adhikary, et al., 2012) introduces formulas for determining *DIF* for RC beams based on their slenderness and longitudinal reinforcement.

3. Analysis idealisation

Idealisation brings necessary simplification into solving structural engineering problems. A certain degree of simplification is implemented in every structural analysis, including accidental events of impact to RC walls. Idealisation needs to be implemented carefully to ensure that the effect of it is either negligible or increases safety of the design. It is desired to achieve results as accurate as possible but not posing a safety risk to the design.

Models used for structural analysis of RC elements subjected to impact loads can be idealised in several aspects:

- Geometry – Beams and columns are modelled as bars, slabs and walls are modelled as plates. Elements are represented by their axis/central plane. Three-dimensional problems are modelled in two dimensions if the section is constant in out-of-plane direction.
- Material – Reinforced concrete is usually modelled as homogeneous material, in majority of cases with elastic behaviour and uncracked. Strain rate effects are usually neglected.
- Loads – Dynamic aspect of load is often simplified into equivalent static load (ESL).
- Analysis type – Linear analysis is used in majority of engineering practices.
- Connections and supports – Joints and supports are usually modelled as either fully fixed or fully allowing translation/rotation in one or more dimensions.

Effects of idealisation on results of structural analysis can be evaluated by comparing results from idealised models to real behaviour (experimentally investigated) or comparing results from idealised models to more accurate (less idealised) models. Evaluating the differences between more and less idealised models or idealised models and reality is the core of structural engineering

research. Outcomes of such research bring development in design methods and increase in result accuracy.

4. Review of related research

As described in Section 3, structures subjected to impact loading can be idealised in many ways. The influence of various idealisations on analysis results were and still are in focus of many researchers. This section brings an overview of published research in this field, emphasising modelling idealisations.

Material properties are heavily idealised aspect in structural modelling. Section 7.c presents that RC behaviour is influenced by strain rate effects. Idealisation by neglecting strain rate effects is conservative in case of impact loading events, however, considering it may prevent unnecessary overdesign. While the phenomenon of strain rate effect is already well known, it is still the subject of research as it is not yet fully quantitatively described. In common engineering practice, the idealisation by neglecting strain rate effect is often driven by its unclarity.

(Juhász, et al., 2017) presents an experimental programme conducted on beam elements with bar and dispersed reinforcement (fibre reinforced concrete (FRC) and synthetic fibres). The specimens were subjected to three-point bending tests with various speed of loading. The objective of the experiment was to obtain load-displacement and load-crack mouth opening displacement (CMOD) diagrams representing the behaviour of the beams under various loading rates. Performance under quasi-static loading was the benchmark for evaluating load rate effects; the quasi-static tests were performed according to standard three-point bending test according to (RILEM TC 162-TDF, 2002). The article concludes that loading rate is significant factor in performance of FRC beams and concrete beams reinforced with synthetic fibres. (Adhikary, et al., 2012) presents a wide experimental and numerical investigation of RC beams subjected to impact loading induced by a drop-hammer mechanism. The beams in focus were loaded in their midspan. Experimental data were compared to complex three-dimensional dynamic simulations. The research evaluates *DIF* for varying load rates, beam geometry and reinforcement. The author declares large scatter of experimental results and concludes that the experimental set up has noticeable effect on the outcomes and suggests unification of experimental techniques. This idea agrees with a conclusion stated by (Pajak, 2011) which provides a summary of experimental programmes carried out in the field of high-velocity loading of concrete structures. Within the experiments, wide range of loading rates was studied and corresponding *DIF* values were determined. Two main types of testing technique were used in the experiments to achieve desired load rates: Drop hammer test and Split Hopkinson Pressure Bar (SHPB) test. The authors conclude that the obtained value of *DIF* depends not only on loading rate, but also on the testing method, as each testing method brings different circumstances influencing the measurement.

Loads are a subject of idealisation as well as material properties of the structure, especially in case of dynamic events. Dynamic analysis of impact requires deep knowledge of mechanics and also requires more advanced software than common static analysis does. Computational time is as well significantly longer for

dynamic analysis. These are the reasons why the dynamic aspect of the load is replaced by an equivalent static force (ESF) very often. Determining ESF depends on many factors and some of those are difficult to quantify. That makes determining ESF an uneasy task. The method proposed in (EN 1991-1-7, 2006) involves vast simplifications of the complex problem which makes the outcoming ESF value less trustworthy. Finding more accurate values of ESF is a topic to research by many.

(Choi, et al., 2005) proposes a method to transform dynamic loads to ESF. ESF are calibrated according to displacement induced by the dynamic loads using numerical simulation. The article points out the fact that there is a lag between displacement and stress induced by the dynamic loads, and therefore, the stresses induced by the dynamic loads do not correspond to stresses induced by the ESF. The study is performed on a two-dimensional frame model, neglecting out-of-plane distribution of internal forces. (Majeed, et al., 2019) explains the difference between impact force (that can be expressed as ESF and can be determined from kinetic energy balance) and contact force on a case of a boulder fall event. Contact force acts locally at the surface of the target, while ESF can be used only to determine its effects on global behaviour of the target structure. The study is supported by extensive experimental programme in which the magnitude of the contact force is evaluated. The study concludes that the contact force reaches much higher magnitudes than ESF in the early stage of the impact event. The magnitude of contact force is strongly dependent on compressive stiffness of both striking object and target structure. The authors provide a practical chart for engineers to find contact force values for various design situation, enabling them to avoid complex numerical modelling. (Zhou, et al., 2017) investigates behaviour of RC bridge piers during vehicle collision using advanced dynamic analysis in LS-DYNA software. One of the goals of the research is to evaluate standardized values of ESF from (EN 1991-1-7, 2006), (AASHTO-LRFD, 2012) and (JTG D60, 2004). The study concludes that for some of the investigated loading scenarios, the values of ESF provided in the mentioned standards are inappropriately low and their use leads to underestimated design. This indicates that further development in the field of dynamic load simplification is needed.

Bridge piers/columns under impact loading are extensively researched by many, since traffic accidents are not rare, and bridges are a part of critical infrastructure. Researchers took a variety of approaches in their work, conducting both experimental and numerical investigations, analysing both load and structural response. Following text contains only a small example of work published to this topic.

Impact loading on concrete columns is researched by (Mestrovic, et al., 2008) who focuses on probabilistic approach to determine impact loading. (Do, et al., 2018) uses numerical modelling to obtain peak impact force during an accident and finds the relationship between peak impact force and engine weight. Interference of lateral impact load and static axial force in concrete columns is researched by (Liu, et al., 2017) where experimental the testing was supplemented with numerical modelling. The influence of pre-existing axial force in a column on impact performance was examined also by (Abdelkarim, et al., 2017) who conducted finite element method (FEM) investigation of several structural

parameters; peak dynamic force and ESF were evaluated for various conditions and compared against standardized values. Impact on concrete columns caused by rockfalls was presented by (Mavrouli, et al., 2010) who analysed the whole accidental situation from calculation of the event probability, through structural response evaluation, to evaluation of robustness of the whole building and calculation of damage index.

Structural response to impact is also studied on concrete structures with enhanced mechanical properties, using ultra-high performance concrete (UHPC), FRC, carbon fabric reinforced concrete, etc. The aim of such research is to find a suitable material for structures exposed to risk of impact loading. A few selected publications on this topic are outlined in following text, not to give the reader the full review of possible material solutions, but to give illustrative examples.

(Yoo, et al., 2017) studies behaviour of UHPC and FRC elements under impact and blast loading. The study focuses on structural performance of various types of fibres and the influence of fibre orientation. Fibre reinforced polymer enhances impact performance of concrete structures, according to review by (Pham, et al., 2016). (Horská, et al., 2015) presents results of experimental programme on FRC slabs subjected to drop-hammer impact tests. The effects of fibre types and volume and slab thickness are evaluated. Structural response to impact is compared to quasi-static performance; elements with dispersed reinforcement are compared to unreinforced concrete slabs. Steel fibres are concluded to increase structural resistance to impact, while the effect of polypropylene fibres in concrete mix is negligible. (Sovják, et al., 2013) experimentally investigates ultra-high performance fibre reinforced concrete (UHPFRC) subjected to projectile impact. The research results show that UHPFRC with steel micro fibres improves impact performance of the tested slabs compared to standard FRC.

Contrarily to the research on beams and columns, the issue of impact load on plate elements is not as frequently researched. When it is, the objective is often to evaluate the impact loading or qualitatively compare performance of various material modifications, as illustrated by the review above. Quantification of internal forces and their distribution in the two perpendicular directions of plate elements is rarely studied. The distribution of the internal forces in both directions of plates plays a huge role for the plate element design, especially when a concentrated load is applied.

(Salama, 2012) presents the issue of concentrated loads applied on rectangular two-way slabs supported at all four edges and proposes expressions for maximum bending moment values for each direction. The expressions were verified with the results of elastic analysis performed in FEM software. The proposed method is convenient as it requires only hand calculations. (Koktan, et al., 2019) studies differences between the results of two- and three-dimensional analysis of foundation slab on elastic half-space. The findings of the study result into proposal of a method where the results of the two-dimensional analysis are altered so that their accuracy is close to results of three-dimensional elastic half-space models. (Özel, et al., 2013) presents a study on the differences of two- and three-dimensional modelling of concrete faced rockfill dams subjected to dynamic loads. The study is focused on earthquake events and their effects on

crack opening, as the crack width is crucial for water retaining structures. (Yong, et al., 2020) focuses on experimental study of real-scale precast cantilever wall segments. The wall segments are subjected to impact load acting at the top edge of the wall and in the middle of the wall length. The aim was to develop a numerical simulation that agrees with the experiment in wall displacement. Contact force was also evaluated. Related research was presented by (Yong, et al., 2020), where the original study was broadened to investigate interaction of pre-existing static loading with accidental impact actions. These combined actions were modelled as well, and the model agrees with the outcomes of the experiment. Both the original and subsequent research consider load position in the middle of the wall length, neglecting the possibility of asymmetrical actions and results. Further investigation is required to understand effects of unsymmetrically loaded walls. Central position of the load and symmetry of the results are not very likely to occur in real application.

The aim of research is not only to describe the phenomenon of RC structures under impact loads, but also apply the outcomes and use them in practice. For that, some researchers developed practical tools to be at hand to engineers designing such structures.

A spreadsheet-based design tool for cantilever RC retaining walls was proposed by (Kaveh, et al., 2020). The tool uses optimisation methods to provide efficient design, minimising cost of concrete and steel reinforcement. The design considers the wall to be subjected to lateral soil pressure and surface surcharge. Both static and dynamic effects are considered. A two-dimensional model of the retaining wall was used for the analysis. (Sagar, et al., 2016) focuses as well on retaining wall optimisation and cost reduction. Both stability and structural resistance are the criteria for the optimisation, generating a section with satisfying factor of safety and minimum cost. The optimisation was performed on a two-dimensional model of a soil retaining wall. Efficient design of cantilever RC walls is the topic of (Bhatti, 2006). Spreadsheet tool was developed to design efficient wall section. The used model is two-dimensional and allows variable geometry, soil conditions and surface surcharge. (Hu, et al., 2018) developed a design tool to evaluate reliability of a retaining wall affected by a nearby railway traffic. Uncertainties in material parameters and reinforcement placement enter the evaluation, returning probability of structural failure. A two-dimensional model was used for the analysis. (Horská, 2020) presents a tool for structural analysis and assessment of a retaining wall subjected to arbitrarily set soil and hydrostatic conditions. In one step calculation, the tool analyses three design scenarios – flood event, rapid drawdown, and dry season. On a two-dimensional model, overturning, sliding, and bearing capacity failures are verified and decisive internal forces were evaluated.

Overviewing the research conducted in the field of concrete structures under impact loads, following conclusions are made:

- Strain rate effect is a recognised phenomenon influencing impact performance of RC structures. To idealise material models and simplify dynamic structural analysis, reliable *DIF* values are needed. Quantification of the strain rate effect through *DIF* is a complex problem requiring vast experimental investigation. That is the reason why strain rate effect was

not fully and reliably standardized, and so is rarely considered by structural designers. While extensive work was already done in this area, introducing the idealisation through *DIF* in standards was not yet completed, and therefore opens opportunities for further research.

- Idealisation of the dynamic aspect of impact force by introducing ESF is already standardised and used in practice. However, many researchers found that the standardised values are not only inaccurate, but sometimes also unsafe. For that, further research is desirable in this field.
- Bar elements (beams, columns) are researched much more widely than plate elements (walls, slabs) for their impact load structural performance. This is perceived as a gap and an opportunity for researchers to extend their scope. It is acknowledged that broadening of a two-dimensional problem into a three-dimensional problem brings multitude of new issues to be considered and addressed.
- The issue of idealisation of three-dimensional problems by using simpler two-dimensional models is not fully researched. That is despite the fact that such approach is widely used in practice. It is deemed by the author of this thesis that research should meet the requirements of practice and help solving issues encountered by engineers in their daily work, making their results satisfactorily accurate and easy to achieve. Idealised two-dimensional models are often used even for plate elements subjected to concentrated loads, for which they are very inappropriate as they do not consider force distribution in the plane of the plate. Since this discrepancy was not in focus of many researchers but is crucial for correct structural design, it was chosen as topic of this thesis.

5. Standardization of structural design to impact loading

This Section provides a description of standardised methods used for the design of RC elements under impact loading that are used in the Czech Republic, majority of European countries and several other countries outside Europe.

The Eurocode (EN 1991-1-7, 2006) categorizes accidental design situations into two groups: 1) Identified accidental actions, 2) Unidentified accidental actions. The design strategies differ for the two groups.

Identified actions can be prevented or reduced, as they are anticipated. Since the identified accidental actions can also be quantified, the structural elements can be designed to sustain such actions. Identified actions also allow the structure to be designed with sufficient robustness to prevent excessive damage extent.

Unidentified actions cannot be anticipated or quantified. For that reason, more general approach to the design needs to be chosen. Possible provisions include alternative load paths, designing key elements to notional accidental action and ensuring sufficient ductility by correct choice of materials.

The design strategy should be chosen respecting the probability of action occurrence, including the prevention systems and the consequence of structural failure. Usually, a certain risk level must be accepted.

The Eurocode section on Impact covers following areas: impact from road vehicles, impact from forklift trucks, impact from trains, impact from ships, the hard landing of helicopters on roofs. Either dynamic analysis or static analysis with ESF can be used. Conservatively, it can be assumed that the impacting body absorbs all the energy, which is in line with the theory of hard impact. Strain rate effects can be taken into consideration in dynamic analysis but should be neglected in equivalent static analysis. Neglecting strain rate effects is a conservative approach.

For accidental actions caused by road vehicles, forklifts, and derailed rail traffic, selected equivalent static force values are tabulated in the Eurocode for specific target structures and category of traffic.

Annex C of the Eurocode offers an explanation of mechanical principles applied in determination of ESF, that can be applied in order to perform approximate dynamic design. Annex C also classifies impact into two categories – hard and soft impact. In case of hard impact, kinetic energy of the colliding object is mainly dissipated by the impacting body, which is the case of a road vehicle colliding with a concrete structure. The structure is assumed to be rigid and immovable. The colliding object deforms linearly during the impact. The impact force is defined by mechanical properties of the colliding object, see Equation 3.

$$F = v_r\sqrt{km} \qquad \textit{Equation 3}$$

where	v_r [m/s]	is colliding object velocity at impact
	k [N/m]	is equivalent elastic stiffness of the colliding object
	m [kg]	is mass of the colliding object

A traffic accident against a structure classifies as hard impact as the stiffness of the structure is assumed to be much larger than the stiffness of the vehicle. A vehicle is geometrically and materially complex object an no two vehicles are the same, and it is difficult to express its stiffness k that enters Equation 3. For that, it can be simplified as an equivalent impacting object that is homogeneous and has a simple prism shape. Stiffness k and mass m of such object has expressed in Equation 4 and Equation 5.

$$k = EA/L \qquad \textit{Equation 4}$$

where	E [Pa]	is equivalent elasticity modulus
	A [m^2]	is equivalent cross-sectional area
	L [m]	is equivalent length

$$m = \rho AL \qquad \textit{Equation 5}$$

where ρ [kg/m^3] is equivalent mass density

While the simplification above enables to use basic principle of mechanics, the parameters of equivalent impacting object entering the basic equations are still difficult to determine. Complex numerical modelling or real scale experiments are the only reliable way for obtaining the parameters.

The impact force F given by Equation 3 applies on the surface of the structure. Dynamic effects may amplify the force as it travels through the structure. The amplification factor ϕ_{dyn} may reach the value of 2.0.

A short description of the conceptual approach to ULS design of structures subjected to impact is provided in (fib Model Code, 2010). Structural analysis is categorized into three levels according to its complexity. Level 1 uses quasi-static equivalent loads and neglects strain rate effects. Level 2 involves dynamic aspect of the problem and applies the load to the structure as standardized pressure-time curves. Level 3 involves detailed dynamic analysis where the load is determined individually for the specific load scenario. Model Code also suggests values of *DIF* for concrete and reinforcement to use in Level 2 and 3 design.

Note: The symbols used in this Section are adopted from (EN 1991-1-7, 2006) and are excluded from the list of symbols of this dissertation. Some of the symbols of this Section are used elsewhere in this dissertation while describing a different quality.

SECTION B – Investigation of differences in two- and three-dimensional modelling of cantilever walls subjected to concentrated loads

The review of research in Section 4 presented variety of topics related to impact loading, RC response, and differences between two- and three-dimensional modelling. The scope of these topics is very wide, and although a lot of work has already been was done in this field, not all structures and load situations were covered by researchers yet. Section B of this thesis aims to research a problem that is related to all the topics mentioned above, however, was not a subject of any reviewed research: two- versus three-dimensional modelling of cantilever RC walls subjected to a concentrated impact load that is idealised as ESF. The investigation presented in this Section respects the principles presented in Section 7 and its findings are intended to be used with standardised design methods presented in Section 5.

Section B is structured as follows:

- Section 6 demonstrates the importance of the topic on simple examples and explains how the outcomes of this research can be used in engineering practice.
- Section 7 is the core of the research. Comparative study of two- and three-dimensional modelling is presented, analysing the effects of wall and load parameters on the peak value of vertical bending moment. Based on the findings, correction coefficients are proposed to rectify the error of two-dimensional modelling of the problem. Correction coefficients are then used in development of a practical tool for engineers to enable them simple, but accurate design of cantilever walls subjected to concentrated loads.
- Section 8 summarises the findings of the research and states the area of their applicability.

6. Cantilever walls subjected to impact loading

Structural design of a cantilever walls subjected to ESF was chosen to be the field of interest in this investigation. Practical approach was taken when addressing the problem in order to satisfy not only the academic aspect of the study, but also to provide conclusions that can be easily adopted by structural designers in their everyday work.

Some of the outcomes of this study can be generalized and applied not only to cantilever wall analysis subjected to ESF but also to elements with similar structural character and behaviour patterns subjected to any concentrated load perpendicular to the wall plane.

a. Topic importance and motivation

Typical representative of cantilever walls is a retaining wall. Retaining walls are structures that usually don't attract attention and are often overlooked by public as their main purpose is not architectural; however, their technical function makes them important part of both urban and rural areas.

Even though retaining walls are a very common type of structure, their structural design is often simplified in a way, that can lead to over- or under-dimensioning and, in some cases, even to both within one wall. Faulty simplification of design procedure results in construction cost increase, unnecessarily inflated carbon footprint, and in extreme situations may lead to damage of the wall and elements in close vicinity of the wall.

Following sections describe a simplified approach that is often mistakenly adopted by structural designers. The possible errors rising from such approach are presented, demonstrating the importance of deeper understanding of the topic.

b. Common design approach

The common approach to cantilever wall design is illustrated on an example of a retaining wall in coastal area or areas with risk of fluvial flooding. The main purpose of such wall is double: to retain water in case of flood event, and to resist impact in case of traffic accident; see Figure 1 as an example. When designing dimensions and reinforcement of such wall, usually a conservative approach is chosen, modelling the structure as a cantilever wall, fixed against rotation at the base. Such approach neglects possible rotations of the retaining wall as a whole (including the base), and therefore returns conservative internal forces which inevitably results in unnecessary overdesign. Apart from being conservative, this approach also does not require any knowledge about foundation conditions and backfill parameters, which makes this method very often the only feasible way of design, as geotechnical survey may not be available.

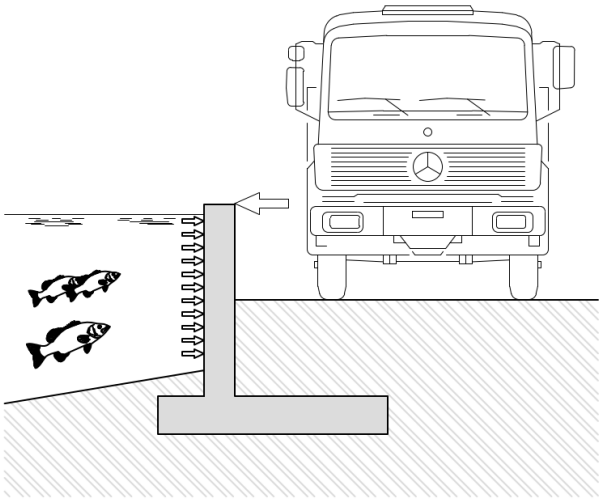

Figure 1: Design situations

Since Eurocode allows use of ESF for impact loading modelling, it is the generally preferred method used for the design of retaining walls. Such approach is appreciated mainly for its simplicity and low demands on software, as software for dynamic analysis is not purchased very often by companies that do not specialise in dynamic actions.

Majority of structural designers use linear FEM analysis for the same reason as stated above – simplicity and availability of software. For simple structures even

a hand calculation might be an option. Even though non-linear analysis would give more precise results, software demands and analysis duration make its use in many cases impractical, as demonstrated in Section 7.e.ii.

The three simplifications described above (fixed wall support at the wall base, the use of ESF, linear FEM analysis) have been adopted in the cantilever wall investigation presented in this thesis, as the results coming out of the analysis are expected to be used in structural design practise, and so the issue is approached in similar manner.

c. Issues of two-dimensional modelling

Cantilever walls, such as the retaining wall described in the section above, are often of significant lengths, providing continuous, uninterrupted flood protection to land side areas. For that reason, they can be classified as a linear infrastructure. Linear infrastructures are specific by having all sections identical over the whole length, which encourages the designing engineers to use a two-dimensional model for the structural analysis. However, having identical geometry in all sections is only one of the conditions that allow simplification of a three-dimensional problem to a two-dimensional model. The second condition is having the loads uniformly distributed over the wall length. In case of the example retaining wall, the second condition is met for the flood event scenario, where the water level is even in the whole length of the coast. However, in case of traffic accident, the impact force is concentrated in only a small area, which compromises the use of two-dimensional models during structural analysis. Thus, the results from two-dimensional models do not correctly represent the behaviour of the structure and lead to inaccurate results.

Despite the reasons stated above, most designers still choose to use two-dimensional modelling for linear infrastructures. Not all designers may have access to advanced three-dimensional modelling software, and in their case, a simplified two-dimensional calculation (often prepared with no specialized software at all) is the only option to carry the design.

Very often, the vehicle impact load scenario with concentrated loading force is the only obstacle standing in the way of a reliable two-dimensional modelling. This fact encouraged the topic choice of this thesis

Two examples of a cantilever wall subjected to a concentrated load were prepared to demonstrate how inaccurate results may be obtained by using two-dimensional models on three-dimensional problems. Example no. 1 presents a 2m high and 14m long retaining wall designed to withstand vehicle impact ESF of 75 kN located at the wall top edge. ESF position along the length of the wall cannot be strictly specified as the load case is of accidental character. Design of the structure must therefore appreciate all the possible positions of the ESF for the structure to be safe.

Firstly, a simplified two-dimensional hand calculation of a maximum bending moment was prepared, see Figure 2 (left). The two-dimensional model represents 1 m of wall length, so the loading force is also distributed to 1 m of wall length without any appreciation of the fact that the wall may be longer in longitudinal direction. With this approach, the wall would be designed for maximum bending

moment of 150 kNm/m along the whole wall length, follow the simple calculation steps in Table 2.

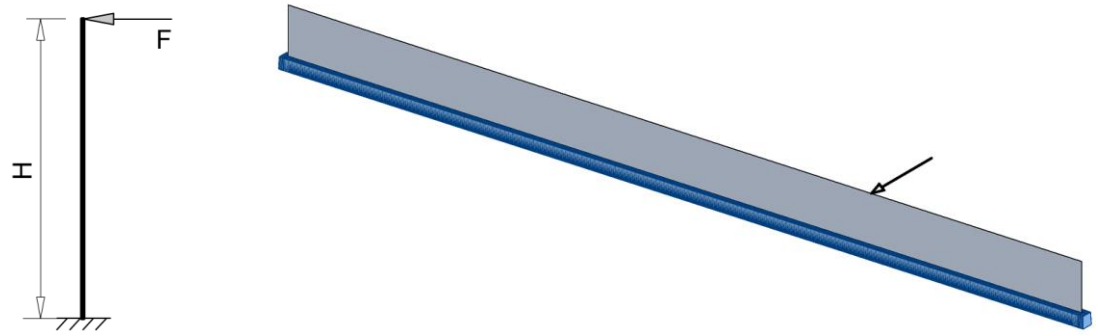

Figure 2: Two-dimensional model (left), three-dimensional model (right)

H [m]	2	Wall height equal to vertical load position from the wall base
F [kN/m]	75	Load force
$M_{2D,max}$ [kNm/m]	75 x 2 = 150	Maximum bending moment

Table 2: Example no. 1 - moment obtained on two-dimensional model

Secondly, a three-dimensional model of the case was prepared, respecting the real wall length and point nature of the load force, see Figure 2 (right). To cover all possible force positions, 15 load cases were set up, varying the force position along the wall top with 1 m step. The vertical reinforcement of the wall should be designed to a bending moment from an envelope of the load cases. The results (see Figure 3) show that the maximum bending moment value is 105 kNm/m, which is 70 % of the maximum bending moment obtained on the two-dimensional model. More importantly, this peak value occurs only at the edge parts of the wall. In the rest of the wall length the bending moment value at the base is approximately 37 kNm/m, which is 25 % of the two-dimensional model result.

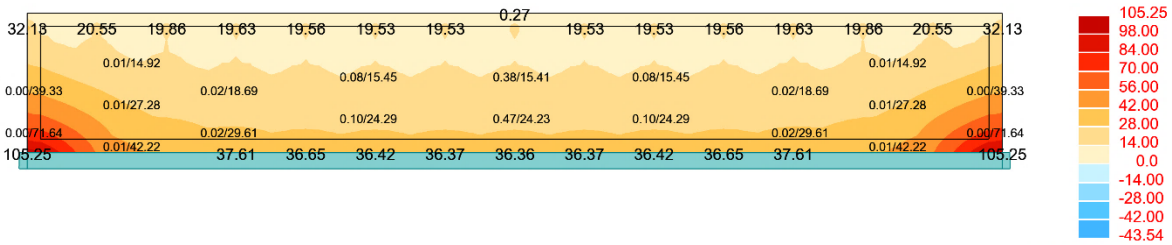

Figure 3: Example no. 1 – bending moment obtained on three-dimensional model

The comparison presented above clearly shows that, in that specific case, simplification the problem to two-dimensional model brings significant over-dimensioning and results in unnecessary increase in reinforcement or wall thickness demand, causing rise of construction costs and carbon footprint.

Example no. 2 will show that in some conditions, two-dimensional modelling may lead not only to over-dimensioning, but also under-dimensioning. Similar two- and three-dimensional model comparison was prepared like in example no. 1, differing only in geometry and load – wall height 1 m, wall length 70 m, load force 20 kN.

Two-dimensional approach gives maximum bending moment equal to 20 kNm/m. For further convenience, the value was related to itself (maximum bending moment obtained by two-dimensional modelling), obtaining relative maximum bending moment equal to 1. See summary in Table 3. Respecting assumption of two-dimensional modelling, this value would be adopted as a basis for structural design of the wall throughout its length. This result is represented in a graph, see Figure 4. The graph shows only one half of the wall length, as the problem is symmetrical.

H [m]	1	Wall height equal to vertical load position from the wall base
F [kN/m]	20	Load force
$M_{2D,max}$ [kNm/m]	20 x 1 = 20	Maximum bending moment
$M_{rel,max}$ [-]	20/20 = 1	Relative maximum bending moment

Table 3: Example no. 2 - moment obtained on two-dimensional model

Three-dimensional model of the problem was prepared in the same manner as it was in case of example no. 1. Like in previous example, bending moment values were concentrated in the edge parts of the wall. Since maximum values are always situated at the bottom fixed edge of the wall, results on the wall cut at the bottom were extracted to see only the relevant values that can be plotted in a graph. Relative values of maximum bending moment were calculated by relating the moments to the maximum bending moment obtained from two-dimensional modelling. The relative maximum bending moment was plotted in a graph to show the course over the wall length, see Figure 4.

Comparison of the two curves in graph in Figure 4 shows that in majority of the wall length the two-dimensional modelling gives overly conservative results. While the relative bending moment on two-dimensional model is equal to 1, three-dimensional modelling gives value of 0.49. On the other hand, 0.4 m of wall length on either end shows higher values of relative bending moment when using three-dimensional modelling when compared to the two-dimensional. The relative bending moment resulting from the three-dimensional model is equal to 1.28 at the very end of the wall. Therefore, the edge parts of the wall from example no. 2 might be under-designed and the structure may be potentially hazardous.

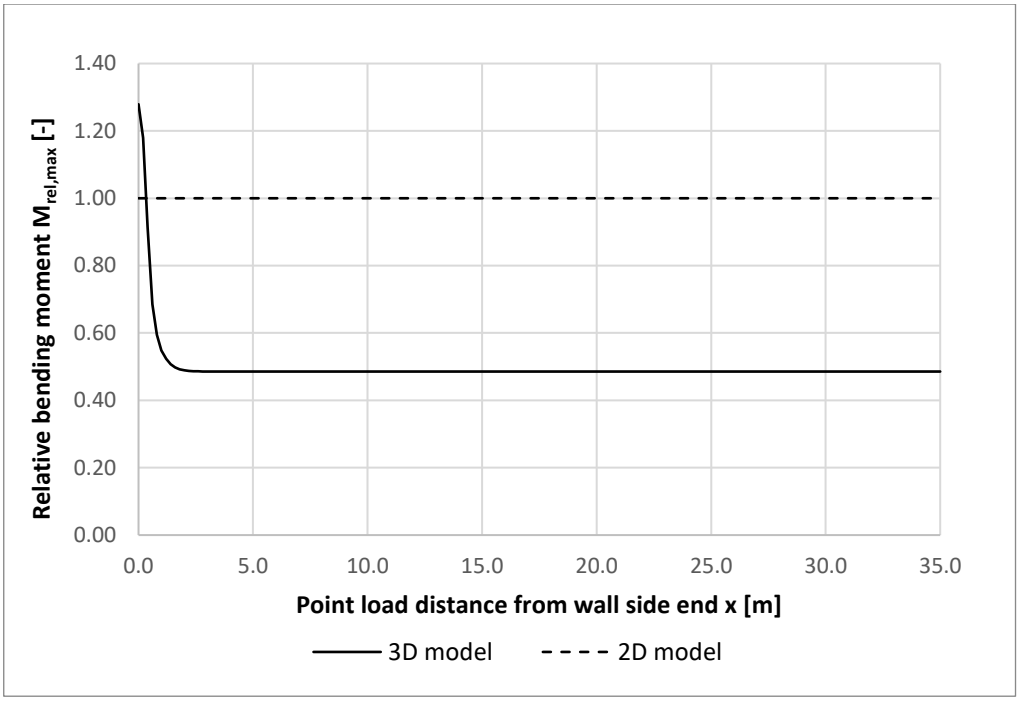

Figure 4: Example no. 2 – relative bending moment on two- and three-dimensional model

The two examples above demonstrate how two-dimensional modelling of retaining walls can be misleading. This thesis aims to quantify the error brought by such simplification and proposes a solution that would enable the designers to keep using the simplification by two-dimensional modelling while increasing accuracy of their results.

There are several reasons why two-dimensional modelling provides inaccurate results in internal forces:

- Two-dimensional models incorrectly assume even distribution of loads and internal forces over the wall length, as they assume all vertical sections of the wall to be identical in their geometry, boundary conditions and loads.
- Two-dimensional models neglect the interaction with the parts of the wall that are outside the loaded length. They presume that the considered 1 m long segment of the wall deforms independently from the rest of the wall length.
- Two-dimensional models neglect boundary conditions at the side faces of walls.
- Two-dimensional models neglect torsional effects that are consequent to the two points above.

7. Comparative study of two- and three-dimensional modelling

The previous section of this thesis presented the reasons why the idealisation and simplification of using two-dimensional analysis are misleading when modelling cantilever walls subjected to impact loading. In this section, the error of such simplification is quantified through a comparative study. Two- and three-dimensional models were prepared to analyse an identical design scenario of impact loaded cantilever wall (described in detail in the section below).

The reference parameter observed in the comparative study is the peak value of bending moment in vertical direction, as it is decisive for the design of the main load bearing vertical reinforcement. All values of bending moment obtained from three-dimensional models include torsional effects according to Wood-Armer theory (Wood, 1968).

As the three-dimensional modelling is presumed to be more accurate and better representing real behaviour of the structure, the deviation of the results obtained from two-dimensional models from the results obtained on three-dimensional models is determined to be the error of two-dimensional simplification. The error was quantified for all examined design scenarios, generalized, and used for a development of correction coefficients. Correction coefficients rectify the inaccuracy caused by two-dimensional simplification.

a. Hypotheses of the analysis

The wall in focus was modelled as a vertical cantilever fixed the bottom edge, see Figure 5. Deformability of the ground was neglected. No backfill was considered to be restraining the wall stem. Equal boundary conditions were used in both two- and three-dimensional models. The two-dimensional model consists of a single bar with no sectional and material properties, as they do not have any effects on the resulting bending moment. The three-dimensional model of the wall was created as a shell element.

The wall was subjected to a concentrated load located at its top edge. The dynamic character of the impact force caused by traffic accident was expressed as ESF. Strain rate effects caused by the dynamic character of the load were neglected.

The results were obtained from linear analysis. The peak bending moment value in vertical direction was result of interest and subject of comparison. In case of the two-dimensional model, the calculations were prepared in MS Excel, as their simplicity does not require any specialized structural software and can be done manually. The three-dimensional analysis was prepared in Robot Structural Analysis, which is a FEM software.

All model idealisations, simplifications and assumptions were chosen to provide more onerous results than what would occur on the real structure to ensure that the design based on those results is safe.

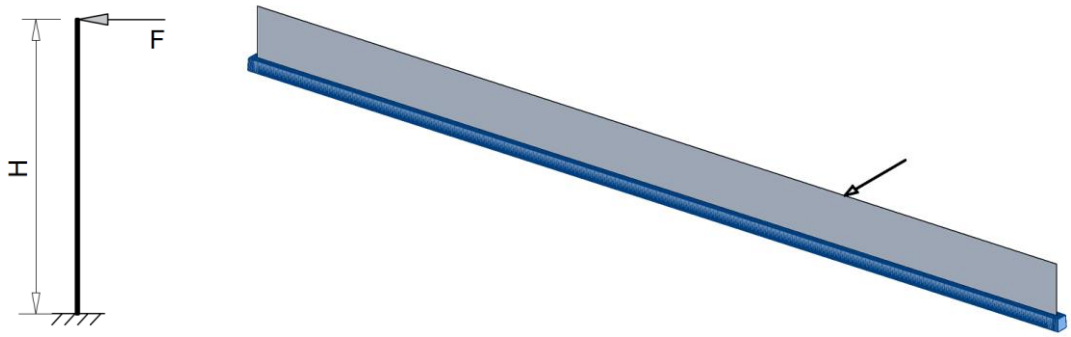

Figure 5: Two-dimensional model (left), three-dimensional model (right)

For many cases examined in this thesis, it was necessary to simulate a wall of infinite length, so that the proximity of the wall end would not affect the distribution of internal forces. To practically achieve that on a three-dimensional model of a finite length, the load was placed in the centre of the top wall edge, and the length was modelled large enough so that there were zero forces and deformations on the side ends of the wall. It was experimentally tested that for all cases studied in this thesis, the wall length of 70 m was sufficient for simulation of an infinite wall.

The nomenclature used is presented in Figure 6.

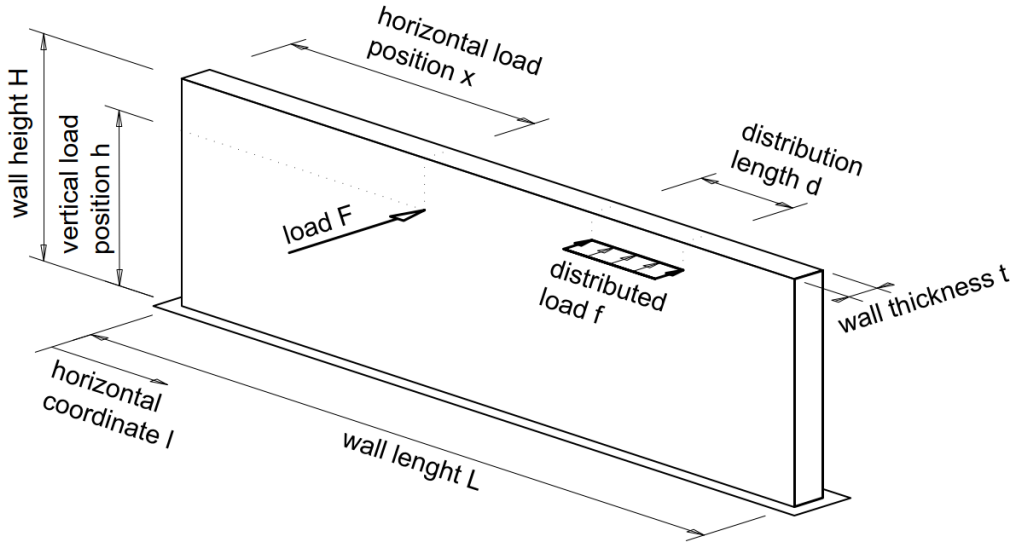

Figure 6: Nomenclature

b. Bending moment distribution approximation

The peak bending moment in vertical direction is decisive for the design of reinforced concrete section. In case of a cantilever wall subjected to a concentrated load, the peak bending moment occurs at the base of the wall below the load. If such problem is analysed using a two-dimensional model, all of the bending moment at the wall base is concentrated into one point, creating an extreme peak. However, when more accurate three-dimensional model is used, the bending moment at the wall base distributes over the horizontal length of the

wall. The peak still occurs below the position of the load, but its value differs from two-dimensional models due to the moment horizontal distribution. For further use in the study, it is practical to analyse the course of the moment distribution over the wall length at the wall base.

A set of three-dimensional models was prepared to evaluate the horizontal course of bending moment at the wall base. All modelled walls were 70 m long which is sufficient length to simulate infinite wall (see Section 7.a for more details). All modelled walls were 300 mm thick, concrete class C30/37 was used. The load was a single force of 1000 kN located at the wall top in the horizontal centre (x = 35 m), see Figure 7. Wall height H ranged from 0.6 to 6.0 m with 0.2 m step.

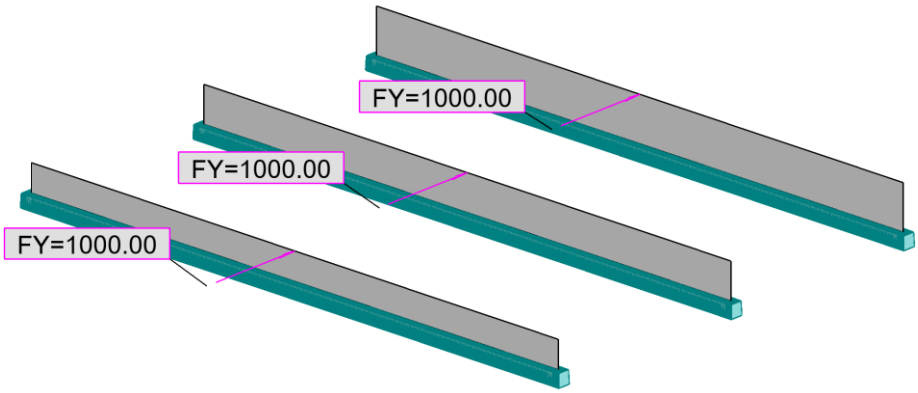

Figure 7: Example of models used for the analysis of bending moment distribution

The course of bending moment M_{3D} over the wall length at its base was obtained, see an example of such result in Figure 8. For more convenient result processing, the relative values of the bending moments M_{rel} were calculated, see Equation 6.

$$M_{rel} = \frac{M_{3D}}{M_{2D}} \qquad \textit{Equation 6}$$

where M_{3D} [kNm/m] is the bending moment obtained from a three-dimensional model

M_{2D} [kNm/m] is the bending moment obtained from a two-dimensional model

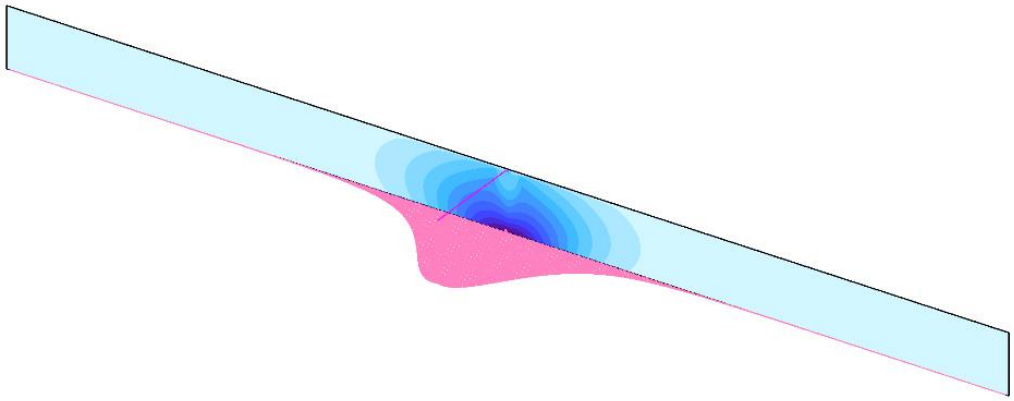

Figure 8: The course of bending moment over the wall length at its base

The results are summarised in a graph in Figure 9. The graph shows the dependence of the relative bending moment M_{rel} on horizontal position l at the wall base. Due to the geometrical symmetry of the problem, the results are plotted only for one half of the wall length, starting at l = 35 m. The plotted area of the graph ends at l = 50 m as the curves reached zero relative bending moment at that point. The legend of each individual curve is not provided for easy orientation. The curve with the highest peak corresponds to the shortest wall within the examined range (H = 0.6 m), the curve with the lowest peak corresponds to the tallest wall within the examined range (H = 6.0 m).

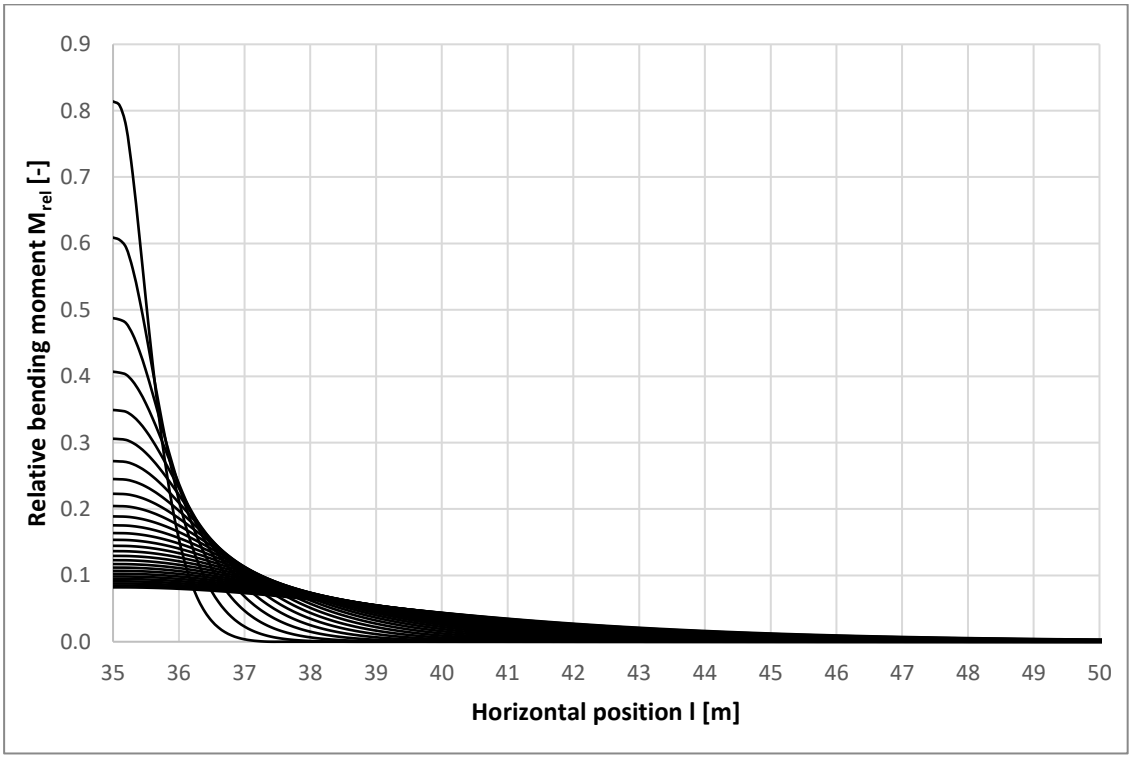

Figure 9: Dependence of relative bending moment on horizontal position

The aim of this Section is to analytically describe or approximate the course of the relative bending moment curves by a function, that has clearly defined parameters. For that, one of the curves was chosen for function fitting. Applicability of the function on the rest of the curves was verified subsequently.

The curve chosen for function fitting was the curve of wall height H = 2.0 m. The values of the horizontal axis were shifted to obtain the peak value at l = 0, not l = 35 m. The shift creates coordinate l_p which refers to the horizontal distance from the curve peak. The shape of the curve suggests that the best fit can be achieved with a bell-shaped function. For that, five bell-shaped functions were chosen to approximate the relative bending moment curve:

- Gaussian function (Normal distribution)
- Algebraic function (root of polynomial equation)
- Hyperbolic secant (derivative of Gudermannian function)
- Witch of Agnesi (probability density function of Cauchy distribution)
- Derivate of logistic function (scaled version of the derivate of hyperbolic tangent function)

Table 4 contains analytical description of the bell-shaped functions and values of parameters best describing the moment curve shape. The values of all parameters were set according to two criteria – to obtain the peak value identical to the peak relative bending moment, and to copy the curve shape with the most precision.

	Function	Analytical description	Parameters
1.	Gaussian function	$f(x) = ae^{\frac{-x^2}{2\sigma^2}}$	$a = 0.245$ $\sigma = 1.742$
2.	Algebraic function	$f(x) = \frac{a}{(b + cx^d)^e}$	$a = 0.245$ $b = 1.000$ $c = 0.200$ $d = 2.000$ $e = 1.500$
3.	Hyperbolic secant	$f(x) = \frac{a * 2}{e^x + e^{-x}}$	$a = 0.490$
4.	Witch of Agnesi	$f(x) = \frac{ba^3}{x^2 + ca^2}$	$a = 0.245$ $b = 1.000$ $c = 0.200$
5.	Derivate of logistic function	$f(x) = \frac{ae^x}{(1 + e^x)^2}$	$a = 0.980$

Table 4: Approximation functions

Note: The symbols used as function parameters in Table 4 are commonly used for their description and are excluded from the list of symbols of this dissertation. Some of the symbols used in this table are used elsewhere in this dissertation while describing a different quality. In the context of this Section, the x symbol used in Table 4 as a variable of the function is equal to horizontal position l, with a shift of 35 m.

The dependence of relative bending moment M_{rel} on horizontal position l with the 35 m shift is displayed in Figure 10 along with all five approximation curves.

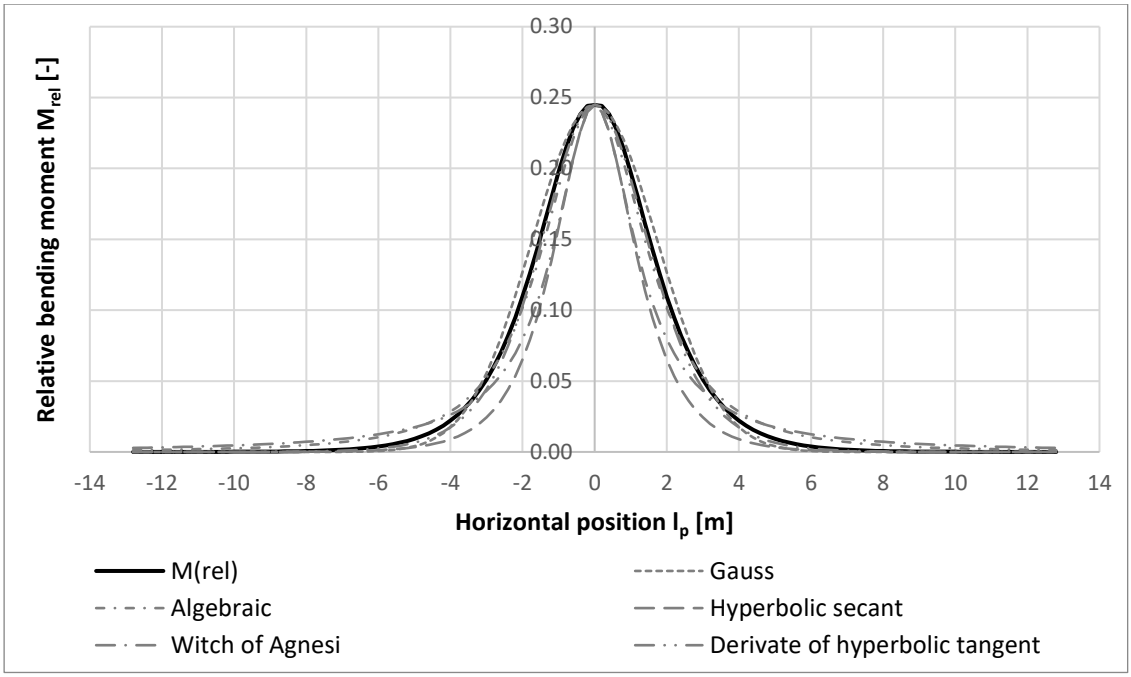

Figure 10: Approximation functions

The best fitting curve was chosen according to three criteria:

- Accuracy. The error of approximation was evaluated as a percentage related to the area under the curve. Table 5 summarises the error of each approximation curve.
- Safety of use. The approximation must provide more onerous results to be applicable in engineering practice safely. This is evaluated by comparing the areas under the curves; the approximation function must be equal or larger than the moment curve, not smaller. See Table 5 for summary.
- Clear definition of parameters. The parameters defining the approximation function need to be clearly defined based on the wall geometry. They need to be easily obtained for various wall heights. Table 5 shows summary of parameter clarity.

	Curve	Area under the curve [-]	Approximation error [%]	Safety	Clear definition of parameters
	Relative bending moment	1.04	-	-	-
1.	Gaussian function	1.07	3.0	safe	Parameters clear: • a is equal to the peak value, which is known for various wall heights H, according to

					Section 7.d.ii of this thesis; • σ is linearly dependent on wall height H, as described further in this section.
2.	Algebraic function	1.08	4.0	safe	Parameters unclear.
3.	Hyperbolic secant	0.77	26.0	unsafe	Parameters clear: dependent on peak bending moment.
4.	Witch of Agnesi	0.99	4.3	unsafe	Parameters unclear.
5.	Derivate of logistic function	0.98	5.6	unsafe	Parameters clear: dependent on peak bending moment.

Table 5: Evaluation of approximation functions

Table 5 shows that Gaussian function is the only approximation meeting all three criteria. Gaussian function was therefore chosen as the best fit to describe the horizontal course of bending moment over wall base.

The Gaussian function was used as an approximation of the bending moment distribution for the whole range of wall heights H, see the graph in Figure 11. Parameters of the approximation function (a, σ) were fitted for all examined wall heights. It was observed that the parameters are dependent on the wall height H in following manner:

- Parameter a directly describes the peak of the curve. The peak value is dependent on wall height H. It is identical to correction coefficient k_2, that is determined in Section 7.d.ii.
- Parameter σ is linearly dependent on wall height H, as it is clear from the graph in Figure 12. The graph shows σ values dependent on wall height H, including the trendline best describing the linear dependence. The dependence of parameter σ on wall height H is expressed in Equation 7.

$$\sigma = 0.834H + 0.056 \qquad \textit{Equation 7}$$

where $H\,[\mathrm{m}]$ is the wall height

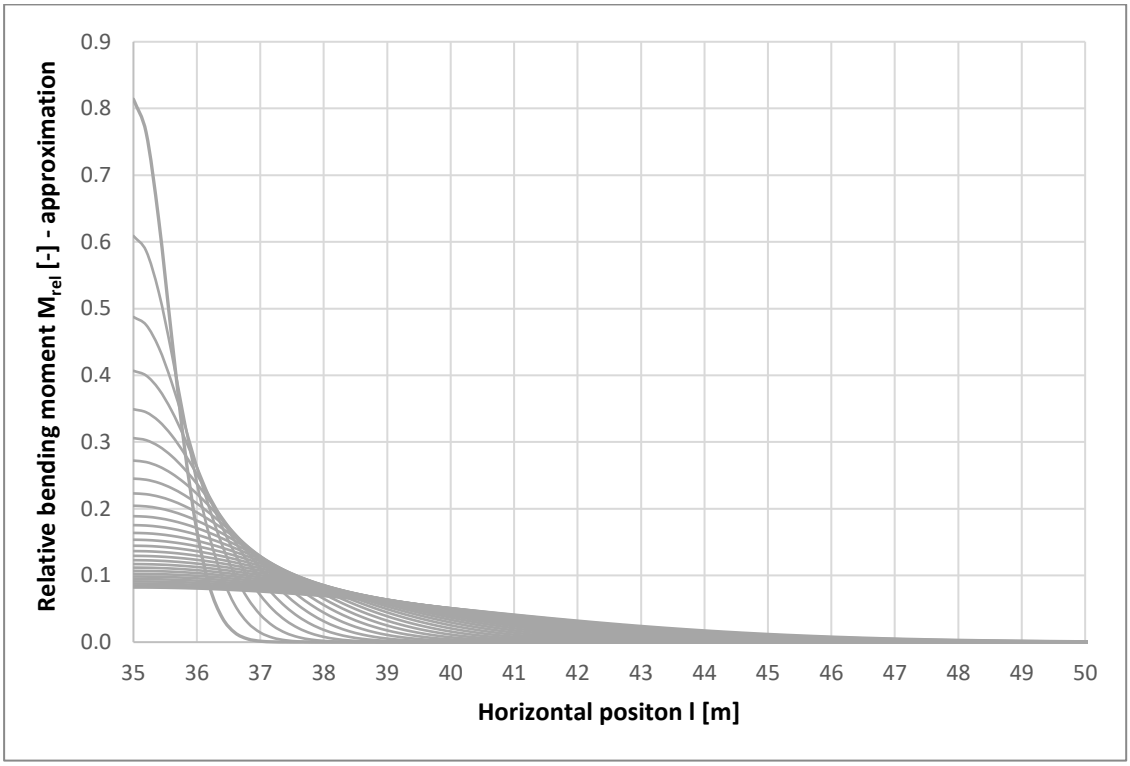

Figure 11: Approximation of relative bending moment course for various wall heights

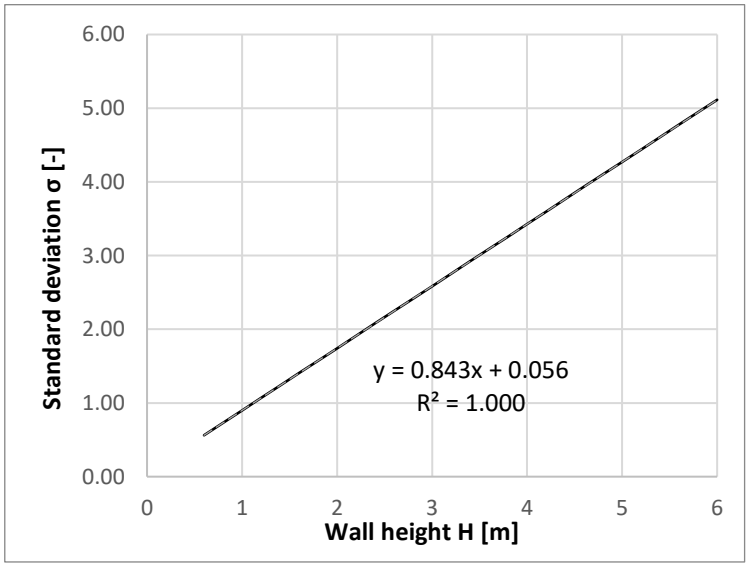

Figure 12: Dependence of σ parameter on wall height

For more convenient comparison, all curves of relative bending moment and all curves of Gaussian approximation were plotted in one graph, see Figure 13.

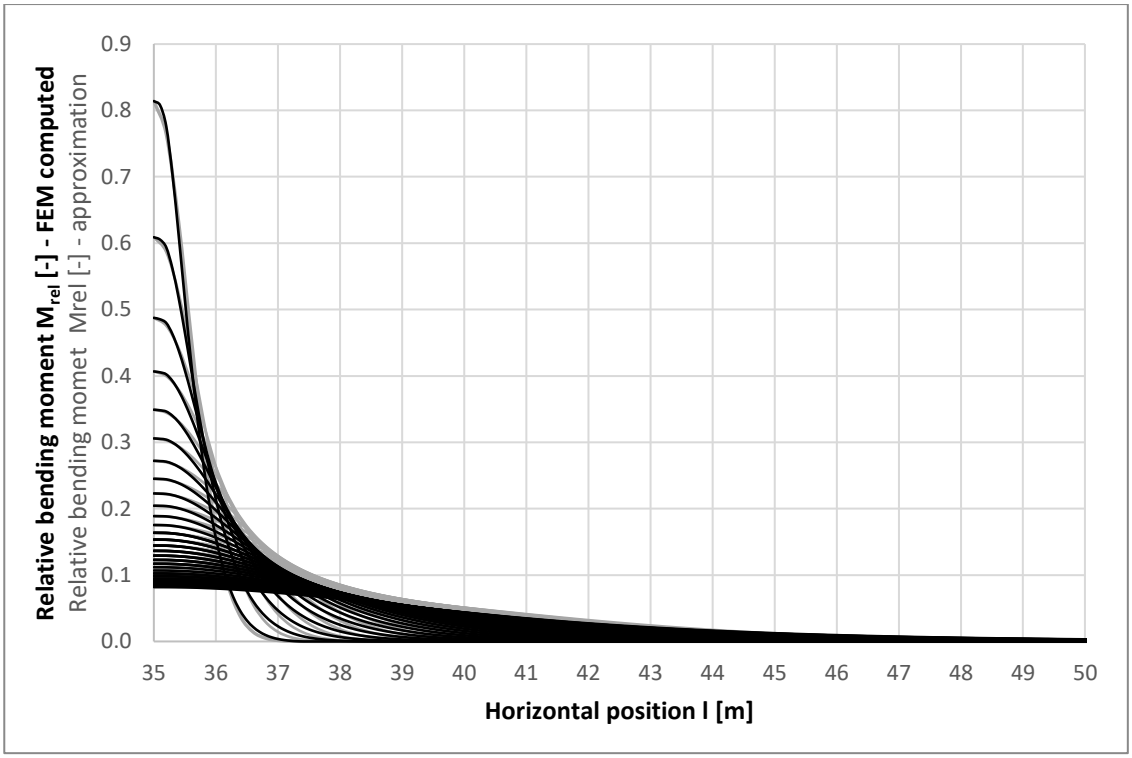

Figure 13: Course of bending moment and its approximation curves for various wall heights

To conclude the findings of this Section, the approximation of the course of the bending moment M_{rel} over the wall length at its base can be expressed by Equation 8 andEquation 9 using the general form of Gaussian function and implementing specific parameters.

$$f(x) = ae^{\frac{-x^2}{2\sigma^2}} \qquad \textit{Equation 8}$$

$$M_{rel} = k_2 e^{\frac{-{l_p}^2}{2(0.834H+0.056)^2}} \qquad \textit{Equation 9}$$

where a, σ [-] are parameters of Gaussian function (not defined in the list of symbols)

k_2 [-] is the correction coefficient according to Section 7.d.ii

l_p [m] is the horizontal distance from the peak bending moment

c. Wall zones

Depending on the circumstances in the vicinity of the cantilever wall, the position of the point load representing vehicle impact may or may not be known. If the wall is fully exposed to the impact, the exposed wall length L_{ex} is equal to the full wall length L, and the load may be applied on any point of the structure, and therefore, the design needs to cover all possible positions. If only certain areas of the wall are exposed to the impact, only a specific part of the wall is influenced, see Figure 14.

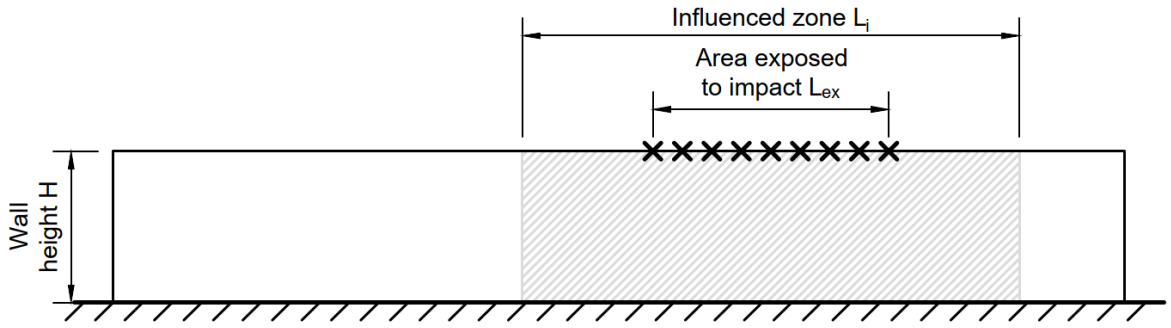

Figure 14: Influenced zone

The influenced zone L_i is defined as the length of the wall that has non-zero bending moment values in vertical direction, see Figure 15. Behind the borders of this zone, the wall remains intact. The influenced half-length $L_{i/2}$ is defined as the horizontal distance between the point load at the end of the area exposed to impact and the position of the nearest zero bending moment. For a wall subjected to a single point load the influenced wall length is double the influenced half-length. As the peak bending moment is located directly below the load force position and their horizontal coordinate is equal, it also means that the influenced half-length $L_{i/2}$ is also the horizontal distance from the load force position to zero bending moment.

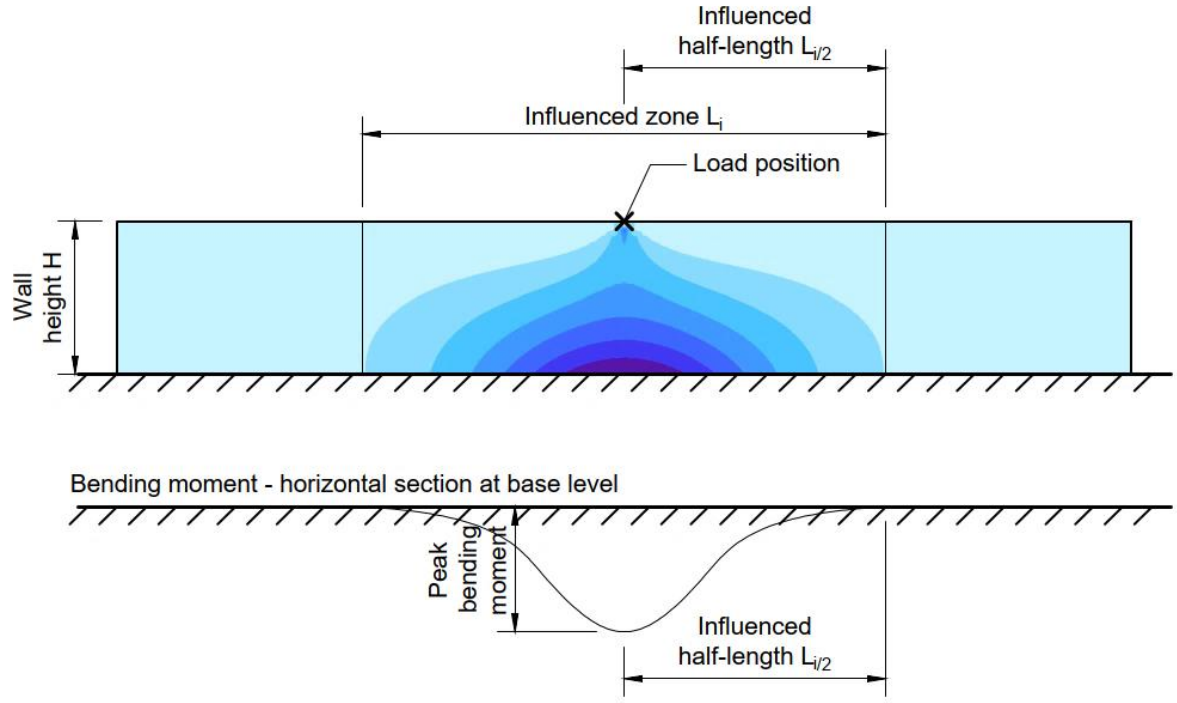

Figure 15: Influenced half-length

i. Influenced zone of infinite wall

To quantify the length of the influenced zone on an infinite wall subjected to a single point load, a set of three-dimensional models was prepared. A wall of length

L = 70 m (to simulate infinite length, see Section 7.a) and thickness t = 300 mm was subjected to a point load F = 1000 kN located at the top wall edge in the centre of the wall length (x = 35.0 m). Various wall heights H were examined, ranging from 0.6 m to 6.0 m with 0.2 m step.

The course of relative bending moment M_{rel} over the wall length was observed. The graph in Figure 16 displays the results. The horizontal axis of the graph shows the representative part of the wall length. It starts at the centre of the wall (l = 35.0 m) and ends in positions where the curves approach zero bending moment (l = 50.0 m). The bending moments in positions behind l = 50.0 m are so close to zero that they are not shown to emphasise the depicted part of the graph. The bending moments in positions before l = 35.0 m are symmetrical to the ones after this mark. There are two curves highlighted dashed in the graph – the curve of 0.6 m wall height and the curve of 6.0 m wall height. These two curves are the beginning and end of the examined range of wall heights. The legend for the rest of the curves is not displayed to keep clarity in the graph.

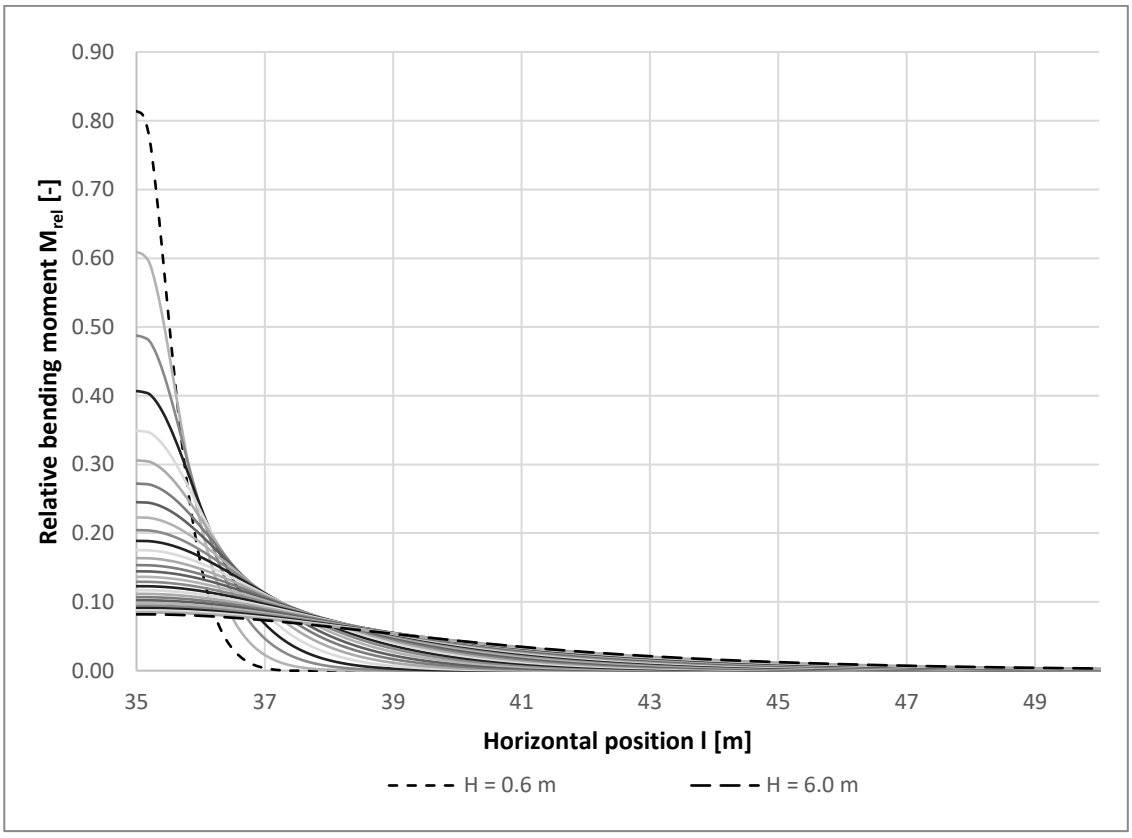

Figure 16: Influenced half-length of infinite wall subjected to a single point load

The curve of 0.6 m wall height has the highest peak of relative bending moment $M_{rel,max}$. The bending moment obtained on this three-dimensional model is 81 % of the bending moment that is obtained on a two-dimensional simulation of the problem. While the peak value of relative bending moment $M_{rel,max}$ is the highest of the examined range of wall heights, the influenced zone is the shortest. The curve decreases rapidly and reaches zero relative bending moment at l = 37.0 m. Since the graph shows values after l = 35.0 m mark, the influenced half-length $L_{i/2}$ equals to 37.0 − 35.0 = 2.0 m, and therefore, the influenced length L_i is 4.0 m.

On the other side of the examined wall height spectrum, the curve of 6.0 m wall height has the lowest peak of relative bending moment $M_{rel,max}$. The bending moment obtained on this three-dimensional model is 8 % of the bending moment that is obtained on a two-dimensional simulation of the problem. While the peak value of relative bending moment $M_{rel,max}$ is the lowest of the examined range of wall heights, the influenced zone is the longest. The curve decreases slowly from the peak and reaches zero relative bending moment at l = 48.4 m. Since the graph shows values after l = 35.0 m mark, the influenced half-length $L_{i/2}$ equals to 48.4 − 35. 0 = 13.4 m, and therefore, the influenced length L_i is 26.8 m.

The results for the whole range of the examined wall heights are presented in Figure 17 andFigure 18. The graph in Figure 17 shows the dependence of the influenced L_i wall length on wall height H. The graph in Figure 18 shows the dependence of the influenced wall half-length $L_{i/2}$ on wall height H. The trend of the curve in Figure 17 can be analytically expressed, see Equation 10. Therefore, the dependence of the influenced wall length L_i on the wall height H can be expressed, see Equation 11. Similarly, the curve describing dependence of the influenced half-length $L_{i/2}$ was determined, see Equation 12.

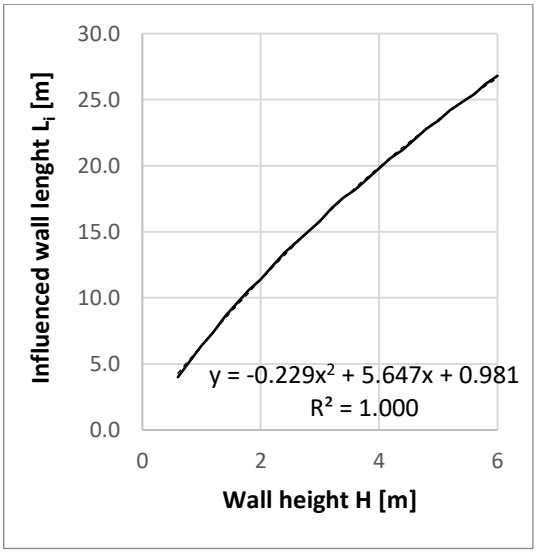

Figure 17: Influenced wall length dependence on wall height

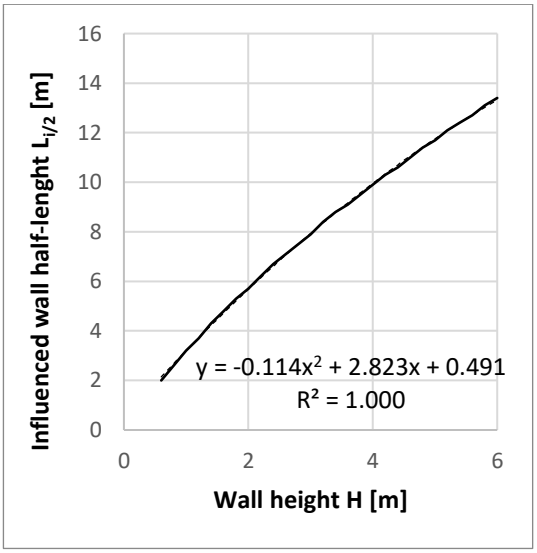

Figure 18: Influenced wall half-length dependence on wall height

$$y = -0.229x^2 + 5.647x + 0.981 \qquad \textit{Equation 10}$$

$$L_i = -0.229H^2 + 5.647H + 0.981 \qquad \textit{Equation 11}$$

$$L_{i/2} = -0.114H^2 + 2.823H + 0.491 \qquad \textit{Equation 12}$$

where H [m] is the height of the wall

The equations presented above apply to walls of infinite length, or walls of finite length where the position of the point load is known to be at least $L_{i/2}$ from wall end.

The modelling was repeated for load force F = 80 kN. The results were identical to those with load force F = 1000 kN, proving that the influenced zone is independent from load magnitude.

ii. Influenced zone of finite wall

The proximity of a wall edge undoubtedly affects the influenced zone of the wall. In case of an infinite wall subjected to a single point load, the influenced zone L_i is double the distance from the peak to zero bending moment and the influenced half-length $L_{i/2}$ is equal to the distance from the load force horizontal position to zero bending moment. It is obvious that in case of finite walls with loads positioned near wall side edges, the influenced half-length on the edge side from the peak will be reduced to the limits of the wall, see Figure 19. In this section of the thesis, there was examined if the half-length on the central side from the peak bending moment is identical for finite and infinite walls.

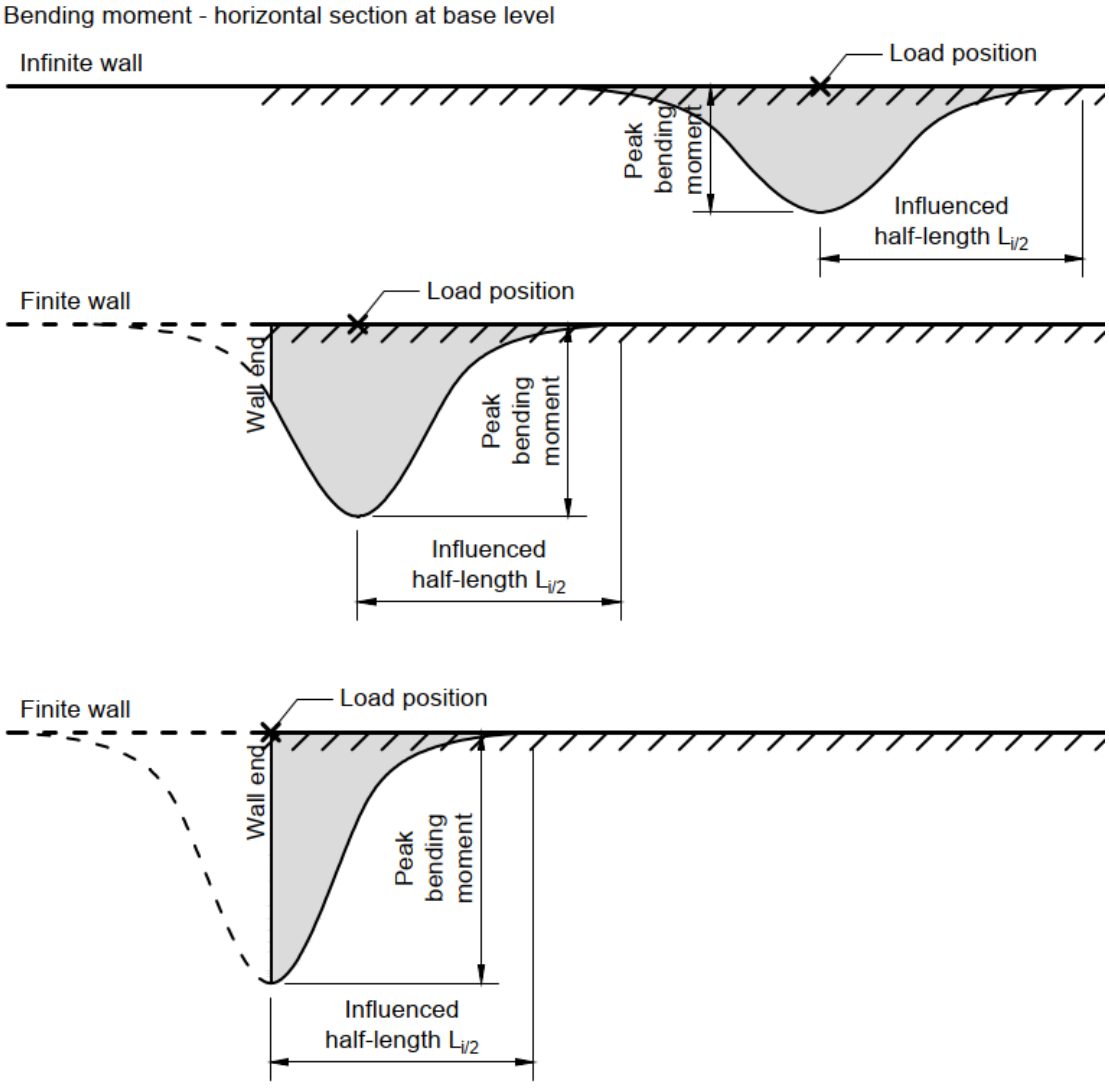

Figure 19: Influenced half-length of infinite and finite wall

To determine the influenced half-length of finite wall subjected to a point load, a three-dimensional model of a wall was prepared. The wall of length L = 70 m, height H = 2.0 m and thickness t = 300 mm was subjected to a point load F = 160 kN. The position of the load was variable, ranging from x = 0.0 m to x = 35.0 m, creating 176 load cases.

The dependence of the relative bending moment M_{rel} on horizontal position l is presented in the graph in Figure 20. for all load positions from x = 0.0 m to x = 12.4 m. The curves of further load positions are not displayed as the trend of the curves is monotonic for load positions behind x = 12.4 m. The distance between the peak position and the position where the curve reaches zero is 5.6 m for all presented curves, see illustration of this result in Figure 21. This means, that the influenced half-length in the direction to the centre of the wall is independent from the position of the load force. The proximity of wall end manifests itself only as a rise in the bending moment peak value and does not result in larger wall length affected by the load.

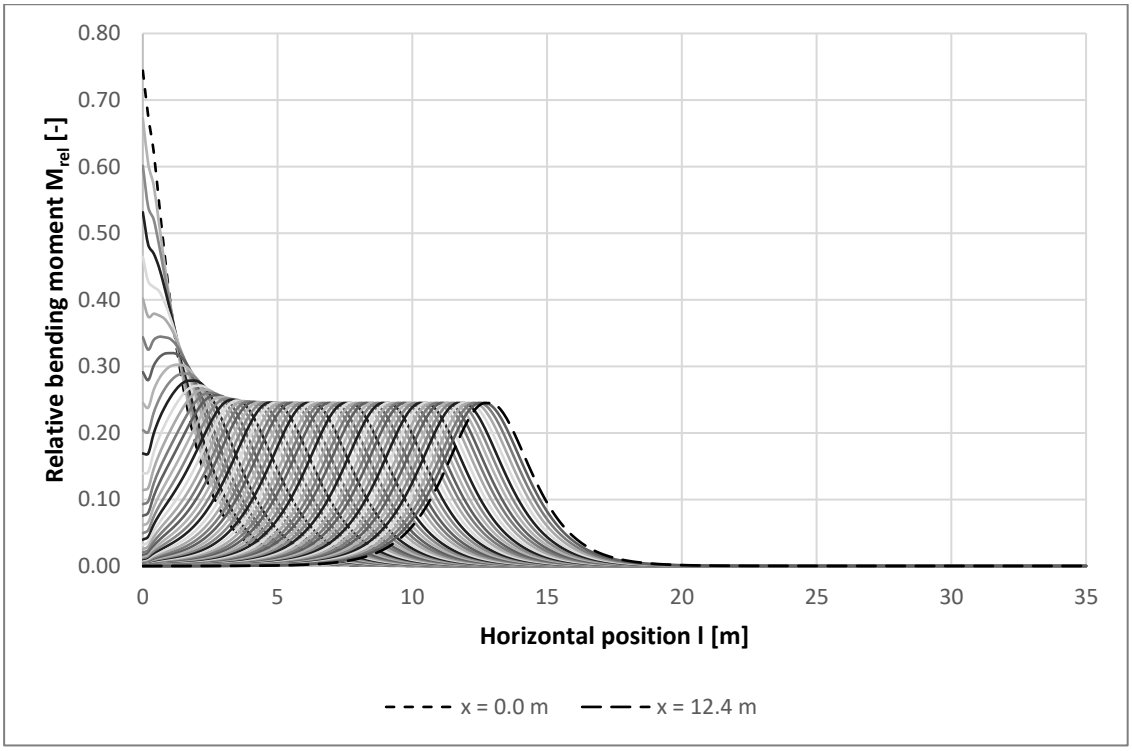

Figure 20: Influenced half-length of a finite wall

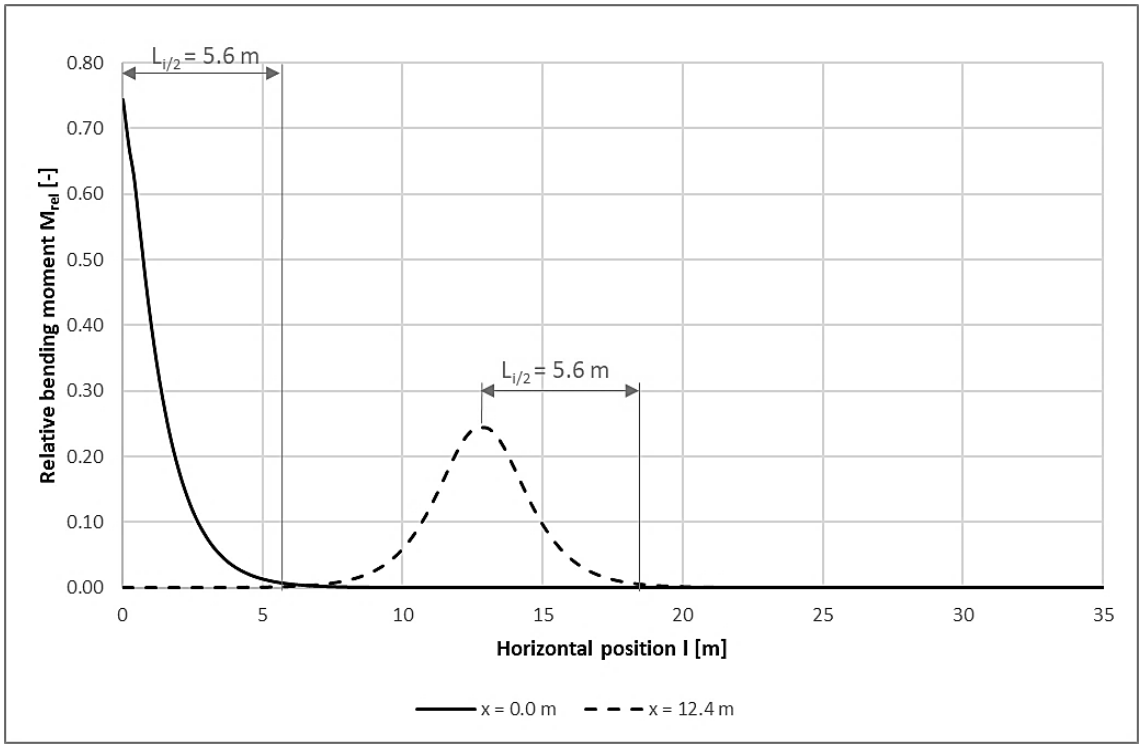

Figure 21: Equal influenced wall half-length for edge and non-edge load position

The findings from this and the previous Section can be summarised as follows:

- For walls with areas exposed to impact further than $L_{i/2}$ from wall edge ($x_{min} \geq L_{i/2}$), the influenced zone L_i can be expressed by Equation 13.
- For walls with areas exposed to impact closer than $L_{i/2}$ to wall edge ($x_{min} < L_{i/2}$), the influenced zone L_i can be expressed by Equation 14.

$$L_i = 2L_{i/2} + L_{ex} \qquad \textit{Equation 13}$$

$$L_i = x_{min} + L_{ex} + L_{i/2} \qquad \textit{Equation 14}$$

where x_{min} is the distance between the wall end and the closest impact load position
L_{ex} is the length of the wall exposed impact
$L_{i/2}$ Is the half-length defined in Equation 12

iii. Central and edge zones

If a wall is fully exposed to impact load, the internal forces in the areas in proximity of wall side edges are strongly influenced. Since the purpose of this study is to obtain reliable results for convenient structural design, it is handy to establish wall zones within which specific rules for the analysis will apply.

Two major wall zones are introduced: a) Central zone; b) Edge zone, see Figure 22.

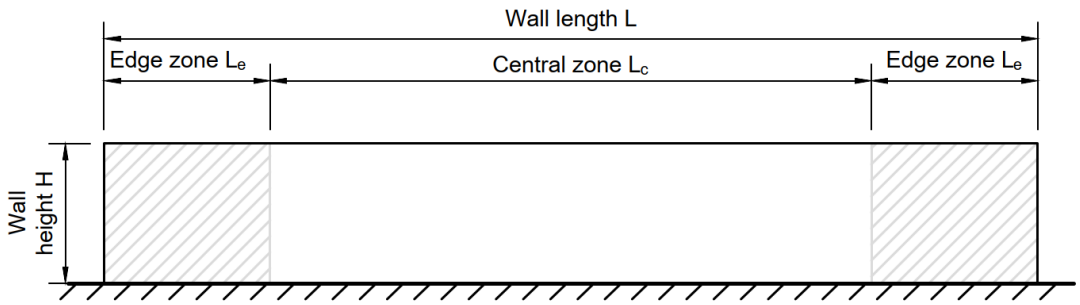

Figure 22: Central and edge zones

The central zone is the part of the wall where the peak bending moment is not influenced by the proximity of the wall edge. Generally, the bending moment in the central zone is smaller than bending moment obtained from a two-dimensional model.

The edge zone is the part of the wall in which the peak bending moment is increased due to the proximity of the wall edge. Generally, the bending moment in the edge zone is higher than the bending moment in the central zone; in some cases, it may even exceed the bending moment obtained from a two-dimensional model.

The position of the interface between edge and central zone is defined by size of the wall edge zone L_e. In this section, the size of L_e is determined. For that purpose, the three-dimensional model of a wall from the previous section was analysed. The wall of length L = 70 m, height H = 2.0 m and thickness t = 300 mm was subjected to a point load F = 160 kN. The position of the load was variable, ranging from x = 0.0 m to x = 35.0 m, creating 176 load cases. The results of this analysis were already presented in the previous section in Figure 20. While in the previous section it was analysed if the horizontal distance between the peak bending moment and zero bending moment is equal for impact forces applied at the wall edge and in a distance from edge (Figure 20), in this section, it is observed for what load position the peak bending moment value is increased in comparison to an infinite wall.

The graph in Figure 23 presents relative bending moments M_{rel} over the wall length for various load position x. The peak values of the curves representing load cases where the load position is further than 4.4 m from the wall edge is constant M_{rel} = 0.24. The peak value starts to increase at x = 4.2 m and increases with decreasing x, reaching M_{rel} = 0.74 at x = 0.0 m. The wall edge zone is equal to the range of positions where the trend of moment peaks is not constant. In this case, the wall edge zone L_e = 4.2 m. As it was proven in the previous section, this result is independent from the load magnitude.

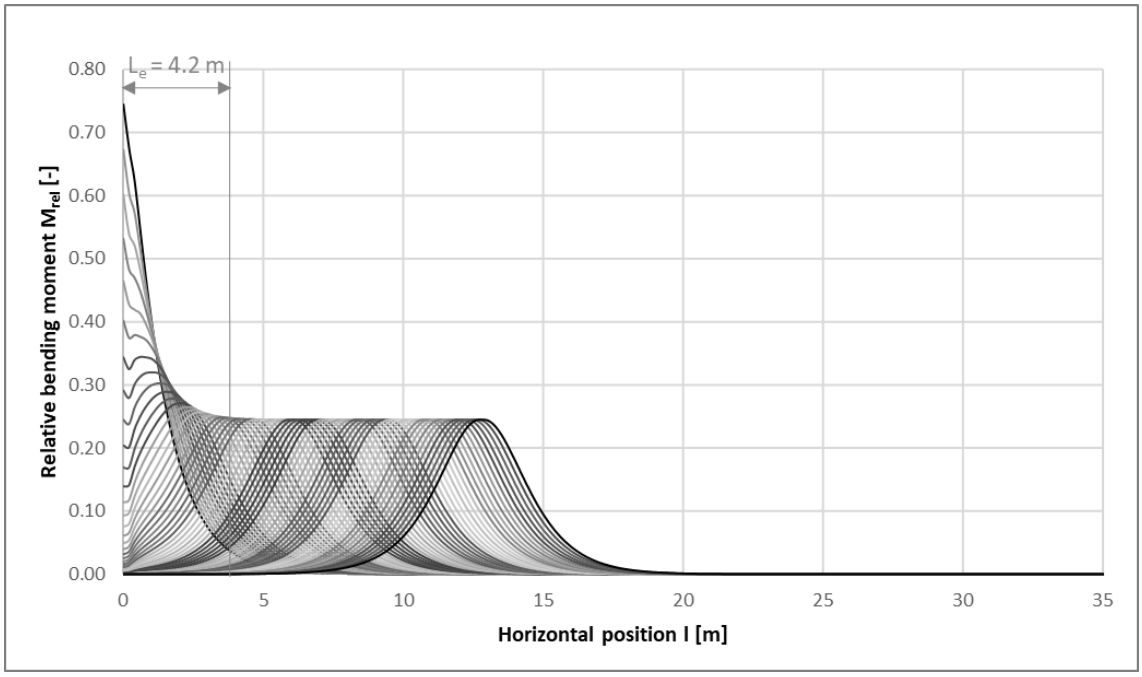

Figure 23: Wall edge zone

The analysis was repeated for various wall heights *H* ranging from 1 m to 5 m with 1 m step. The dependence of the edge zone length L_e on wall height *H* is presented in a graph in Figure 24. The curve can be described by Equation 15, and therefore the dependence of the edge zone length L_e on wall height *H* follows Equation 16.

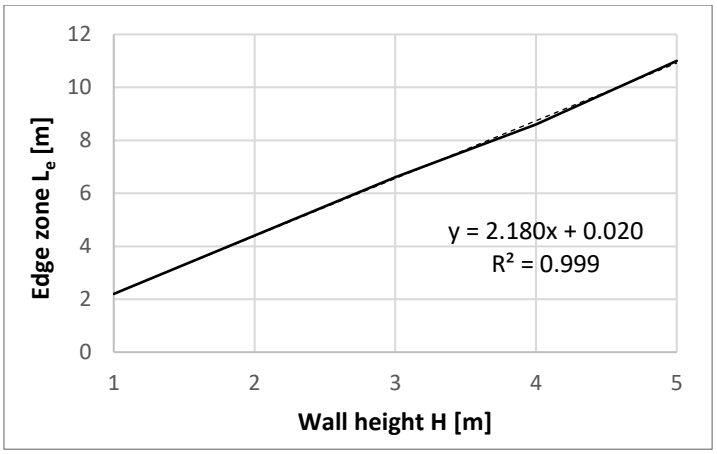

Figure 24: Wall edge zone dependence on wall height

$$y = 2.180x + 0.020$$ *Equation 15*

$$L_e = 2.180H + 0.020$$ *Equation 16*

where *H* is the height of the wall

Knowing the size of the edge zones L_e, the central zone L_c can be determined as the remaining part of the wall length L, see Equation 17.

$$L_c = L - 2L_e \qquad \textit{Equation 17}$$

The definition of central and edge zones of the wall according to the equations stated above is important for a correct use of calculation methods presented in this thesis.

It is important to distinguish between influenced wall half-length $L_{i/2}$ and edge zone length L_e, as they might seem to be equal, but they are not. The influenced half-length is the distance between the peak bending moment and zero bending moment on a wall subjected to a single point load. The edge zone is the distance between peak bending moment at the wall edge and the position past which the peak bending moment no longer decreases in case of a wall that is fully exposed to impact loading and therefore there are infinite possible positions of the load. This is further explained in Figure 25, where the distance $L_{i/2}$ spans from peak of the black curve to the position where the black curve reaches zero bending moment. Contrarily, the distance L_e spans from the absolute peak of all curves to the point where the envelope of the peaks stabilizes at a constant value.

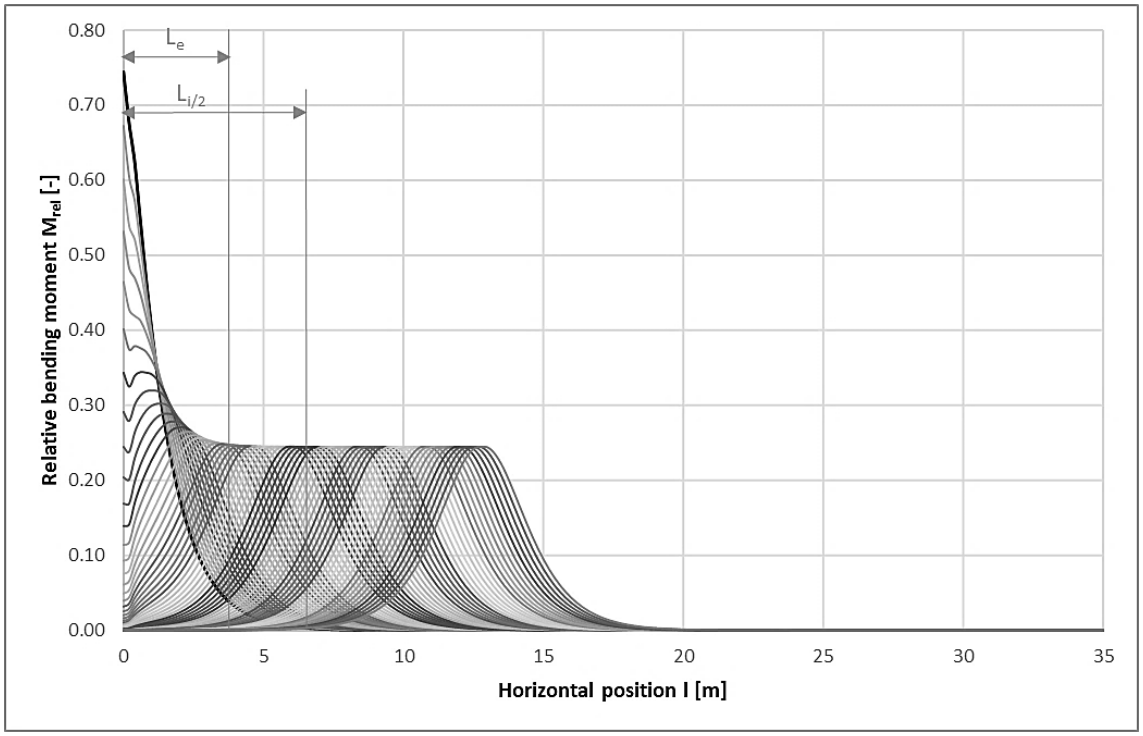

Figure 25: The difference between influenced wall half-length end edge zone

iv. Zone sensitivity to moment precision

The definition of zones in Sections above was determined by detecting at what point of wall length the bending moment reaches a certain value or zero. It needs to be mentioned that such approach is very sensitive to the bending moment value precision. As the curve of bending moments approaches a constant value,

its inclination becomes lower. For that, a small difference in bending moments means a large difference in horizontal position, see Figure 26.

The equations presented in the previous sections are based on results of relative bending moments that have the precision of 0.00. This means that the rounding error is 0.005, i. e. 0.5 %.

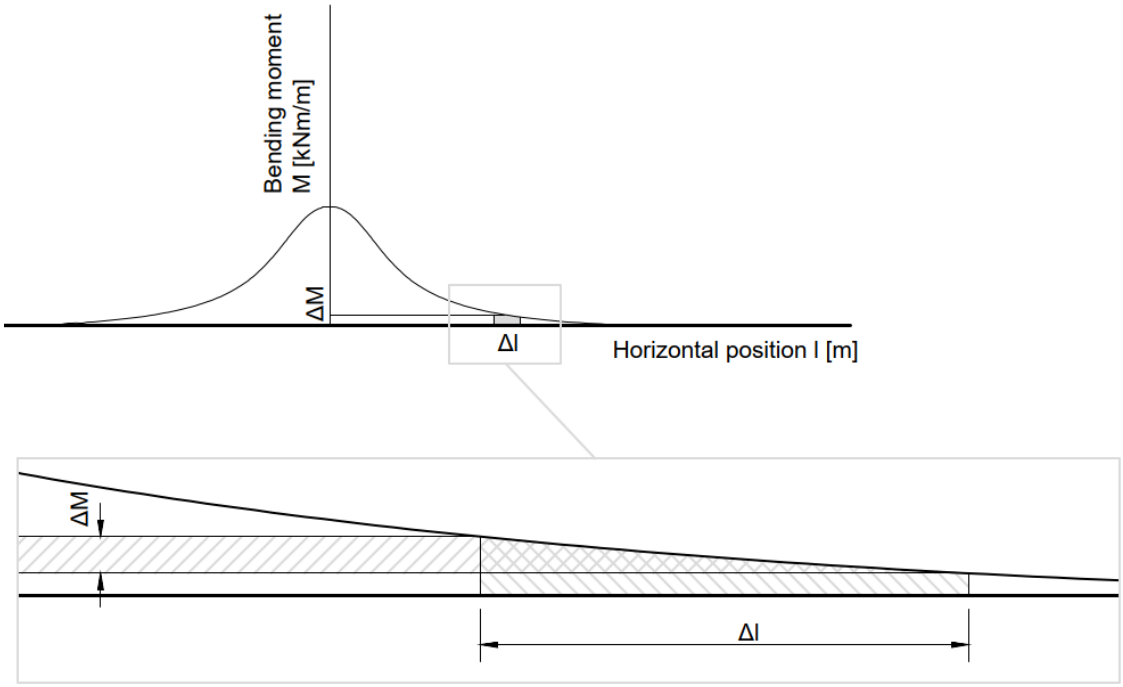

Figure 26: Sensitivity of wall zones to moment precision

d. Effects of parameters influencing bending moment distribution

The distribution of bending moment over the structure and its peak value are affected by several parameters of the structure and load. The effects of each individual parameter on the peak value of bending moment are analysed in following Subsections. The evaluated parameters are listed as follows:

1. Wall length
2. Wall height
3. Wall thickness
4. Load magnitude
5. Load distribution
6. Vertical load position
7. Horizontal load position
8. Concrete class
9. Reinforcement
10. Edge supports

As the objective of this thesis is to provide results of vertical bending moment with precision of three-dimensional modelling with use of only two-dimensional hand calculation, the effects of each individual parameter listed above is incorporated as a correction coefficient to be applied on the maximum value of bending

moment $M_{2D,max}$ from a two-dimensional model. Interaction between the parameters and its effects on resulting value of peak bending moment $M_{3D,max}$ is as well evaluated where applicable.

i. Wall length

The peak bending moment on three-dimensional models of a retaining wall is strongly dependent on wall length L, as the length provides space for distribution of bending moment in horizontal direction. The more the bending moment is distributed, the smaller is its peak value. Since the objective of this thesis is to obtain peak values of bending moments with precision equal to three-dimensional modelling with use of simplified two-dimensional models on long retaining walls, it is crucial to classify the walls according to their length, and thus define applicability of the findings presented further in the thesis.

One of the findings described in Section 7.c is the definition of influenced wall length L_i. Based on that, a hypothesis is proposed regarding the effects of wall length:

A wall with length L equal to or larger than the influenced wall length L_i is classified as a long wall and can be divided into central and edge zones. The peak bending moment caused by a point load placed in the central zone on the top edge of such wall is equal to the peak bending moment on an infinite wall caused by that load.

To validate the hypothesis, a set of three-dimensional models was prepared. A wall was subjected to a point load of 20 kN placed in the centre of the top wall edge. The wall was modelled with thickness of 300 mm, C30/37 concrete class was used. Three wall heights were examined – 1 m, 2 m, and 3 m. The wall length was variable, ranging between 0.2 m and 20.0 m with 0.2 m step. The values peak bending moment in vertical direction $M_{3D,max}$ were observed. The results are presented in Figure 27 on a graph of peak bending moment $M_{3D,max}$ dependence on wall length L.

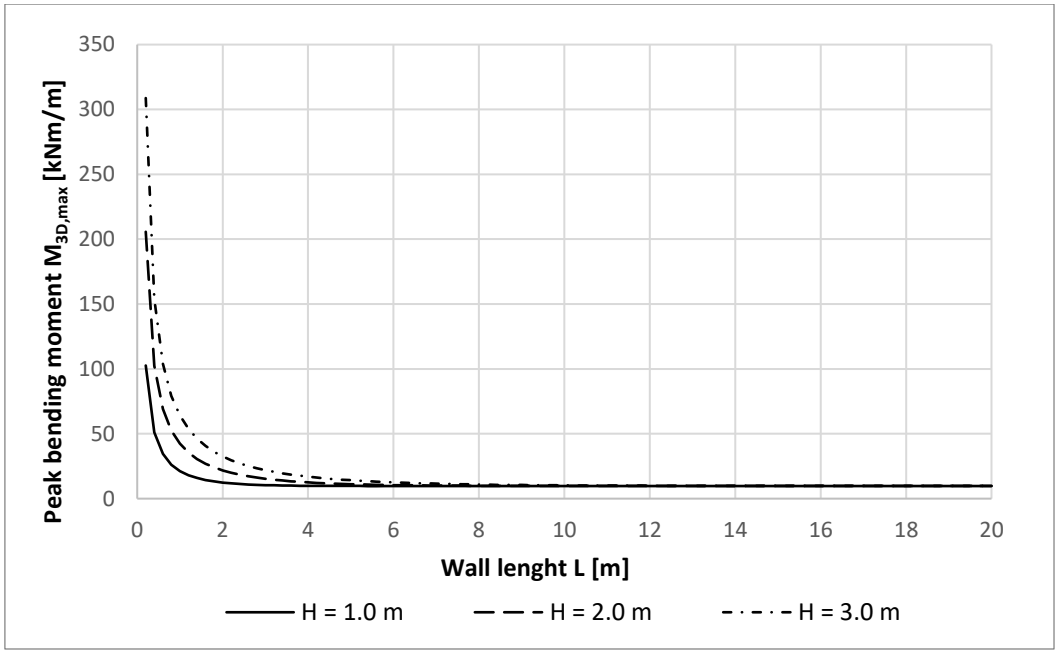

Figure 27: Peak bending moment dependence on wall length

All three curves in the graph of Figure 27 decrease with increasing wall length, which confirms the assumption that large wall lengths provide enough space for bending moment distribution, and thus decrease the peak value.

For more convenient result processing, the relative values of the bending moments M_{rel} were calculated, see Equation 18.

$$M_{rel,max} = \frac{M_{3D,max}}{M_{2D,max}} \qquad \textit{Equation 18}$$

where $M_{3D,max}$ [kNm/m] is the peak bending moment obtained from a three-dimensional model

$M_{2D,max}$ [kNm/m] is the maximum bending moment obtained from a two-dimensional model

$$M_{2D,max} = FH \qquad \textit{Equation 19}$$

where

F [kN] is the loading force

H [m] is the wall height, equal to vertical load position in this case

The dependence of relative bending moment $M_{rel,max}$ on wall length L is presented in Figure 28.

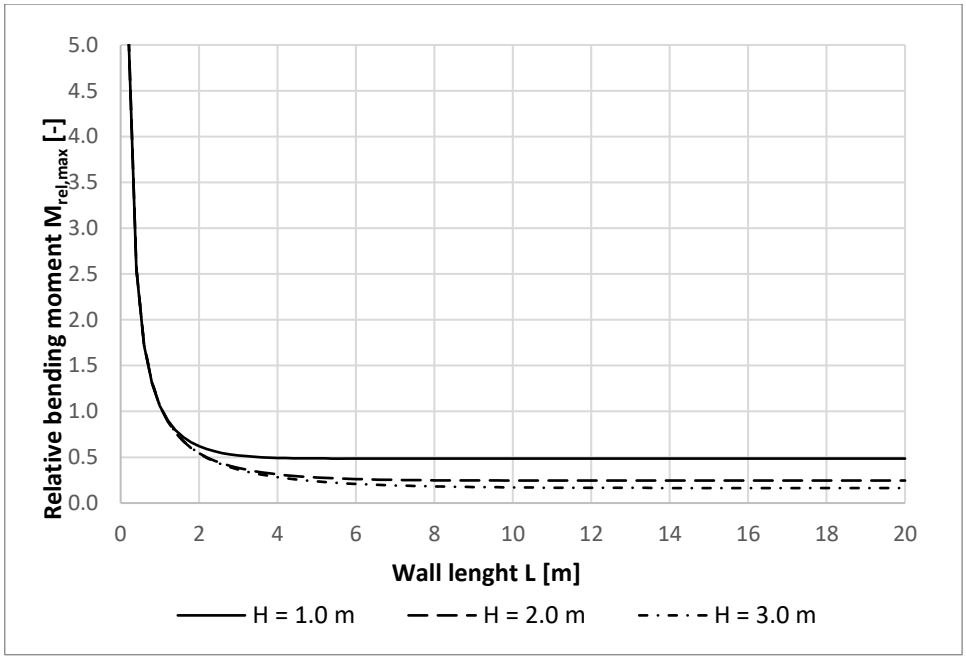

Figure 28: Relative bending moment dependence on wall length

Validation of the hypothesis stated above requires proving that for wall lengths L larger than influenced wall length L_i, the peak bending moment $M_{rel,max}$ does not differ from the peak bending moment $M_{rel,max}$ on infinite wall. In other words, for walls longer than L_i, the peak bending moment should remain constant regardless increasing wall length L. To evaluate that, the influenced wall lengths L_i for all wall heights H are calculated according to Equation 11 in Section 7.c.i and presented in Table 6.

wall height H [m]	influenced wall length L_i [m]
1.0	6.4
2.0	11.4
3.0	15.9

Table 6: Influenced wall length for examined wall heights

The influenced lengths L_i were introduced into the detail of the $M_{3D,max}$-L graph as vertical borders, see Figure 29.

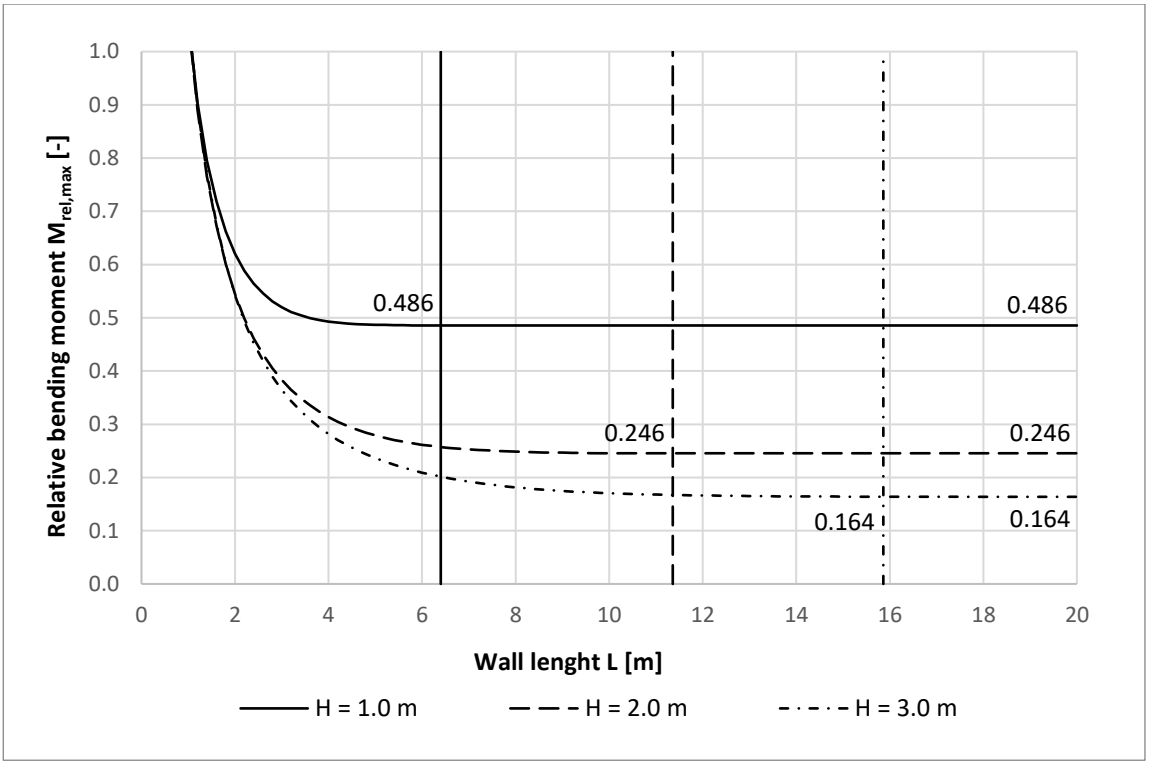

Figure 29: Relative bending moment dependence on wall length with marked influenced lengths

The graph shows the specific values of relative bending moment $M_{rel,max}$ for the wall lengths L equal to the influenced wall length L_i. The values are equal to the relative bending moment values for the longest walls of the examined range, which are shown in the graph as well. This proves that the relative bending moment $M_{rel,max}$ for wall length L_i is equal to the relative bending moment $M_{rel,max}$ for longer walls. The values of relative bending moments $M_{rel,max}$ remain constant for walls with lengths L larger than L_i in all three cases of examined wall heights. The hypothesis stated at the beginning of this Section is thus validated.

Based on the findings presented above, it can be concluded that walls with length L equal to or larger than the influenced wall length L_i can be categorized as long walls, that have defined central and edge zones. When the load of such wall is placed in its central zone, the behaviour of the wall is equal to behaviour of an infinite wall. Walls shorter than L_i are categorized as short walls and need individual approach in their modelling. They are not a subject of the study presented in this thesis and the findings described in the other Sections of this thesis are not applicable to them.

It is advised to always use three-dimensional modelling for the analysis of walls with length L smaller than L_i to obtain reliable results. For walls with length L smaller than or equal to 1.0 m, it is advised to use two-dimensional beam models.

ii. Wall height

The cantilever wall analysed in this thesis is in default assumed to be subjected to a loading force placed at the top wall edge. For that, the wall height H is equal to

the vertical position of the force *h*, and therefore, the wall height *H* strongly affects the peak bending moment as it defines the lever arm of the force.

A set of three-dimensional models was prepared to evaluate the effects of wall height *H*. A wall with length of 70 m was subjected to a load of 20 kN placed in the centre of the wall horizontally, at the top wall edge vertically. The wall was modelled with thickness of 300 mm, C30/37 concrete class was used. Wall heights ranged between 0.6 and 6.0 m with 0.2 m step.

The peak bending moment in vertical direction $M_{3D,max}$ was observed for all examined wall heights. The peak value is situated in the central section of the wall for all cases. The dependence of peak bending moment $M_{3D,max}$ on wall height *H* is summarised in a graph in Figure 30.

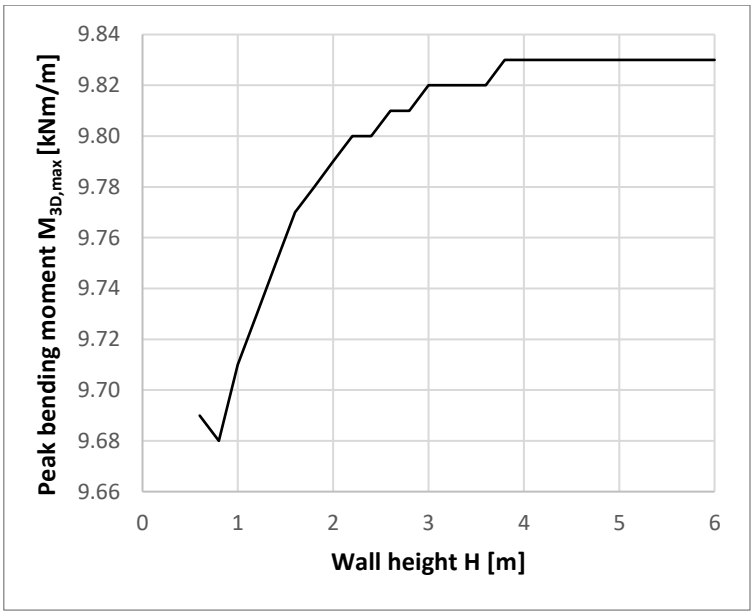

Figure 30: Peak bending moment dependence on wall height

The graph in Figure 30 shows general increase of the peak bending moment $M_{3D,max}$ with increasing wall height *H*, with the exception of the very beginning of the curve corresponding to wall heights up to 1.0 m. A possible cause of this discrepancy at the beginning of the height range is that the wall is too short for using a plate element for its modelling. The curve is not entirely smooth as the software provides results with precision of two decimal places, and for that close values appear to be equal.

The vertical axis of the graph in Figure 30 shows quite narrow range of values. To put the values in perspective, Figure 31 provides the results shown with the baseline at zero bending moment.

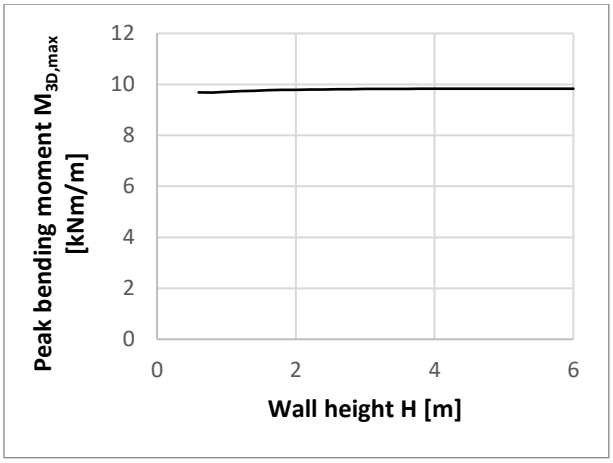

Figure 31: Peak bending moment dependence on wall height

This new perspective reveals that the resulting values of peak bending moment $M_{3D,max}$ are in fact very close for all examined wall heights. Hence, the effect of the wall height H is much less significant in three-dimensional modelling than it is in two-dimensional modelling, where there is a linear dependence between wall height H and peak bending moment $M_{2D,max}$ according to Equation 20.

$$M_{2D,max} = FH \qquad \textit{Equation 20}$$

where F [kN] is the point load force
H [m] is the wall height, equal to vertical load position h in this case

In case of three-dimensional models, the peak bending moment $M_{3D,max}$ increases very slowly with increasing wall height H, while the increase is more rapid on two-dimensional models. The reason for that is that the tree-dimensional model provides wider influenced area into which the bending moment can spread, and therefore, its peak is reduced.

To obtain the relationship between the results on two- and three-dimensional models, the relative peak bending moment $M_{rel,max,2}$ is introduced as a ratio of the value obtained from the three-dimensional model to the value obtained from the two-dimensional model, see Equation 21.

$$M_{rel,max,2} = \frac{M_{3D,max}}{M_{2D,max}} \qquad \textit{Equation 21}$$

where $M_{3D,max}$ [kNm/m] is the peak bending moment obtained from a three-dimensional model
$M_{2D,max}$ [kNm/m] is the peak bending moment obtained from a two-dimensional model

The dependence of the relative peak bending moment $M_{rel,max,2}$ is plotted in Figure 32. For all inspected wall heights, the peak relative bending moments obtained from the three-dimensional models were smaller than the ones obtained from the two-dimensional models. Increasing wall height *H* leads to a decrease of relative bending moment $M_{rel,max,2}$. For a wall with the height of 0.6 m, the bending moment from the three-dimensional model is 81% of the moment from the two-dimensional model. For a wall with the height of 6.0 m, it is 8%.

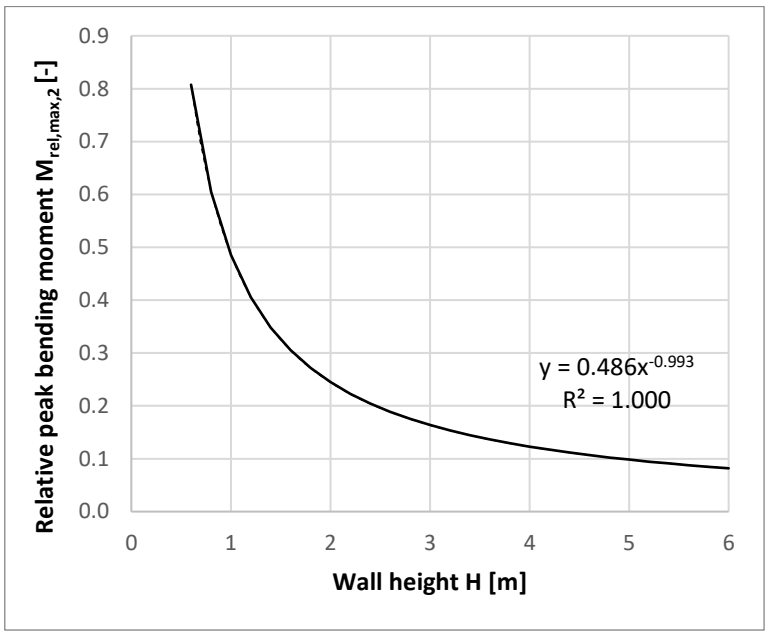

Figure 32: Relative peak bending moment dependence on wall height

A trendline of the curve of the relative peak bending moment $M_{rel,max,2}$ was found, see Equation 22. The precision of the equation is satisfactory as its determination coefficient R^2 is equal to 1.000. The trendline function can be used as a correction coefficient k_2 dependent on wall height *H*, see Equation 23.Equation 23

$$y = 0.486x^{-0.993} \qquad \textit{Equation 22}$$

$$k_2 = y = 0.486x^{-0.993} = 0.486H^{-0.993} \qquad \textit{Equation 23}$$

The correction coefficient k_2 can be applied on the peak bending moment $M_{2D,max}$ obtained from the two-dimensional analysis, returning modified value that approximates a value that would have been obtained from the three-dimensional model, see Equation 24. The correction coefficient k_2 compensates the error of the two-dimensional analysis. The correction coefficient is applicable to the central zone of very long walls as defined in Section 7.c.

$$M_{3D,max} = k_2 M_{2D,max} = 0.486H^{-0.993}FH = 0.486FH^{0.007} \qquad \textit{Equation 24}$$

To generalize the use of correction coefficient k_2 defined in Equation 23, its applicability was tested for changing conditions in the other parameters defining the wall and load (according to the list in Section 7.d). Further paragraphs contain the results of this testing, considering the wall and load parameters one by one and their potential interference with the outcomes from above.

Wall length: The analysis of wall height influence on the peak bending moment was conducted for the case of an infinite wall or a finite wall with length L equal to at least L_i with the loading force F placed in the central zone, as defined in Section 7.c. For shorter walls or walls with the loading force F placed in an edge zone, the ratio of peak bending moments on the three- and two-dimensional models differs. Hence, the correction coefficient k_2 as defined by Equation 23 is not applicable in such cases. Applicability of the correction coefficient k_2 on an infinite wall or a finite wall with length L equal to at least L_i is given by the definitions of infinite/finite walls and central/edge zones from Section 7.c. Within those boundaries, the correction coefficient k_2 is independent from wall length L.

Wall thickness: To test whether the variability of wall thickness t affects the correction coefficient k_2, a set of verification models was prepared. Wall heights H selected for verification were ranging from 1.0 to 6.0 m with 1.0 m step. Each wall selected for verification was assigned with a thickness different from the default thickness 300 mm. Peak bending moment $M_{3D,max}$ was obtained from the models, and approximated using Equation 24 as well. Both values were then compared, and the error of the approximation evaluated. See summary in Table 7.

wall height H [m]	wall thickness t [mm]	FEM computed peak moment $M_{3D,max}$ [kNm/m]	approximated peak moment $M_{3D,max}$ [kNm/m]	approximation error [%]
1.0	150	9.80	9.72	0.8
2.0	200	9.82	9.77	0.5
3.0	250	9.83	9.80	0.4
4.0	350	9.83	9.81	0.2
5.0	400	9.83	9.83	0.0
6.0	500	9.83	9.84	0.1

Table 7: Verification of correction coefficient sensitivity to wall thickness

Table 7 shows that the approximation error is under 1% for wall with thicknesses t varying from 300 mm, which is acceptable. Therefore, it is concluded that the correction coefficient k_2 is independent from wall thickness t.

Magnitude of load: To test whether load magnitude F affects the correction coefficient k_2, a set of verification models was prepared. Verification models were identical to the original set with the exception of the load force F, which was set from the original value of 20 kN to 160 kN. The peak values of bending moment $M_{3D,max}$ were obtained for the two cases. To be able to compare the results, relative values of the peak bending moment $M_{rel,max,2}$ were expressed according to Equation 21. Table 8 summarises the outcomes for all examined wall heights H and both load forces F.

Wall height H [m]	F = 20 kN		F = 160 kN		error [%]
	$M_{3D,max}$ [kNm/m]	$M_{rel,max,2}$ [-]	$M_{3D,max}$ [kNm/m]	$M_{rel,max,2}$ [-]	
0.6	9.69	0.808	77.55	0.808	0.0
0.8	9.68	0.605	77.47	0.605	0.0
1.0	9.71	0.486	77.64	0.485	0.1
1.2	9.73	0.405	77.83	0.405	0.0
1.4	9.75	0.348	78	0.348	0.0
1.6	9.77	0.305	78.13	0.305	0.0
1.8	9.78	0.272	78.23	0.272	0.0
2.0	9.79	0.245	78.32	0.245	0.0
2.2	9.80	0.223	78.38	0.223	0.0
2.4	9.80	0.204	78.43	0.204	0.0
2.6	9.81	0.189	78.47	0.189	0.0
2.8	9.81	0.175	78.51	0.175	0.0
3.0	9.82	0.164	78.53	0.164	0.0
3.2	9.82	0.153	78.56	0.153	0.0
3.4	9.82	0.144	78.57	0.144	0.0
3.6	9.82	0.136	78.59	0.136	0.0
3.8	9.83	0.129	78.6	0.129	0.1
4.0	9.83	0.123	78.61	0.123	0.0
4.2	9.83	0.117	78.62	0.117	0.0
4.4	9.83	0.112	78.63	0.112	0.0
4.6	9.83	0.107	78.63	0.107	0.0
4.8	9.83	0.102	78.64	0.102	0.0
5.0	9.83	0.098	78.64	0.098	0.0
5.2	9.83	0.095	78.65	0.095	0.0
5.4	9.83	0.091	78.65	0.091	0.0
5.6	9.83	0.088	78.65	0.088	0.0
5.8	9.83	0.085	78.65	0.085	0.0
6.0	9.83	0.082	78.65	0.082	0.0

Table 8: Verification of correction coefficient sensitivity to load magnitude

Table 8 shows that the difference between the values of relative peak bending moment $M_{rel,max,2}$ for loads 20 kN and 160 kN is equal or very close to 0.0% in all cases. The non-zero errors may be explained by the fact that the values obtained from the software are rounded to two decimal places. Since the correction coefficient k_2 is equal to the relative peak bending moment $M_{rel,max,2}$, it is concluded that the correction coefficient k_2 is independent from load magnitude F.

Load distribution: The correction coefficient k_2 was determined specifically for the loads concentrated to one point. Load distribution has major effect on moment distribution and therefore its peak value (as described in Section 7.d.v). Different correction coefficient and design method is proposed for walls subjected to distributed loads, see Section 7.d.v. Correction coefficient k_2 is not applicable in such situations.

Load vertical position: The correction coefficient k_2 was determined specifically for the loads placed at the top wall edge so that the vertical load position h is equal to the wall height H. Cases where the vertical load position h is not equal to the wall height H are analysed in Section 7.d.vi. While the definition of the k_2 coefficient according to Equation 23 still applies for walls with vertical load position h different from the wall height H, it is used differently to obtain the peak bending moment $M_{3D,max}$ and because of that, Equation 24 does not apply. See Section 7.d.vi for details and explanation.

Load horizontal position: The correction coefficient k_2 was determined specifically for the loads placed on infinite walls or in central zones of finite walls. Cases where the loads are placed in the edge zones of finite walls are analysed in Section 7.d.vi. Different correction coefficient and rectification method is proposed for walls subjected to loads placed in the edge zones, see Section 7.d.vi. Correction coefficient k_2 is not applicable in such situations.

Concrete strength: To test whether concrete strength f_c affects the correction coefficient k_2, a set of verification models was prepared. Verification models were identical to the original set with the exception of concrete strength f_c, which was set from the original value of 30 MPa to 50 MPa (by using concrete class C50/60 instead of C30/37). The peak values of bending moment $M_{3D,max}$ were obtained for the two cases. Table 9 summarises the outcomes for all examined wall heights H and both concrete strengths f_c.

wall height H [m]	$M_{3D,max}$ [kNm/m]		error [%]
	C30/37	C50/60	
0.6	9.56	9.55	0.1
0.8	9.58	9.57	0.1
1.0	9.61	9.60	0.1
1.2	9.66	9.65	0.1
1.4	9.69	9.69	0.0
1.6	9.71	9.71	0.0
1.8	9.74	9.73	0.1
2.0	9.75	9.75	0.0
2.2	9.76	9.76	0.0
2.4	9.78	9.77	0.1
2.6	9.78	9.78	0.0
2.8	9.79	9.79	0.0
3.0	9.80	9.79	0.1
3.2	9.80	9.80	0.0
3.4	9.80	9.80	0.0
3.6	9.81	9.80	0.1
3.8	9.81	9.81	0.0
4.0	9.81	9.81	0.0
4.2	9.81	9.81	0.0
4.4	9.82	9.81	0.1
4.6	9.82	9.81	0.1

wall height H [m]	$M_{3D,max}$ [kNm/m]		error [%]
	C30/37	C50/60	
4.8	9.82	9.82	0.0
5.0	9.82	9.82	0.0
5.2	9.82	9.82	0.0
5.4	9.82	9.82	0.0
5.6	9.82	9.82	0.0
5.8	9.82	9.82	0.0
6.0	9.82	9.82	0.0

Table 9: Verification of correction coefficient sensitivity to concrete strength

Table 9 shows that the difference between the values of peak bending moment $M_{3D,max}$ for concrete class C30/37 and C50/60 is equal or very close to 0.0% in all cases. Therefore, it is concluded that the correction coefficient k_2 can be applied to walls of various concrete strength f_c.

Reinforcement: The correction coefficient k_2 was determined specifically for the reinforcement equal in horizontal and vertical direction. Cases where the reinforcement differs in the two directions are analysed in Section 7.d.ix. See Section 7.d.ix for details and explanation.

Wall edge restraints: The correction coefficient k_2 was determined specifically for the loads placed on infinite walls or in central zones of finite walls. Since wall edge restraints affect only edge zones of finite walls, as examined in Section 7.d.x, the correction coefficient k_2 remains applicable in central zones of walls regardless their side edge restraints.

iii. Wall thickness

A set of three-dimensional models was prepared to evaluate the effects of wall thickness. A wall with length of $L = 70$ m was subjected to a load of $F = 20$ kN placed in the centre of the wall horizontally, at the top wall edge vertically. C30/37 concrete class was used. Wall heights H ranged between 1.0 and 6.0 m with 1.0 m step. Wall thickness t ranged between 100 mm and 600 mm with 100 mm step.

The peak bending moment in vertical direction $M_{3D,max}$ was observed for all examined wall heights and thicknesses. The dependence of the peak bending moment on wall thickness is summarised for all wall heights in a graph in Figure 33.

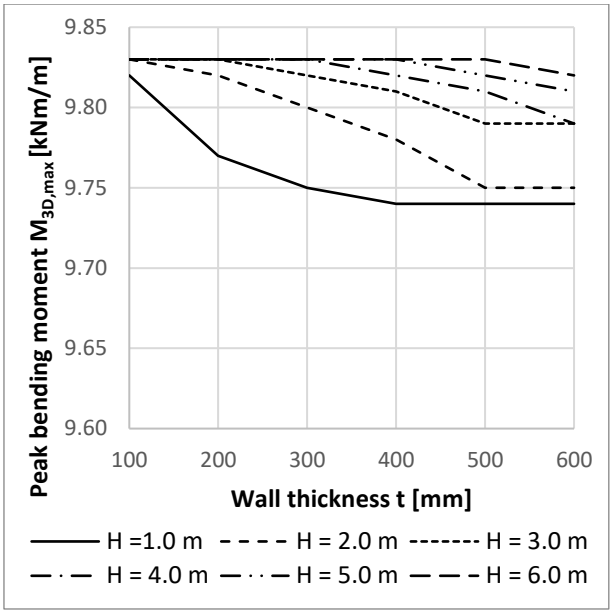

Figure 33: Peak bending moment dependence on wall thickness

The graph in Figure 33 shows that the peak bending moment $M_{3D,max}$ decreases with increasing wall thickness *t* for all wall heights *H*. However, the rate of decrease differs for various wall heights *H*; the decrease is more rapid for shorter walls.

The graph in Figure 33 presents the curves with a clear trend, however, it is important to put the results into perspective by broadening the vertical axis to the full range of values starting from zero bending moment $M_{3D,max}$, see Figure 34.

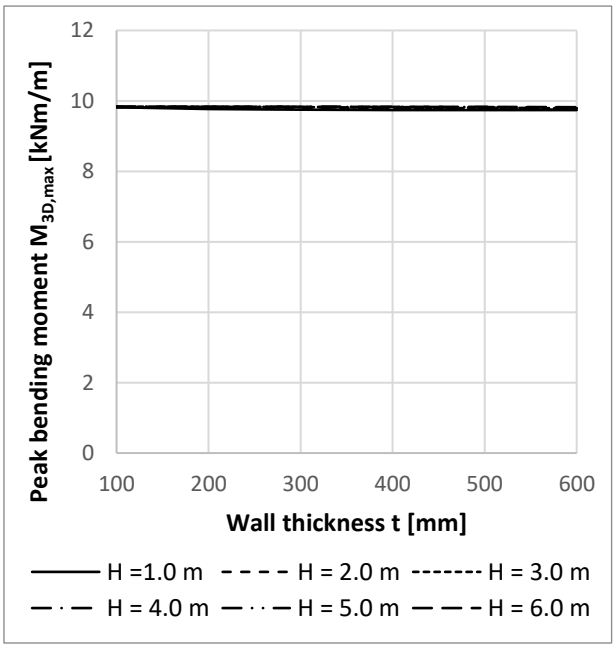

Figure 34: Peak bending moment dependence on wall thickness

Figure 34 shows that, in broader perspective, the bending moment values $M_{3D,max}$ are in fact quasi-constant with increasing wall thickness *t* for all wall heights. For that, it is concluded that there is no need to consider wall thickness as a significant

influence on the peak bending moment. The slight diversions in results may reflect various wall thickness to element size ratio.

All other wall and load parameters examined in this thesis are analysed on a wall with the thickness t = 300 mm. For that reason, the diversion of results for various thicknesses from results of 300 mm thickness is quantified, see Table 10.

wall thickness t [mm]	Diversion [%] in peak bending moment $M_{3D,max}$ from result for wall thickness t = 300 mm					
	H = 1.0 m	H = 2.0 m	H = 3.0 m	H = 4.0 m	H = 5.0 m	H = 6.0 m
100	0.7	0.3	0.1	0.0	0.0	0.0
200	0.2	0.2	0.1	0.0	0.0	0.0
300	0.0	0.0	0.0	0.0	0.0	0.0
400	-0.1	-0.2	-0.1	-0.1	0.0	0.0
500	-0.1	-0.5	-0.3	-0.2	-0.1	0.0
600	-0.1	-0.5	-0.3	-0.4	-0.2	-0.1

Table 10: Diversion in peak bending moment for various wall thicknesses

The values in Table 10 show that the largest diversion applies to short walls and large thicknesses. Contrarily, bending moments of tall thin walls are equal to bending moment of 300 mm thick wall. All the diversions in the examined range of wall heights and thicknesses are below 0.8%. Therefore, it is concluded that wall thickness does not influence the values of resulting bending moment significantly and does not need to be considered as an affecting parameter in the structural analysis.

iv. Magnitude of load

The magnitude of loading force applied on a structure is undoubtedly the major factor influencing the internal forces. In two-dimensional models, the peak bending moment is proportional to the loading force. Equal dependence was assumed to be applicable in three-dimensional modelling, and the assumption was confirmed in Section 7.d.ii. Section 7.d.ii provides comparison of relative bending moment $M_{rel,max,2}$ for a wall loaded in the centre of its top edge with two forces of different magnitude. The results were equal for both loading force values, thus proving that the peak bending moment is independent from load magnitude. The test in Section 7.d.ii was conducted on a wall of infinite length, and the only outcome observed was the peak bending moment value. Section 7.d.ii did not study the effect of load magnitude on the influence length. For that, this Section aims to verify that the relative peak bending moment is independent from the load magnitude even for walls with finite length that is short enough to decrease the influenced length. In other words, it is studied whether load magnitude affects influenced length of the wall.

A set of three-dimensional models was prepared to evaluate the effects of load magnitude. A wall of C30/37 concrete class, with height H = 1 m and thickness t = 300 mm was subjected to a point load F positioned at the top edge in the centre of the wall length. The wall length L ranged between 0.2 m and 10.0 m with 0.2 m step. Three values of load magnitude F were examined: 5 kN, 20 kN, and 160 kN.

The peak bending moment in vertical direction $M_{3D,max}$ was observed for all examined wall lengths L and load magnitudes F. The dependence of peak bending moment $M_{3D,max}$ on wall length L is summarised for all load magnitudes F in a graph in Figure 35.

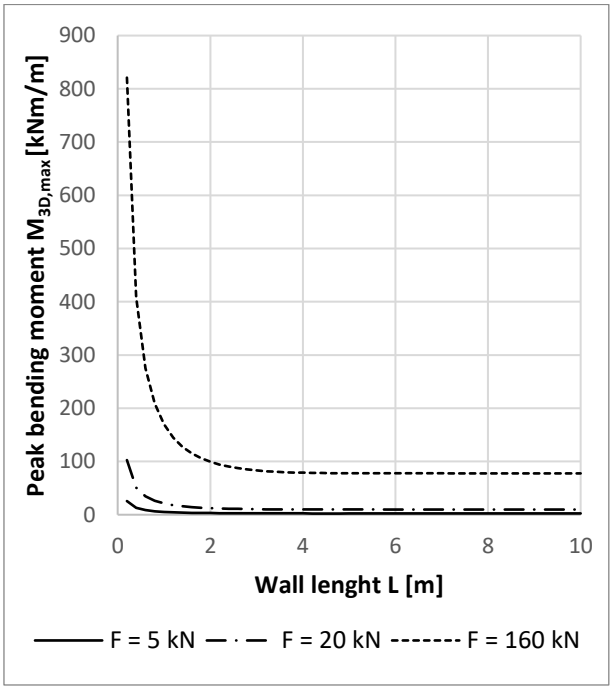

Figure 35: Peak bending moment of various load magnitudes

The values of peak bending moment $M_{3D,max}$ are proportional to the load magnitude F, as it was assumed. Relative peak bending moment $M_{rel,max,2}$ was expressed for more convenient result comparison, see Equation 25 and Figure 36.

$$M_{rel,max,2} = \frac{M_{3D,max}}{M_{2D,max}} \qquad \textit{Equation 25}$$

where $M_{3D,max}$ [kNm/m] is the peak bending moment obtained from a three-dimensional model

$M_{2D,max}$ [kNm/m] is the peak bending moment obtained from a two-dimensional model

The graph in Figure 36 shows that the results are equal for the three load magnitudes F in the whole range of examined wall lengths L. This finding proves that both relative peak bending moment and the influenced length are independent from load magnitude.

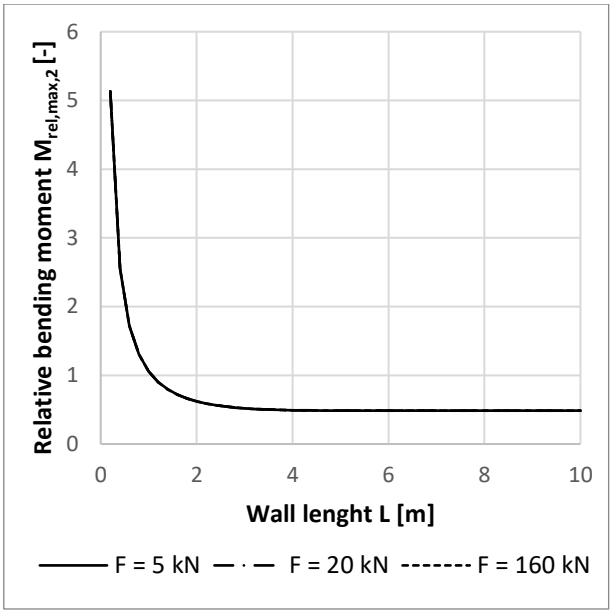

Figure 36: Relative peak bending moments of various load magnitudes

v. Load distribution

Concentrated load is often idealized and modelled as a point load. However, more realistic models consider non-zero area of load application. This section examines structural behaviour of walls subjected to loads distributed over the top wall edge. Such loads were modelled as uniformly distributed linear loads acting on a certain length of the top wall edge.

A set of three-dimensional models was prepared to evaluate the effects of load distribution. A wall with length L = 70 m was subjected to load F =1000 kN placed in the centre of the wall horizontally, at the top wall edge vertically. The wall was modelled with thickness t = 300 mm, C30/37 concrete class was used. Wall heights H ranged between 1 and 4 m with 1 m step. The local x-axis is oriented horizontally, y-axis vertically. The peak value of bending moment $M_{3D,max}$ in vertical direction was evaluated.

The load F was distributed, providing linear loading f applied to the distribution length d, see Table 11 and Figure 37.

The peak bending moment in vertical direction $M_{3D,max}$ was observed for all examined wall heights H and load distributions d. The peak bending moment is situated in the central section of the wall for all cases. The dependence of peak bending moment $M_{3D,max}$ on distribution length d was evaluated for all examined wall heights H, see Table 12. The results are summarised in Figure 38.

Distribution length d [m]	Linear loading f [kN/m]
0	-
0.2	1000/0.2 = 5000
0.5	1000/0.5 = 2000
1	1000/1 = 1000
2	1000/2 = 500
4	1000/4 = 250
8	1000/8 = 125
16	1000/16 = 62.5
20	1000/20 = 50
25	1000/25 = 40

Table 11: Load distribution over the top wall edge

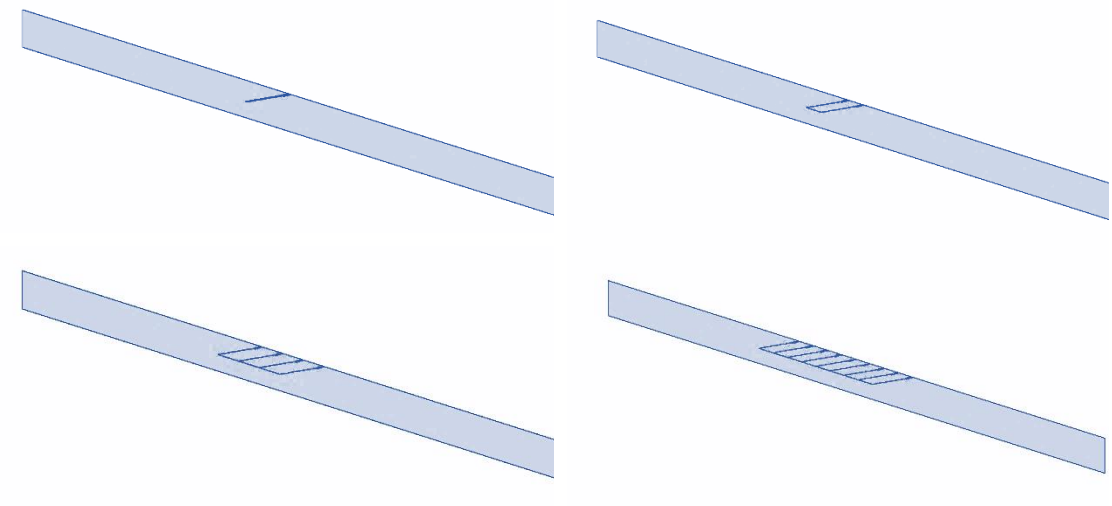

Figure 37: Load distribution over the top wall edge

d [m]	F/d [kN/m]	M_{3D} [kNm/m]			
		H = 1.0 m	H = 2.0 m	H = 3.0 m	H = 4.0 m
0	-	487.43	490.18	491.18	491.52
0.2	5000	484.96	489.52	490.87	491.35
0.5	2000	476.6	487.23	489.83	490.75
1	1000	449.66	479.31	486.13	488.63
2	500	372.54	450.89	472.12	480.41
4	250	239.83	371.12	425.67	451.08
8	125	124.97	238.23	318.39	369.98
16	62.5	62.52	124.84	184.51	237.38
20	50	50.01	99.99	149.23	195.61
25	40	40.01	80.01	119.85	158.75

Table 12: Peak bending moments for various load distribution lengths

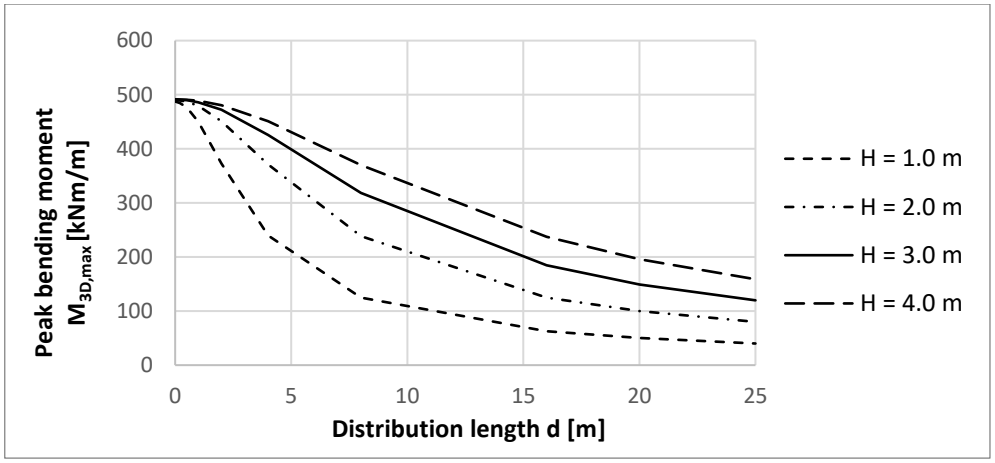

Figure 38: Peak bending moment dependence on load distribution length

For more convenient processing of the data, relative bending moment $M_{rel,max,5}$ was introduced, see Equation 26. The relative bending moment $M_{rel,max,5}$ relates the bending moment values from load acting distribution length d to the bending moment value from a point load.

$$M_{rel,max,5} = M_{3D,max}/M_{3D,max.F} \qquad \textit{Equation 26}$$

where $M_{3D,max}$ [kNm/m] is the peak value corresponding to load applied on distribution length d

$M_{3D,max,F}$ [kNm/m] is the peak value corresponding to load concentrated into a point

Relative bending moment values $M_{rel,max,5}$ are summarised in Table 13 and Figure 39.

d [m]	$M_{rel.max,5}$ [kNm/m]			
	H = 1.0 m	H = 2.0 m	H = 3.0 m	H = 4.0 m
0	1.000	1.000	1.000	1.000
0.2	0.995	0.999	0.999	1.000
0.5	0.978	0.994	0.997	0.998
1	0.923	0.978	0.990	0.994
2	0.764	0.920	0.961	0.977
4	0.492	0.757	0.867	0.918
8	0.256	0.486	0.648	0.753
16	0.128	0.255	0.376	0.483
20	0.103	0.204	0.304	0.398
25	0.082	0.163	0.244	0.323

Table 13: Relative bending moments for various load distribution lengths

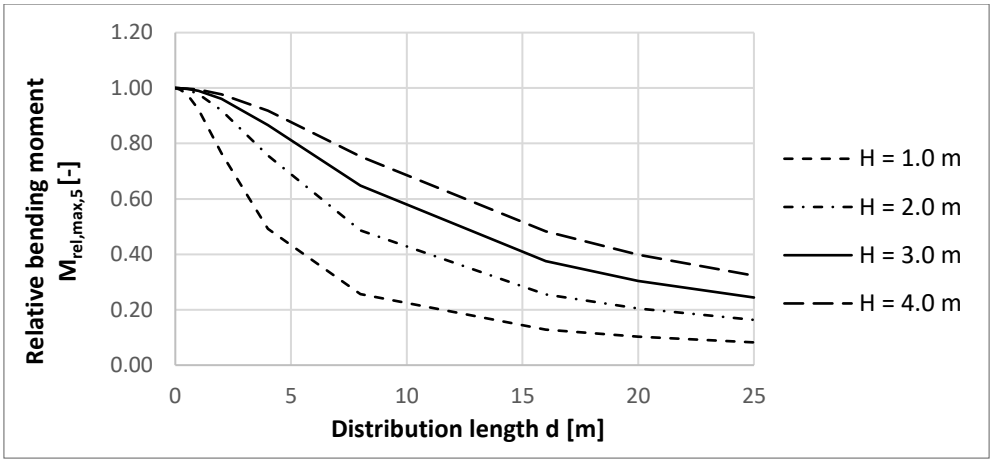

Figure 39: Relative bending moment dependence on load distribution length

The curves in the graph of Figure 38 show that the maximum bending moment $M_{3D,max}$ is reached for the load concentrated to a point. This maximum bending moment was set as a reference moment for the relative values, therefore, the relative bending moment value $M_{rel,max,5}$ is equal to 1.00 for all inspected wall heights H. With increasing distribution length d, the peak bending moment $M_{3D,max}$ and the relative bending moment $M_{rel,,max,5}$ decrease.

The dependence of relative bending moment $M_{rel,max,5}$ on distribution length d cannot be expressed analytically, as the curves describing the trend would be variable of too many parameters that cannot be determined based on provided inputs. However, the dependence can be reliably approximated. Following part of this Section presents the approximation.

The principle of approximation of the dependence of relative bending moment $M_{rel,max,5}$ on distribution length d lies in discretization of the uniformly distributed load F/d into a series of point loads f acting on division element size Δd and summarizing their effects, see Figure 40. The number of division elements is n, see Equation 27.

$$n = d/\Delta d \qquad \textit{Equation 27}$$

where d [m] is the load distribution length
Δd [m] the size of division element

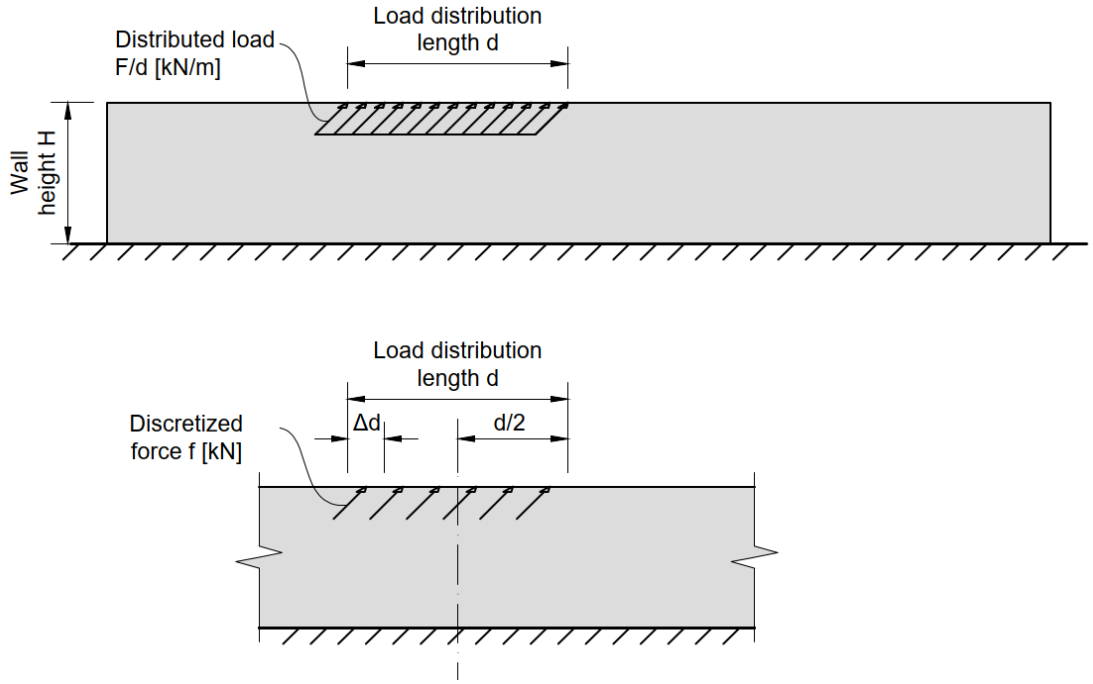

Figure 40: Discretization of uniformly distributed load

The individual effect of each discretized force f can be evaluated as it is proposed in Section 7.b. In general, the course of vertical bending moment over bottom wall edge from a single point load acting on a wall can be approximated by a bell curve that is commonly used as a distribution function, as it explained in Section 7.b, see Figure 41. The bell curve is described with Gauss function $g(x)$, see Equation 28.

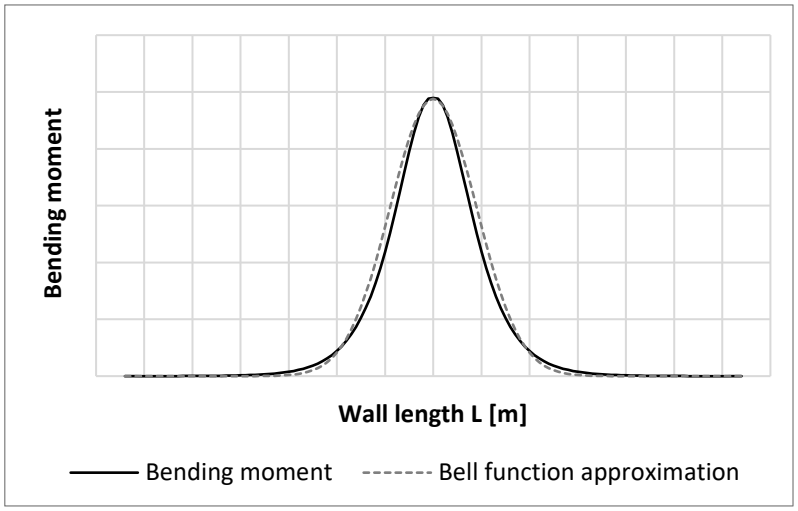

Figure 41: Bell function approximation of bending moment course

$$g(x) = ae^{\frac{-(x-\mu)^2}{2\sigma^2}}$$ *Equation 28*

where a [-] is the peak of the bell curve
x [m] is the variable
μ [m] is the shift of the bell curve peak from x = 0
σ [-] is the standard deviation

For the specific case of a wall subjected to a single point load, the parameters of the curve can be described according to Table 14.

Note: The symbols used as function parameters in Equation 28 and Table 14 are commonly used for their description and are excluded from the list of symbols of this dissertation. Some of the symbols used in this table are used elsewhere in this dissertation while describing a different quality.

parameter	description
a	peak value of a three-dimensional bending moment $M_{3D,f}$ from discretized load f
x	horizontal position on the bottom wall edge
μ	horizontal shift of the peak bending moment to the loading force; $\mu = 0$ in all cases as the peak bending moment is always positioned at the same horizontal position as is the point load
σ	decrease rate of the bending moment with increasing horizontal position x; described in Section 7.b $\sigma = 0.843H + 0.056$

Table 14: Bell curve parameters

The bending moment $m_f(x)$ caused by one individual discretized load f is then determined by applying the parameters from Table 14 on Equation 28, see Equation 29, Equation 30, Equation 31 and Equation 32.

$$m_f(x) = M_{3D,f} * e^{\frac{-(x)^2}{2(0.843H+0.056)^2}} \qquad \textit{Equation 29}$$

$$m_f(x) = k_2 M_{2D,f} * e^{\frac{-(x)^2}{2(0.843H+0.056)^2}} \qquad \textit{Equation 30}$$

$$m_f(x) = (0.486H^{-0.993})fH * e^{\frac{-(x)^2}{2(0.843H+0.056)^2}} \qquad \textit{Equation 31}$$

$$m_f(x) = \frac{(0.486H^{-0.993})FH}{d} * e^{\frac{-(x)^2}{2(0.843H+0.056)^2}} \qquad \textit{Equation 32}$$

where
- H [m] is the wall height
- F [kN] is the total load that is distributed into length d
- f [kN] is the discretized load acting on distance Δd; $f = F/n$
- $M_{3D,f}$ [kNm/m] is the peak value of a three-dimensional bending moment from discretized load f, can be obtained as $k_2 M_{2D,f}$; correction coefficient k_2 described in Section 7.d.ii as $k_2 = 0.486H^{-0.993}$
- $M_{2D,f}$ [kNm/m] is the two-dimensional peak bending moment from the discretized load f; $M_{2D,f} = fH$

The effects of all discretized loads *f* need to be summarised at the centre of load distribution length *d* to obtain the peak bending moment $M_{3D,max}$. Each individual discretized force *f* is in a different position to the centre equal to *x*, see Figure 42. Provided that the number of division elements *n* is an even number, the first (smallest) and the last (largest) value of *x* (x_1, x_n, respectively) is given by Equation 33 and Equation 34.

$$x_1 = \frac{\Delta d}{2} \qquad \textit{Equation 33}$$

$$x_n = \frac{d}{2} - \frac{\Delta d}{2} \qquad \textit{Equation 34}$$

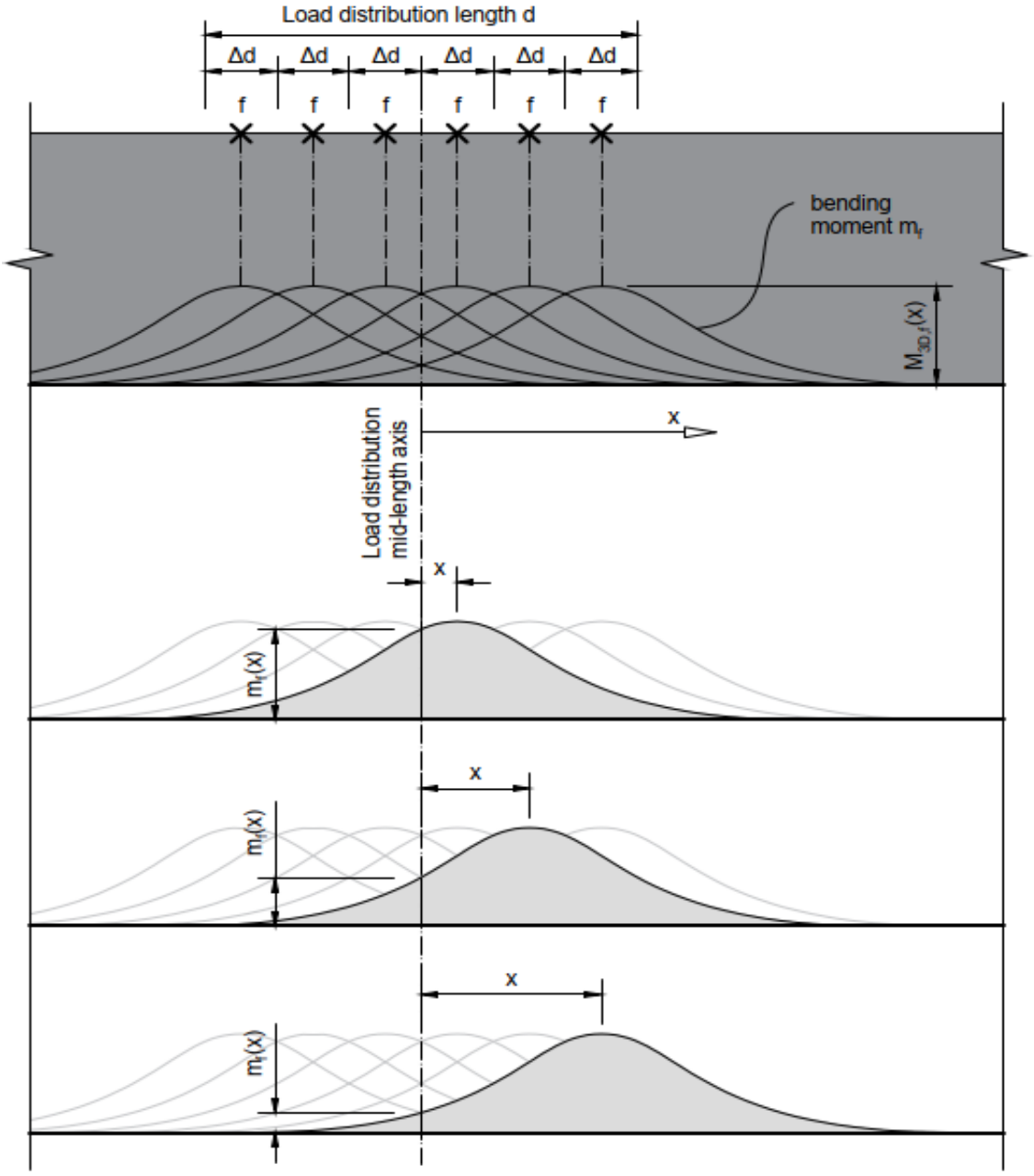

Figure 42: Bending moment effect from individual discretized forces

Using Equation 32, the contribution $m_f(x)$ of all discretized loads *f* to the bending moment $M_{3D,max}$ is determined. Finally, they are summarised to obtain the peak bending moment $M_{3D,max}$ at the centre of load distribution length, see Equation 35 and Equation 36. Due to the symmetry of the bell curve, only a half of the load distribution length needs to be evaluated, provided that the resulting bending moment is doubled.

$$M_{3D,max} = 2\sum_{x_1}^{x_n} m_f(x) \qquad \textit{Equation 35}$$

$$M_{3D,max} = 2\sum_{\Delta d/2}^{\frac{d}{2}-\Delta d/2} \frac{(0.486H^{-0,993})FH}{d} * e^{\frac{-(x)^2}{2(0.843H+0,056)^2}} \qquad \textit{Equation 36}$$

Equation 36 is to be used for determining the peak bending moment on cantilever walls subjected to a load distributed to a certain length along the top wall edge. The equation is applicable to cases where the load is applied outside edge wall zones (defined in Section 7.c), i.e. not in proximity of the wall side edge. Since the equation is based on an approximation of moment distribution curve, and the method uses discretization of a continuous problem, the equation does not provide exact analytical results, and therefore, the error rising from its use needs to be evaluated. For that, a comparison with FEM calculation is provided.

Table 15 summarises the error given by the difference of the approximation from FEM results as a percentage related to FEM result. The error exceeds 5% margin for larger load distribution lengths. The error is more significant for shorter walls. While the error seems to be too large in some of the cases presented in the table, in practice, the concentrated loads are rarely distributed into lengths *d* larger than 1.5 m, as this is a recommended distribution length for many design scenarios stated in (EN 1991-1-7, 2006). The error for distribution lengths *d* smaller than 1.5 m, the errors are acceptable.

d [m]	error in peak bending moment $M_{3D,max}$			
	H = 1.0 m	H = 2.0 m	H = 3.0 m	H = 4.0 m
0	0.29%	0.37%	0.29%	0.16%
0.2	0.01%	0.29%	0.25%	0.14%
0.5	0.67%	0.11%	0.17%	0.09%
1	2.76%	0.51%	0.12%	0.08%
2	7.89%	2.65%	1.21%	0.72%
4	11.18%	7.61%	4.54%	2.92%
8	9.55%	9.47%	9.42%	7.81%
16	9.48%	6.76%	7.28%	8.85%
20	9.50%	6.63%	6.31%	7.41%
25	9.50%	6.61%	5.92%	6.22%

Table 15: Error in peak bending moment

The error was plotted into the graph in Figure 43. The graph shows that all the approximated values of bending moments are larger than the values provided by

FEM analysis. For that, the error is on the safe side and can be accepted in practical use without any safety concerns.

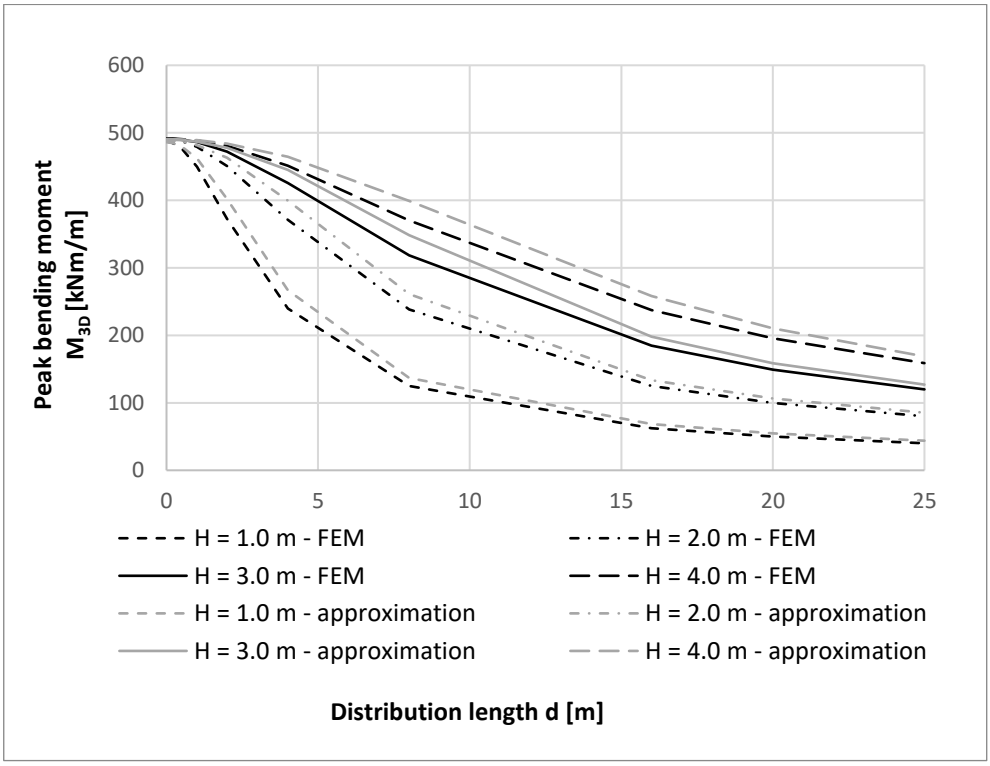

Figure 43: Approximation error of load distribution effects on peak bending moment

A correction coefficient k_5 is introduced to express the relationship between the results of two- and three-dimensional modelling, see Equation 39. The correction coefficient k_5 is to be applied on the maximum value of bending moment obtained from a two-dimensional model $M_{2D,max}$ to obtain value that would have been obtained from a three-dimensional model. The value of the correction coefficient k_5 is determined from the ratio of results on three- and two-dimensional models, see Equation 37 and Equation 38.

$$M_{2D,max} = FH \qquad \textit{Equation 37}$$

$$\frac{M_{3D,max}}{M_{2D,max}} = (2\sum_{\frac{\Delta d}{2}}^{\frac{d}{2}-\frac{\Delta d}{2}} \frac{(0{,}486H^{-0{,}993})FH}{d} * e^{\frac{-(x)^2}{2(0.843H+0{,}056)^2}})/(FH) \qquad \textit{Equation 38}$$

$$k_5 = \frac{M_{3D,max}}{M_{2D,max}} = 2\sum_{\frac{\Delta d}{2}}^{\frac{d}{2}-\frac{\Delta d}{2}} \frac{(0{,}486H^{-0{,}993})}{d} * e^{\frac{-(x)^2}{2(0.843H+0{,}056)^2}} \qquad \textit{Equation 39}$$

vi. Vertical load position

All other parameters of the wall and load investigated in subsections of Section 7.d were examined on the case of wall subjected to the loading placed at its top edge, making vertical position of the load *h* equal to the wall height *H*. This Section analyses the effects of the vertical load position *h* smaller than the wall height *H*.

Since the bending moment strongly depends on lever arm of the load, it is assumed, that increasing vertical load position *h* will bring increase in the peak bending moment $M_{3D,max}$ even though the height of the wall *H* remains constant. This increase is linear when a two-dimensional model is used, as no other parameter than load force *F* and vertical load position *h* affect the value of $M_{2D,max}$, see Equation 40. However, three-dimensional models lack the linearity, as the internal forces can distribute in the horizontal direction, and so other parameters enter the solution of the problem.

$$M_{2D,max} = Fh \qquad \textit{Equation 40}$$

where F [kN] is the point load force
h [m] is the vertical load position

A set of three-dimensional models was prepared to evaluate the effects of vertical load position in the central zone of a wall. A wall with the length L = 70 m was modelled with the thickness t = 300 mm, C30/37 concrete class was used. The point load F = 1000 kN was placed in the middle of wall length. The wall height *H* was fixed at 3.0 m. Vertical load position h varied from 0.0 m to 3.0 m with 0.2 m step.

The peak bending moment in vertical direction $M_{3D,max}$ was observed. The dependence of peak bending moment $M_{3D,max}$ on vertical load position *h* is summarised in a graph in Figure 44.

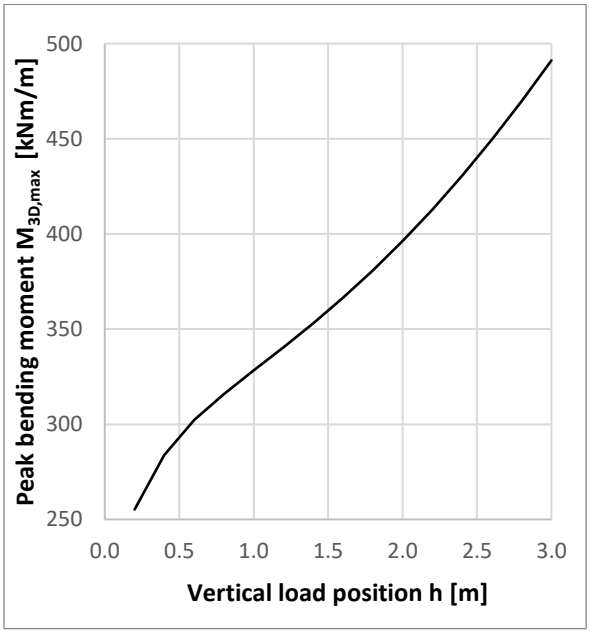

Figure 44: Dependence of peak bending moment on vertical load position

The graph in Figure 44 confirms the assumption, that increasing vertical load position h increases the peak bending moment $M_{3D,max}$ even though wall height H remains constant.

When a two-dimensional model is used, the free height of the wall h' (height of the wall above the load) does not affect the value of the peak bending moment $M_{2D,max}$. To investigate if this principle also applies to three-dimensional models, a graph of peak bending moment $M_{3D,max}$ dependence on the vertical load position h is presented in Figure 45.

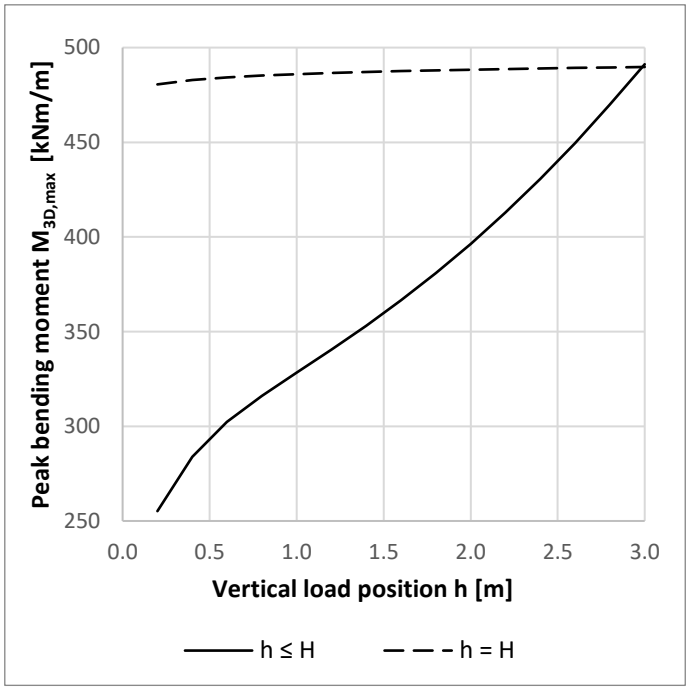

Figure 45: Dependence of peak bending moment on vertical load position

The graph in Figure 45 compares two curves. The first curve is taken from the graph in Figure 44 and corresponds to the situation where the wall height H is fixed at 3.0 m and vertical load position h is variable ($h \leq H$). The free height h' of the wall decreases with increasing vertical load position h. The second curve corresponds to the situation where the wall height H is equal to the vertical load position h ($h = H$), therefore, the free height h' is zero for all cases.

The two curves in Figure 45 differ, thus proving that, unlike in two-dimensional models, the presence of free height of the wall affects the results of three-dimensional models. The peak bending moments $M_{3D,max}$ on the wall with non-zero free height ($h < H$) are smaller than the ones on the wall with zero free length ($h = H$). The gap between the two curves decreases as the vertical load position h reaches wall height H, until the curves meet at $h = H$. The gap between the two curves demonstrates how the free height of the wall causes decrease in peak bending moment. The effect of free wall height is especially remarkable when the load is placed far below the wall top.

Figure 46 explains the free height effect. The figure presents the map of bending moment distribution in the area around the load. Free height of the wall provides additional area for the bending moment to distribute - there are visible non-zero

moments in the area above the level of the load. Such distribution causes decrease in the peak value as the moment is less concentrated. Figure 47 confirms this statement by showing non-zero values of bending moment in vertical section of the panel at the position next to the loading force.

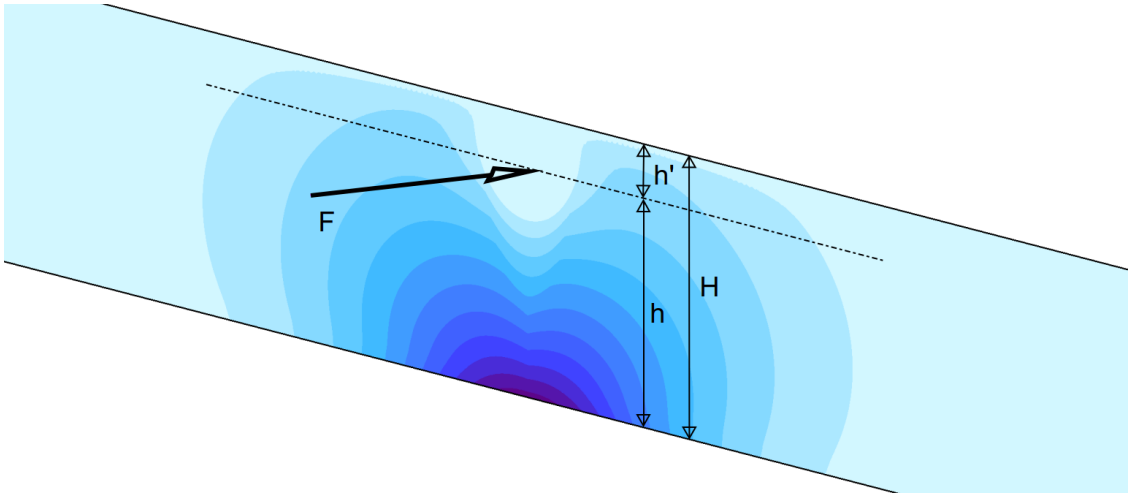

Figure 46: Map of bending moment distribution

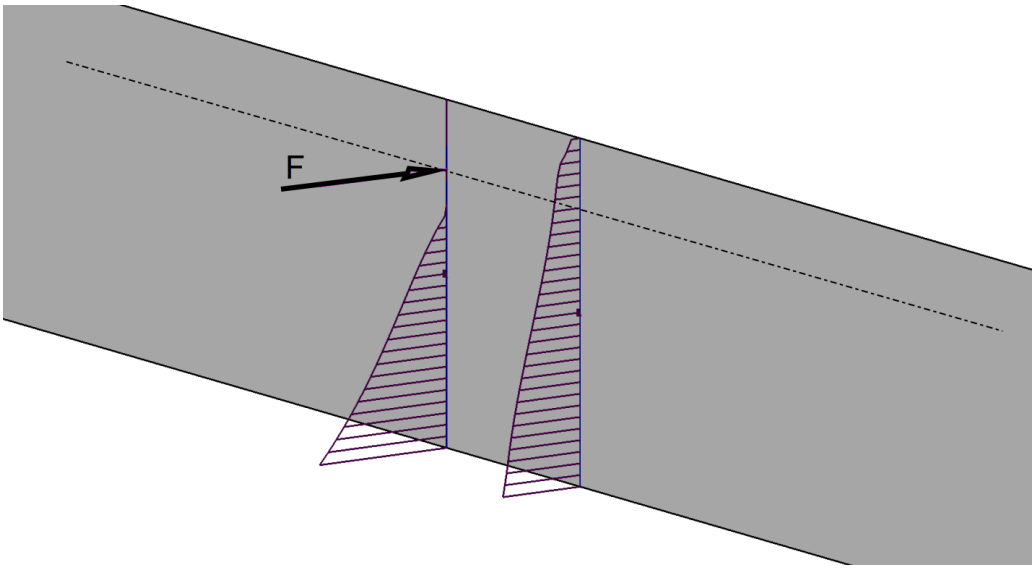

Figure 47: Bending moment distribution over vertical wall cuts

Since the effect of free wall heigh is not reflected in the results obtained from two-dimensional models, it is concluded that two-dimensional simplification of the problem brings severe inaccuracies in the results.

To evaluate the difference between results of three- and two-dimensional modelling, relative peak bending moment $M_{rel,max,6}$ is introduced, see Equation 41. Relative peak bending moment $M_{rel,max,6}$ is defined as a ratio of peak bending moment on a wall with free height above the load to peak bending moment on a wall with neglected free height, see Figure 48 for illustration.

$$M_{rel,max,6} = \frac{M_{3D,max}(h \leq H)}{M_{3D,max}(h = H)}$$ *Equation 41*

where $M_{3D,max}(h \leq H)$ [kNm/m] is the peak bending moment on wall with vertical load position smaller than or equal to wall height

$M_{3D,max}(h \leq H)$ [kNm/m] is the peak bending moment on wall with vertical load position equal to wall height

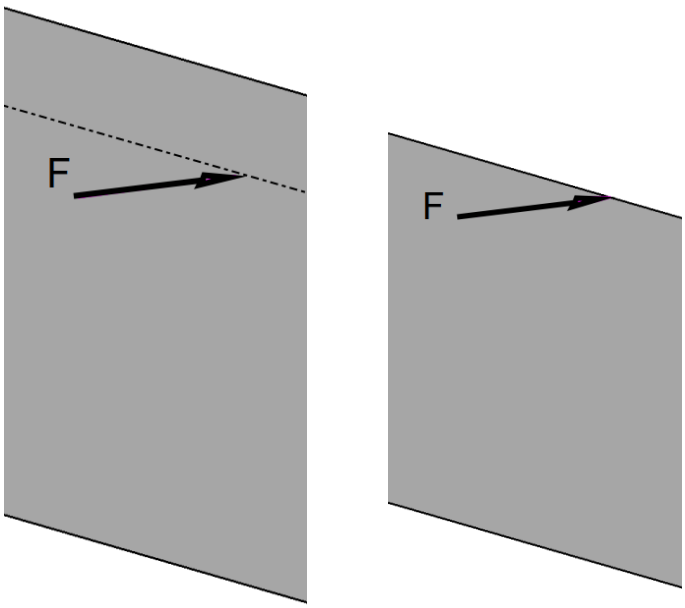

Figure 48: Wall with non-zero free height (left) and neglected free height (right)

The dependence of relative peak bending moment $M_{rel,max,6}$ on relative vertical load position h/H is plotted in Figure 49.

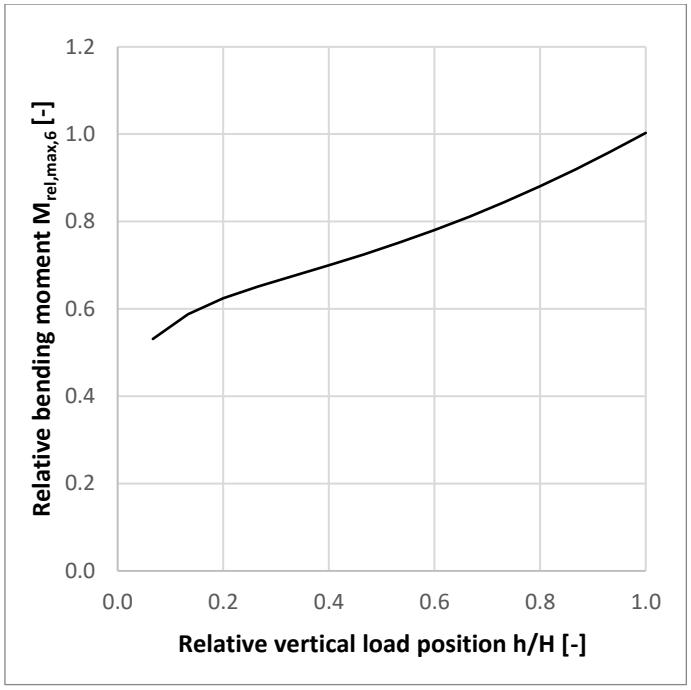

Figure 49: Dependence of relative peak bending moment on relative vertical load position

The curve of the graph in Figure 49 can be devided into a concave and a covex part in its inflection point placed at the relative vertical load positon $h/H = 0.33$. Both parts of the curve are described separately, see Figure 50 and Figure 51.

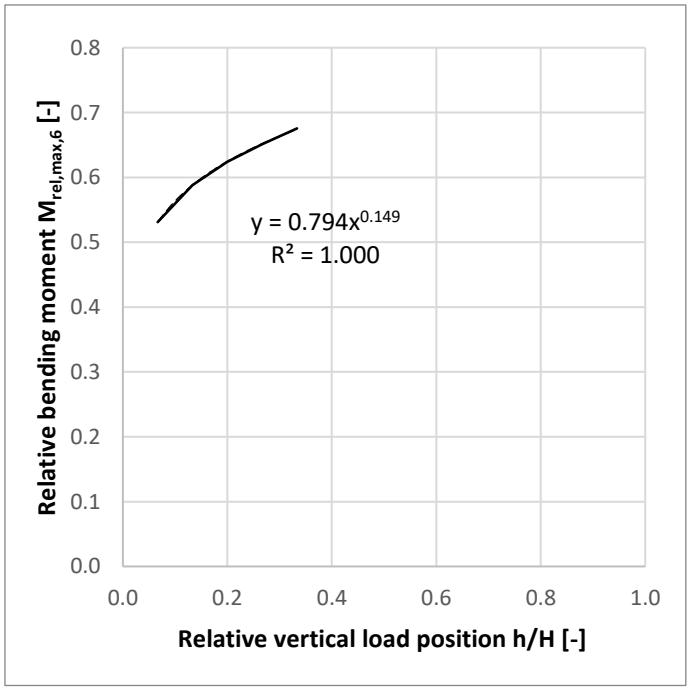

Figure 50: Dependence of relative peak bending moment on relative vertical load position for $h/H \leq 0.33$

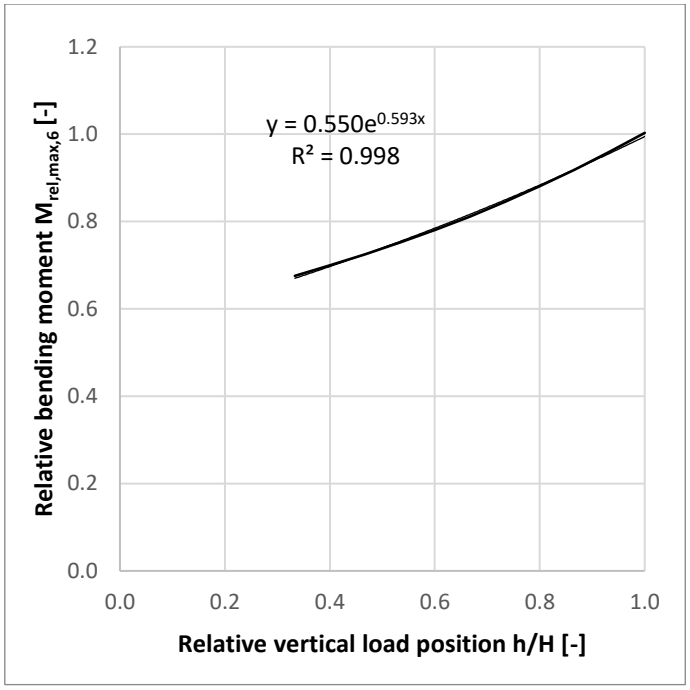

Figure 51: The dependence of relative peak bending moment on relative vertical load position for h/H ≥ 0.33

A trendline was found for both parts of the curve, see Equation 42 andEquation 43 applicable for $h/H \leq 0.33$, and Equation 44 andEquation 45 applicable for $h/H \geq 0.33$. Both trendlines approximate the data satisfactorily as their determination coefficients R^2 are equal to 1.000 and 0.998. The relative peak bending moment $M_{rel,max,6}$ defines the correction coefficient k_6 which compensates neglection of the free wall height.

$$y = 0.794x^{0.149} \qquad \textit{Equation 42}$$

$$k_6 = M_{rel,max,6} = 0.794(\frac{h}{H})^{0.149} \qquad \textit{Equation 43}$$

$$y = 0.550e^{0.593x} \qquad \textit{Equation 44}$$

$$k_6 = M_{rel,max,6} = 0.550e^{0.593(\frac{h}{H})} \qquad \textit{Equation 45}$$

where h/H [m] is the relative vertical load position

The correction coefficient k_6 can be used to determine the peak bending moment $M_{3D,max}$ on a wall with free height above the load using results on equal wall with neglected free height, see Equation 46.

$$M_{3D,max}(h \leq H) = k_6 * M_{3D,max}(h = H) \quad \textit{Equation 46}$$

Since the peak bending moment $M_{3D,max}$ for wall with neglected free height can be approximated using correction coefficient k_2 and two-dimensional peak bending moment $M_{2D,max}$ according to Section 7.d.ii, the equation can be extended to Equation 47,Equation 48 andEquation 49, while Equation 48 applies to $h/H \leq 0.33$ and Equation 49 applies to $h/H \geq 0.33$.

$$M_{3D,max}(h \leq H) = k_6 * k_2 * M_{2D,max} \quad \textit{Equation 47}$$

$$M_{3D,max}(h \leq H) = 0.794(\frac{h}{H})^{0.149} * 0.486h^{-0.993} * Fh \quad \textit{Equation 48}$$

$$M_{3D,max}(h \leq H) = 0.550e^{0.593(\frac{h}{H})} * 0.486h^{-0.993} * Fh \quad \textit{Equation 49}$$

The equations can be used for arbitrary vertical load position h up to the value of wall height H, including the vertical load position h equal to wall height H. For that, the formal expression of the equations can be simplified to Equation 50 applicable to $h/H \leq 0.33$ and Equation 51 applicable to $h/H \geq 0.33$.

$$M_{3D,max} = 0.794(\frac{h}{H})^{0.149} * 0.486h^{-0.993} * Fh \quad \textit{Equation 50}$$

$$M_{3D,max} = 0.550e^{0.593(\frac{h}{H})} * 0.486h^{-0.993} * Fh \quad \textit{Equation 51}$$

The equations above were derived from result of a wall with the height H = 3.0 m. To verify if the equations are applicable for walls of various heights H, a set of verification models was prepared. Table 16 presents wall heights H and vertical load positions h used for the verification. Verification was conducted for the load force F = 1000 kN. All combinations of wall height H and vertical load position h presented in the table were analysed using FEM, obtaining peak bending moment $M_{3D,max}$. Then the peak bending moments $M_{3D,max}$ were approximated using Equation 50 andEquation 51. Both FEM results and approximation are presented in Table 16 and are plotted in Figure 52.

h [m]	H [m]	h/H [-]	$M_{3D,max}$ [kNm/m] - FEM	$M_{3D,max}$ [kNm/m] - approximation	error [%]
3.00	3.00	1.00	491.18	487.39	0.8
3.00	4.50	0.67	398.15	399.97	0.5
2.00	2.00	1.00	490.18	486.01	0.9
2.00	3.50	0.57	375.73	376.94	0.3
1.00	1.00	1.00	487.43	483.65	0.8
1.00	2.50	0.40	337.63	338.85	0.4
4.00	4.00	1.00	491.52	488.37	0.6
1.00	4.00	0.25	318.72	313.87	1.5
2.00	4.00	0.50	362.13	361.31	0.2
5.00	5.00	1.00	491.64	489.13	0.5
1.00	5.00	0.20	314.13	303.61	3.4
2.50	5.00	0.50	363.41	361.87	0.4
6.00	6.00	1.00	491.68	489.76	0.4
1.00	6.00	0.17	311.58	295.47	5.2
3.00	6.00	0.50	364.16	362.33	0.5
0.90	5.00	0.18	310.54	298.66	3.8
1.08	6.00	0.18	313.86	299.04	4.7

Table 16: Verification of k_6 correction coefficient applicability

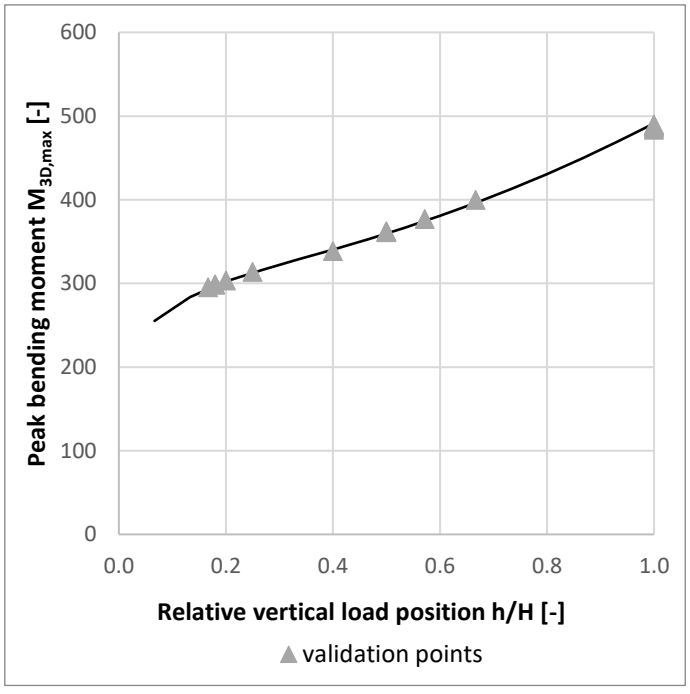

Figure 52: Verification of k_6 correction coefficient applicability

Good agreement of the FEM results and approximation was achieved. The error of the approximation is presented in Table 16. For higher values of relative vertical load position *h/H* the error is satisfactory, under 1.0%. It was established that

maximum error accepted is 5%. According to results of the verification, the margin for this error is $h/H = 0.18$. For relative vertical load positions h/H smaller than 0.18, the equations may give inaccurate results, and therefore, it is recommended to use Equation 50 andEquation 51 only for relative vertical load positions h/H larger than or equal to 0.18.

Equation 50 andEquation 51 are applicable to the walls with loads placed in their central zone. Equivalent approach was taken to determine peak bending moments $M_{3D,max}$ for walls subjected to loads in their edge zone.

A set of three-dimensional models was prepared to evaluate the effects of vertical load position in the edge zone of a wall. A wall with the length L = 70 m was modelled with the thickness t = 300 mm, C30/37 concrete class was used. The point load F = 1000 kN was placed at the side end of the wall. The wall height H was fixed at 3.0 m. Vertical load position h varied from 0.0 m to 3.0 m with 0.2 m step.

The peak bending moment in vertical direction $M_{3D,max}$ was observed. The dependence of peak bending moment $M_{3D,max}$ on vertical load position is summarised in a graph in Figure 53.

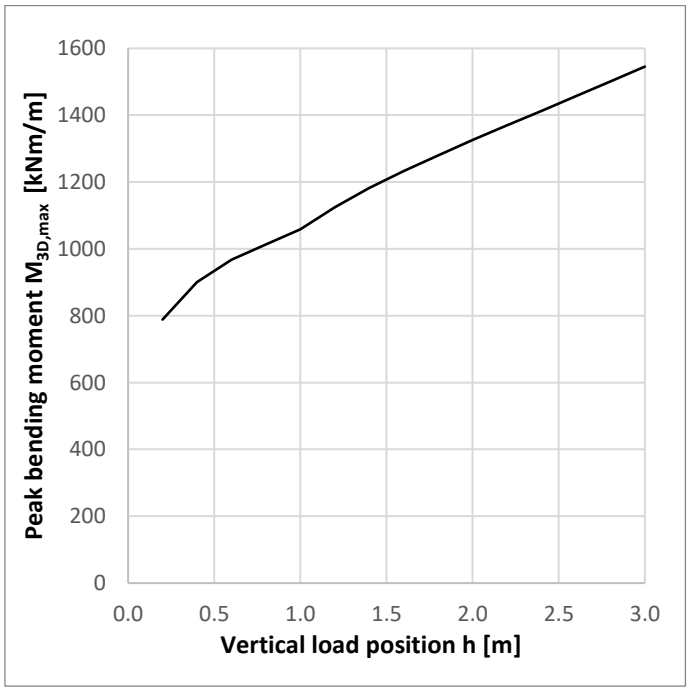

Figure 53: Dependence of peak bending moment on vertical load position

The dependence of relative peak bending moment $M_{rel,max,6}$ on relative vertical load position h/H was determined using equal approach like in case of central zone load position; the outcome is plotted in Figure 54.

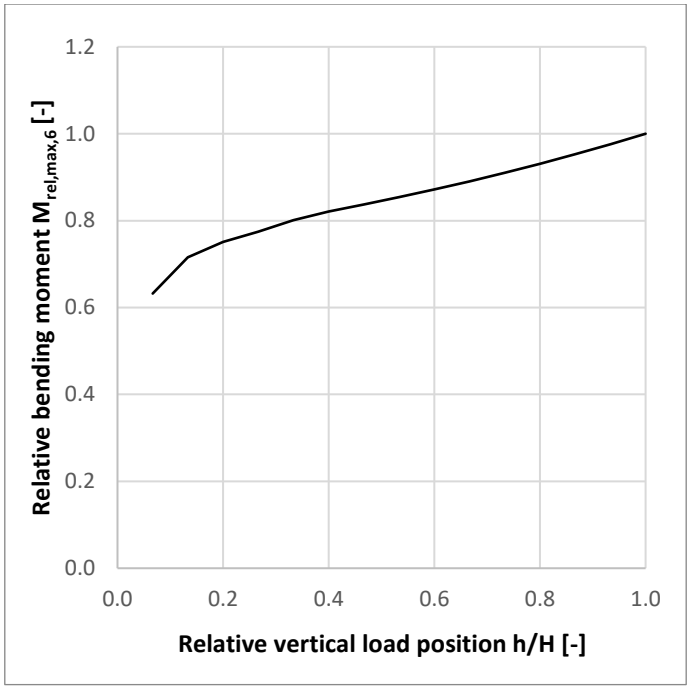

Figure 54: Dependence of relative peak bending moment on relative vertical load position

To analytically describe the curve of Figure 54, it was split into two intervals divided at the point of relative vertical load position h/H = 0.33. Both parts of the curve along with their trendline are presented in Figure 55 andFigure 56. Both trendlines approximate the data satisfactorily as their determination coefficients R^2 are equal to 0.989 and 0.999.

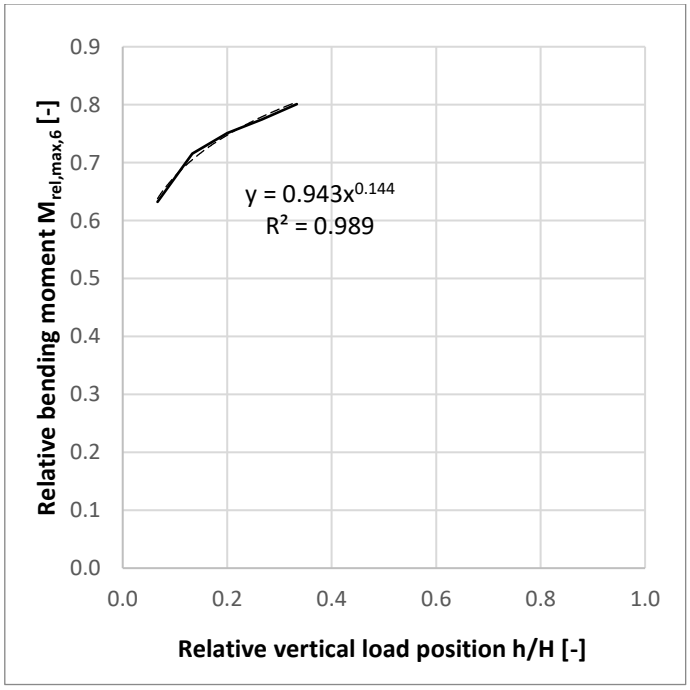

Figure 55: Dependence of relative peak bending moment on relative vertical load position

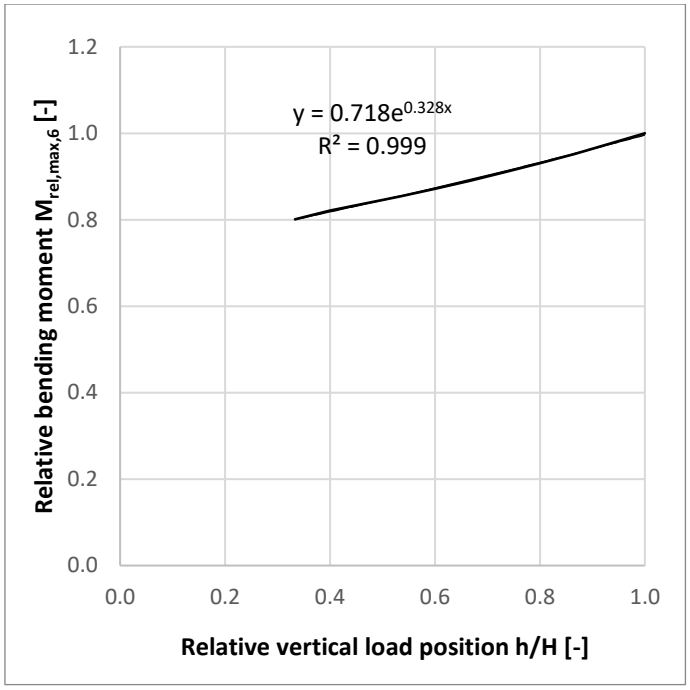

Figure 56: Dependence of relative peak bending moment on relative vertical load position

See Equation 52 and Equation 53 applicable for $h/H \leq 0.33$ and Equation 54 and Equation 55 applicable for $h/H \geq 0.33$ for the trendline functions and their application to express the relative peak bending moment $M_{rel,max,6}$. The relative peak bending moment $M_{rel,max,6}$ defines correction coefficient k_6 which compensates neglection of the free wall height.

$$y = 0.943x^{0.144} \qquad \textit{Equation 52}$$

$$k_6 = M_{rel,max,6} = 0.943(\frac{h}{H})^{0.144} \qquad \textit{Equation 53}$$

$$y = 0.718e^{0.328x} \qquad \textit{Equation 54}$$

$$k_6 = M_{rel,max,6} = 0.718e^{0.328(\frac{h}{H})} \qquad \textit{Equation 55}$$

Correction coefficient k_6 can be used to determine peak bending moment on a wall with free height above the load using results on equal wall with neglected free height, see Equation 56.

$$M_{3D,max}(h \leq H) = k_6 * M_{3D,max}(h = H) \qquad \textit{Equation 56}$$

Since the peak bending moment for a wall with neglected free height can be approximated using correction coefficient k_7 and two-dimensional peak bending moment $M_{2D,max}$ according to Section 7.d.vii, the equation can be extended to Equation 57, Equation 58 andEquation 59, while Equation 57 applies to $h/H \leq 0.33$ and Equation 59 applies to $h/H \geq 0.33$.

$$M_{3D,max}(h \leq H) = k_6 * k_7 * M_{2D,max} \qquad \textit{Equation 57}$$

$$M_{3D,max}(h \leq H) = 0.943(\frac{h}{H})^{0.144} * 1.364h^{-0.898} * Fh \qquad \textit{Equation 58}$$

$$M_{3D,max}(h \leq H) = 0.718e^{0.328(\frac{h}{H})} * 1.364h^{-0.898} * Fh \qquad \textit{Equation 59}$$

The equations can be used for arbitrary vertical load position h up to the value of wall height H, including the vertical load position h equal to wall height H. For that, the formal expression of the equations can be simplified to Equation 60 applicable to $h/H \leq 0.33$ and Equation 61 applicable to $h/H \geq 0.33$.

$$M_{3D,max} = 0.943(\frac{h}{H})^{0.144} * 1.364h^{-0.898} * Fh \qquad \textit{Equation 60}$$

$$M_{3D,max} = 0.718e^{0.328(\frac{h}{H})} * 1.364h^{-0.898} * Fh \qquad \textit{Equation 61}$$

Equation 60 and Equation 61 are applicable to the walls with loads placed in at their side edge. Conservatively, they can be applied to the whole edge zone of the wall. Less conservative, but still safe approach is to assume linear transition of the peak bending moment value in the edge zone between the extreme value from the load placed at the very end of the wall and the value from the load placed in the central zone. For more details on this approach, see Section 7.d.vii where this principle is used and presented.

vii. Horizontal load position

Horizontal position of the load on the top edge of the wall does not affect the peak bending moment in case of infinitely long walls. However, side ends of finite walls cause irregularities when the load is placed near them. According to definitions from Section 7.c.iii, an edge zone is the area where the presence of a side wall end affects the value of bending moments. This section quantifies the peak bending moments of loads placed in edge zones.

A set of three-dimensional models was prepared to evaluate the effects of horizontal load position. A wall with the length L = 70 m was modelled with the thickness t = 300 mm, C30/37 concrete class was used. Wall heights H ranged between 1.0 and 5.0 m with 1.0 m step. The wall was subjected to the load F = 20 kN. The position of the load x varied from 0.0 to 35.0 m with 0.2 m step. The position x = 0.0 m corresponds to the load placed at the side end of the wall; the position x = 35.0 m corresponds to the load placed in the mid-length of the wall.

Due to symmetry of the wall, there is no need for modelling load positions past x = 35.0 m.

The peak bending moment in vertical direction $M_{3D,max}$ was observed for all examined wall heights H. The dependence of peak bending moment $M_{3D,max}$ on the horizontal load position x is summarised in a graph in Figure 57.

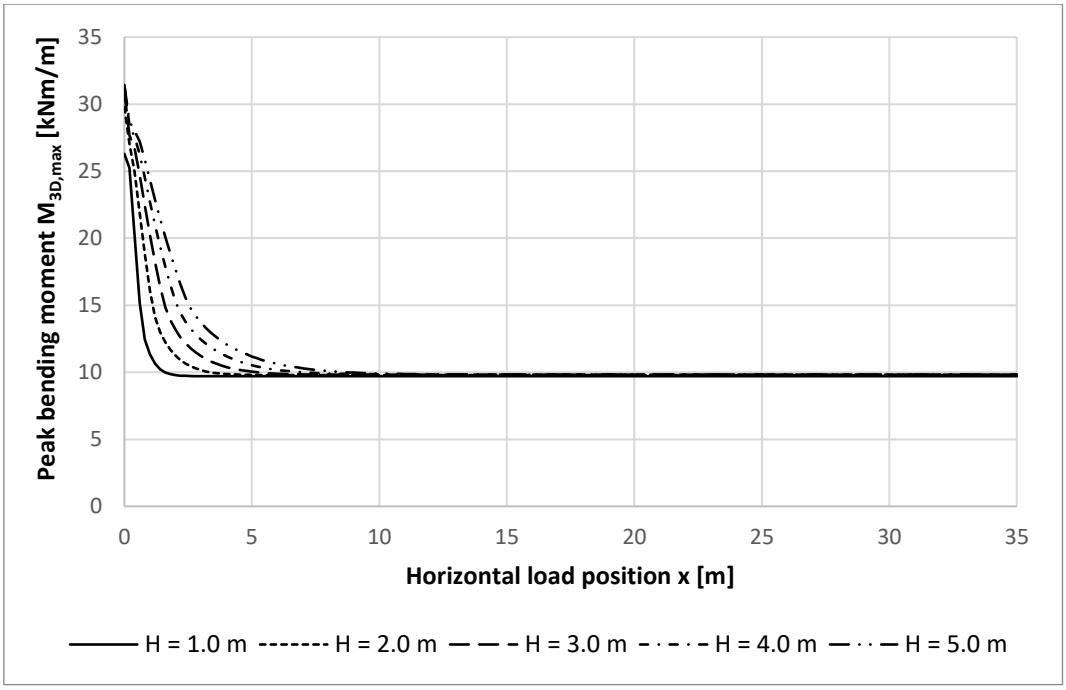

Figure 57: Dependence of peak bending moment on horizontal load position

The graph in Figure 57 shows that the peak bending moment $M_{3D,max}$ increases as the position of the load nears x the wall end for all wall heights H. This can be explained by the fact that there is smaller length for the bending moment to distribute over near the wall end than it is in the central zone of the wall, as described Section 7.c.iii. With smaller space for moment distribution, the moment concentrates on a smaller length which is compensated by higher peaks of moments.

For better interpretation of the results, relative peak bending moment $M_{rel,max,7a}$ was expressed as a ratio of peak bending moment of load position x to peak bending moment of a wall loaded at its central zone, see Equation 62.

$$M_{rel,max,7a} = \frac{M_{3D,max}\,(x)}{M_{3D,max}\,(L - L_e > x > L_e)} \qquad \textit{Equation 62}$$

where $M_{3D,max}(x)$ [kNm/m] is the peak bending moment for load placed in horizontal position x

$M_{3D,max}(L-L_e>x>L_e)$ [kNm/m] is the peak bending moment for load placed in central zone of the wall

The dependence of the relative peak bending moment $M_{rel,max,7a}$ on the horizontal load position x is plotted for all examined wall heights H in Figure 58.

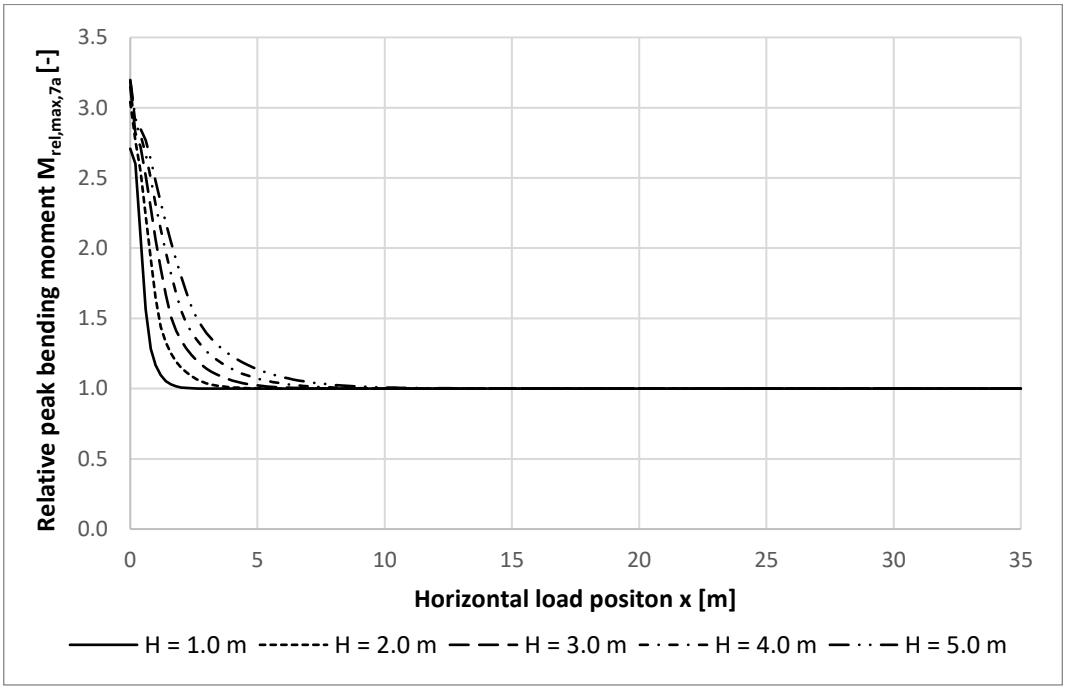

Figure 58: Dependence of relative peak bending moment on horizontal load position

The graph in Figure 58 presents that the peak bending moment of walls loaded at wall end reach up to 3.2x larger values than of walls loaded in their central zone for the examined range of wall heights.

To find the relationship between the peak bending moment on three-dimensional model and simplified two-dimensional model, relative bending moment $M_{rel,max,7b}$ is introduces, see Equation 63.

$$M_{rel,max,7b} = M_{rel,max,2} = \frac{M_{3D,max}}{M_{2D,max}} \qquad \textit{Equation 63}$$

where $M_{2D,max}$ [kNm/m] is the peak bending moment obtained from a two-dimensional model

$M_{3D,max}$ [kNm/m] is the peak bending moment obtained from a three-dimensional model

The dependence of the relative peak bending moment $M_{rel,max,7b}$ on the horizontal load position x is presented in Figure 59. The curves presented correspond to loading force of 20 kN, however, identical curves were obtained for loading forces 160 kN and 1000 kN, proving that the relative bending moment $M_{rel,max,7b}$ is independent from load magnitude F.

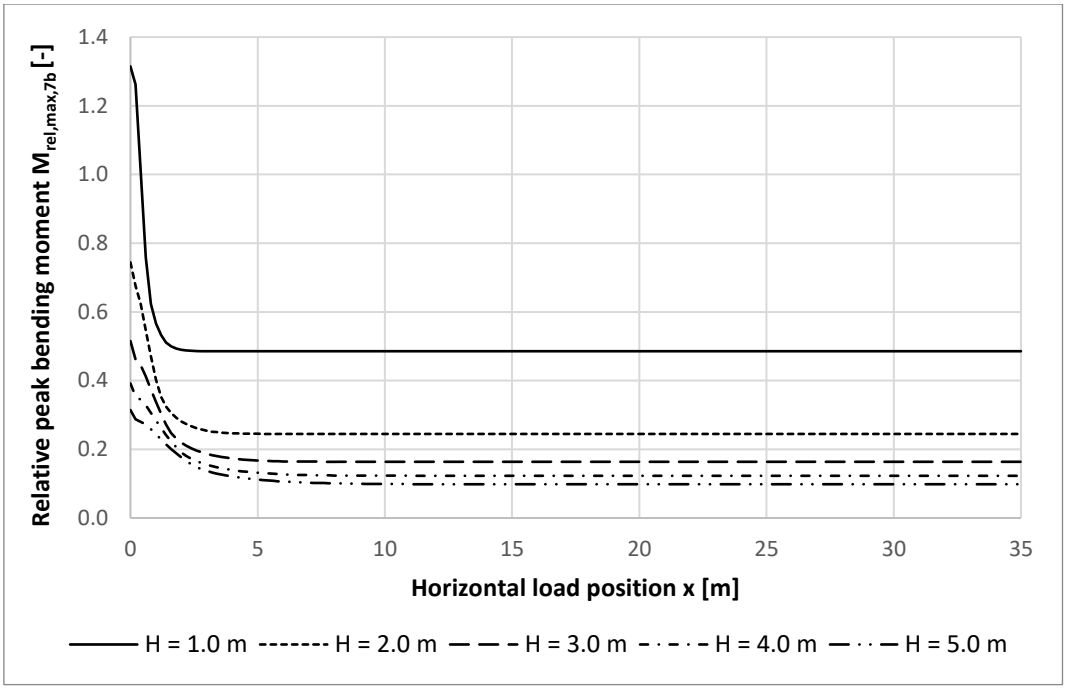

Figure 59: Dependence of relative peak bending moment on horizontal load position

The graph in Figure 59 shows that even though the values of peak bending moment increase with the load position nearing the wall side edge, in most cases, the three-dimensional analysis still bring less onerous results than the simplified two-dimensional analysis, as most of the relative peak bending moment values of $M_{rel,max,7b}$ are smaller than 1.0. However, the curve of 1.0 m high wall reaches relative peak bending moment values $M_{rel,max,7b}$ over 1.0 at the very end of the wall. That means that the results of the three-dimensional analysis are more onerous than of two-dimensional analysis. Thus, it can be concluded that using the simplified two-dimensional analysis is not generally conservative approach and might give unsafe results.

To quantify relative peak bending moment $M_{rel,max,7b}$ for horizontal load position at the wall end, the range of the examined wall heights H was widened to 0.6 m to 6.0 m with 0.2 m step. The dependence of the relative peak bending moment value $M_{rel,max,7b}$ with load placed at wall end on wall height H is presented in Figure 60.

A trendline of the curve of the peak relative bending moment $M_{rel,max,7b}$ was found, see Equation 64. The precision of the equation is satisfactory as its determination coefficient R^2 is equal to 0.999. The trendline function can be used as a correction coefficient k_7 dependent on wall height, see Equation 65.

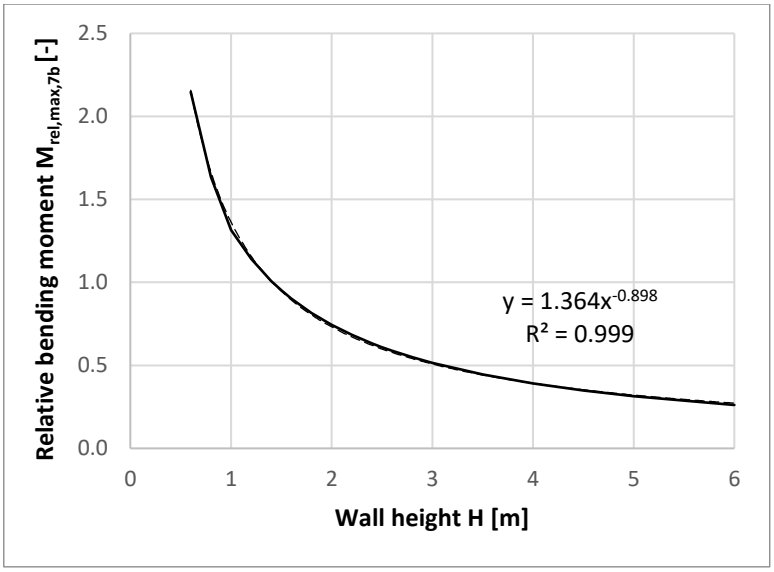

Figure 60: Dependence of relative peak bending moment at wall end on wall height

$$y = 1.364x^{-0,898} \qquad \textit{Equation 64}$$

$$k_7 = M_{rel,max,7b} = y = 1.364x^{-0,898} = 1.364H^{-0,898} \qquad \textit{Equation 65}$$

The correction coefficient k_7 can be applied on the peak bending moment $M_{2D,max}$ obtained from the two-dimensional analysis, returning modified value that approximates a value that would have been obtained from the three-dimensional model, see Equation 66. The correction coefficient k_7 compensates the error of the two-dimensional analysis. The correction coefficient is applicable to the edge zone of walls as defined in Section 7.c.iii.

$$M_{3D,max} = k_7 M_{2D,max} = 1.364H^{-0.898}FH = 1.364FH^{0.102} \qquad \textit{Equation 66}$$

The correction coefficient k_7 helps to obtain the value of the peak bending moment $M_{3D,max}$ caused by a point load placed at the very end of the wall. This value of peak bending moment can conservatively be applied to the whole edge zone of the wall. Less conservative, but still safe approach is to assume a linear decrease in peak bending moment between the very end of the wall and beginning of the central zone. This simplification is presented in graphs in Figure 61. The gap between the exact and simplified curve increases with increasing wall height H, which means that the simplified bilinear curve is more conservative for tall walls than short.

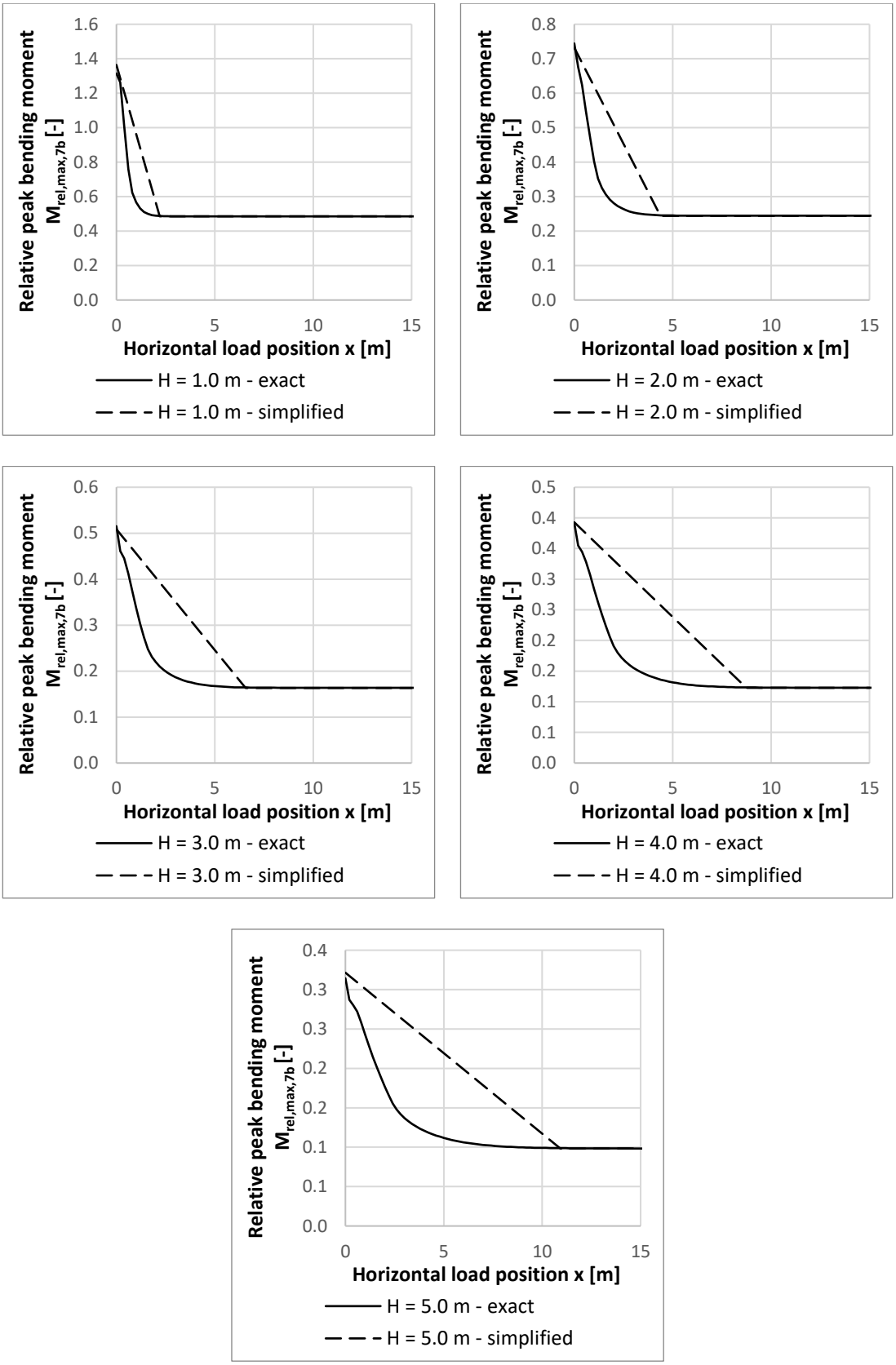

Figure 61: Simplified curves of relative peak bending moment dependence of horizontal load position for various wall heights

viii. Concrete strength

In the structural design according to EN1992-1-1, the strength of concrete is given by concrete class. A set of models was prepared to investigate the influence of concrete class on the peak bending moment in vertical direction of a retaining wall subjected to concentrated loads. A wall with the length L = 70 m was subjected to the point load F = 20 kN placed in the centre of the wall horizontally, at the top wall edge vertically. The wall was modelled with the thickness t = 300 mm. The wall height H ranged between 0.6 m and 6.0 m with 0.2 m step. The peak value of bending moment in vertical direction $M_{3D,max}$ was evaluated. The performance of concrete class C30/37 and C50/60 was compared.

The results of the analysis are presented in the graph in Figure 62 (left). The graph presents peak bending moment values $M_{3D,max}$ for all examined wall heights H. The two curves for concrete class C30/37 and C50/60 are almost identical. Maximum divergence in the values is 0.01 kNm/m, which may be caused by computation method and is negligible.

For further use, it is practical also to show the values of relative peak bending moment $M_{rel,max}$, see the graph in Figure 62 (right). Processing the values of peak bending moment $M_{3D,max}$ into values of relative bending moment $M_{rel,max}$ smoothens even the slight negligible differences between results of C30/37 and C50/60 concrete classes

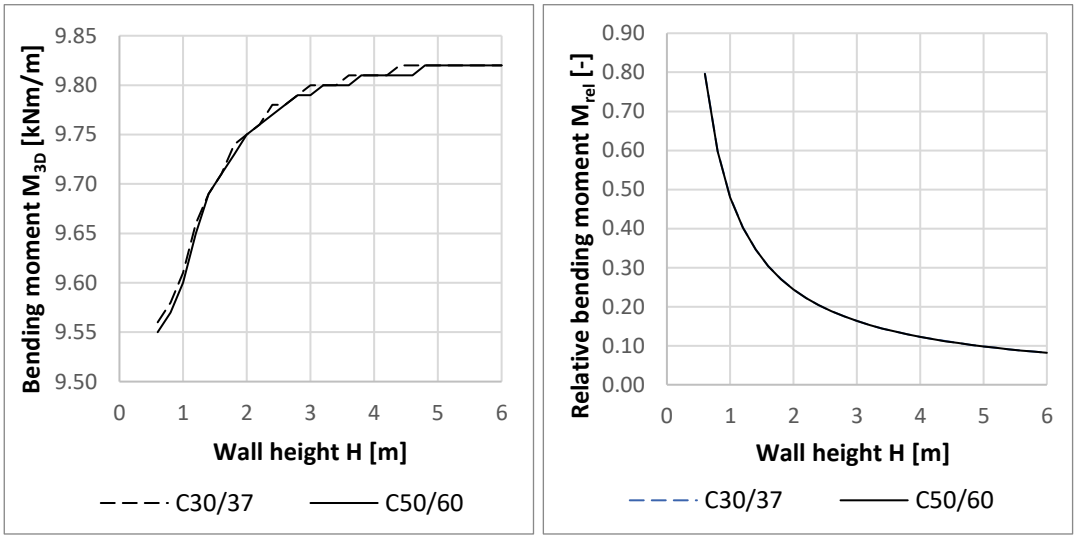

Figure 62: Influence of concrete class on peak bending moment (left), on relative bending moment (right)

Based on the data obtained by this study, it is concluded that the value of peak bending moment is not influenced by concrete strength class.

ix. Reinforcement

Plate elements used in three-dimensional modelling of a wall subjected to a point load usually use predefined material model of concrete. Predefined material models are integrated in majority of commercial FEM software. The definition of the material uses simplifications according to selected standard. The default setting of the material characteristics considers strength and deformability of plain concrete and does not take into account the reinforcement.

The reinforcement of concrete structures increases flexural stiffness of a section. In majority of cases, orthogonal grid of rebars is used, and the reinforcement is oriented in x- and y-direction of a local coordinate system. For concrete elements that are equally reinforced in both x- and y-axis, the ratio of flexural stiffness in x- and y-axis is equal to the ratio of flexural stiffness of unreinforced concrete. Therefore, a point load acting on such element distributes proportionally to the flexural stiffness ratio and equal reinforcement in x and y direction does not affect the load distribution.

However, concrete elements are rarely reinforced equally in their local x- and y-axis. Even if the reinforcement area in the section was equal for both directions, still, the positions of reinforcement in x- and y-axis need to be shifted to avoid rebar collision, thus creating slightly unequal flexural stiffness for the two directions.

The influence of reinforcement was introduced into the study as a flexural stiffness orthotropy. The analysis software used in this study allows modification of the default concrete material model – the flexural stiffness can vary for x- and y-direction. The software requires setting of a stiffness coefficient *k* (see Figure 63), that expresses the ratio of flexural stiffness in local x- and y-axis, see Equation 67. The ratio of bending stiffness of the plate is notated *a* in this thesis.

$$a = k = EI_x/EI_y \qquad \textit{Equation 67}$$

where EI_x is flexural stiffness in x-direction

EI_y is flexural stiffness in y-direction

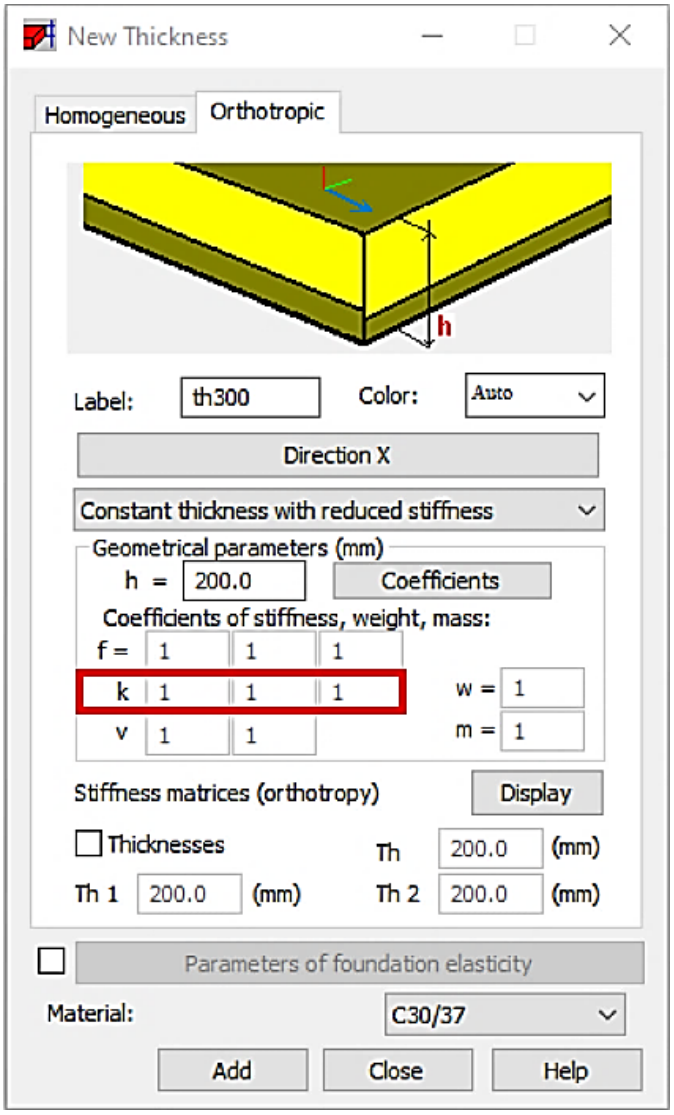

Figure 63: Flexural stiffness orthotropy in Robot Structural Analysis

The influence of unequal reinforcement in x- and y-axis of a retaining wall subjected to a point load was studied on a set of three-dimensional models. A wall with the length L = 70 m was subjected to the point load F = 1000 kN placed in the centre of the wall horizontally, at the top wall edge vertically. The wall was modelled with the thickness t = 300 mm, C30/37 concrete class was used. The wall height H ranged between 1 and 6 m with 1 m step. The local x-axis is oriented horizontally, y-axis vertically. The peak value of bending moment in vertical direction $M_{3D,max}$ was evaluated.

Three values of stiffness coefficient were used, representing three reinforcement options, see Table 17.

	Reinforcement option	Rebars used	$a = EI_x/EI_y$	Note
1	Wall reinforced equally in both directions so that the flexural stiffness is equal for section in horizontal and vertical direction. This is the default setting of concrete material models in majority of structural analysis software.	Not relevant.	1.00	-
2	Wall reinforced with respect to EN1992-1-1 requirement: Horizontal reinforcement area is at least 25% of vertical reinforcement area	Vertical: Ø20 mm, 150 mm spacing, rebar centre 40 mm from wall face, equal at both faces. Horizontal: Ø10 mm, 150 mm spacing, rebar centre 55 mm from wall face, equal at both faces.	0.90	Calculation of *a* value provided in Table 18
3	Wall reinforced to achieve the lowest possible stiffness coefficient regardless standard requirements: Maximum reinforcement in vertical direction allowing concrete workability, absent reinforcement in horizontal direction.	Vertical: Ø32 mm, 40 mm spacing, rebar centre 40 mm from wall face, equal at both faces. Horizontal: absent.	0.43	Calculation of *a* value provided in Table 19

Table 17: Reinforcement options and corresponding stiffness coefficients

parameter	vertical section	horizontal section	description
h [mm]	300	300	section height
b [mm]	1000	1000	section breadth
E_c [GPa]	33	33	concrete elasticity modulus
$Ø_t$ [mm]	20	10	bar diameter of top reinforcement layer
s_t [mm]	150	150	spacing of top reinforcement layer
d_{1t} [mm]	40	55	position of top reinforcement layer from top face
$Ø_b$ [mm]	20	10	bar diameter of bottom reinforcement layer
s_b [mm]	150	150	spacing of bottom reinforcement layer
d_{1b} [mm]	40	55	position of bottom reinforcement layer from bottom face
E_s [GPa]	200	200	reinforcement elasticity modulus
α_e [-]	6.06	6.06	modular ratio
A_c [mm^2]	300 000	300 000	concrete area
A_t [mm^2]	2 094	524	top reinforcement area
A_b [mm^2]	2 094	524	bottom reinforcement area
A_{ti} [mm^2]	12 693	3 173	equivalent top reinforcement area
A_{bi} [mm^2]	12 693	3 173	equivalent bottom reinforcement area
A_i [mm^2]	325 387	306 347	ideal section area
c_c [mm]	150	150	concrete centre of gravity position from top face
c_{At} [mm]	40	55	top reinforcement centre of gravity position from top face
c_{Ab} [mm]	260	245	bottom reinforcement centre of gravity position from top face
c [mm]	150	150	section centre of gravity position from top face
I_c [mm^4]	2 250 000 000	2 250 000 000	moment of inertia - concrete contribution
I_{At} [mm^4]	153 588 974	28 639 266	moment of inertia - top reinforcement layer contribution
I_{Ab} [mm^4]	153 588 974	28 639 266	moment of inertia - bottom reinforcement layer contribution
I [mm^4]	2 557 177 948	2 307 278 533	moment of inertia - ideal section
EI [MNm^2]	84	76	flexural stiffness
a [-]	0.90		flexural stiffness ratio

Table 18: Stiffness coefficient for Reinforcement option 2

parameter	vertical section	horizontal section	description
h [mm]	300	300	section height
b [mm]	1000	1000	section breadth
E_c [GPa]	33	33	concrete elasticity modulus
$Ø_t$ [mm]	32	0	bar diameter of top reinforcement layer
s_t [mm]	40	150	spacing of top reinforcement layer
d_{1t} [mm]	40	40	position of top reinforcement layer from top face
$Ø_b$ [mm]	32	0	bar diameter of bottom reinforcement layer
s_b [mm]	40	150	spacing of bottom reinforcement layer
d_{1b} [mm]	40	40	position of bottom reinforcement layer from bottom face
E_s [GPa]	200	200	reinforcement elasticity modulus
α_e [-]	6.06	6.06	modular ratio
A_c [mm^2]	300 000	300 000	concrete area
A_t [mm^2]	20 106	0	top reinforcement area
A_b [mm^2]	20 106	0	bottom reinforcement area
A_{ti} [mm^2]	121 856	0	equivalent top reinforcement area
A_{bi} [mm^2]	121 856	0	equivalent bottom reinforcement area
A_i [mm^2]	543 711	300 000	ideal section area
c_c [mm]	150	150	concrete centre of gravity position from top face
c_{At} [mm]	40	40	top reinforcement centre of gravity position from top face
c_{Ab} [mm]	260	260	bottom reinforcement centre of gravity position from top face
c [mm]	150	150	section centre of gravity position from top face
I_c [mm^4]	2 250 000 000	2 250 000 000	moment of inertia - concrete contribution
I_{At} [mm^4]	1 474 454 152	0	moment of inertia - top reinforcement layer contribution
I_{Ab} [mm^4]	1 474 454 152	0	moment of inertia - bottom reinforcement layer contribution
I [mm^4]	5 198 908 304	2 250 000 000	moment of inertia - ideal section
EI [MNm^2]	172	74	flexural stiffness
a [-]	0.43		flexural stiffness ratio

Table 19: Stiffness coefficient for Reinforcement option 3

The peak bending moment in vertical direction $M_{3D,max}$ was observed for all examined wall heights H and flexural stiffness ratios a. See the summary of results in Table 20, where the divergence of results from the results corresponding to the stiffness ratio a = 1.00 is expressed as $\Delta M_{3D,max}$.

Wall height H [m]	a [-]	$M_{3D,max}$ [kNm/m]	$M_{3D,max}$ [%]	$\Delta M_{3D,max}$ [%]
1	1.00	487.43	100.00	0.00
	0.90	494.73	101.50	1.50
	0.43	554.78	113.82	13.82
2	1.00	490.18	100.00	0.00
	0.90	498.79	101.76	1.76
	0.43	570.00	116.28	16.28
3	1.00	491.18	100.00	0.00
	0.90	500.11	101.82	1.82
	0.43	574.44	116.95	16.95
4	1.00	491.52	100.00	0.00
	0.90	500.58	101.84	1.84
	0.43	576.14	117.22	17.22
5	1.00	491.64	100.00	0.00
	0.90	500.77	101.86	1.86
	0.43	576.92	117.35	17.35
6	1.00	491.68	100.00	0.00
	0.00	500.84	101.86	1.86
	0.00	577.31	117.42	17.42

Table 20: Increase in bending moment due to reinforcement orthotropy

The graph in Figure 64 presents the dependence of the bending moment divergence $\Delta M_{3D,max}$ on wall height H. For both values of flexural stiffness ratio a equal to 0.90 and 0.43, the divergence in bending moment ΔM_{3D} increases with increasing wall height H. However, the curve trends suggest, that the increase in bending moment converges to a limit.

Extrapolating the trend of the curve of flexural stiffness ratio a = 0.43, the convergence limit of bending moment increase $\Delta M_{3D,max}$ is 17.6 %. For flexural stiffness ratio a = 0.90, it is 1.9 %.

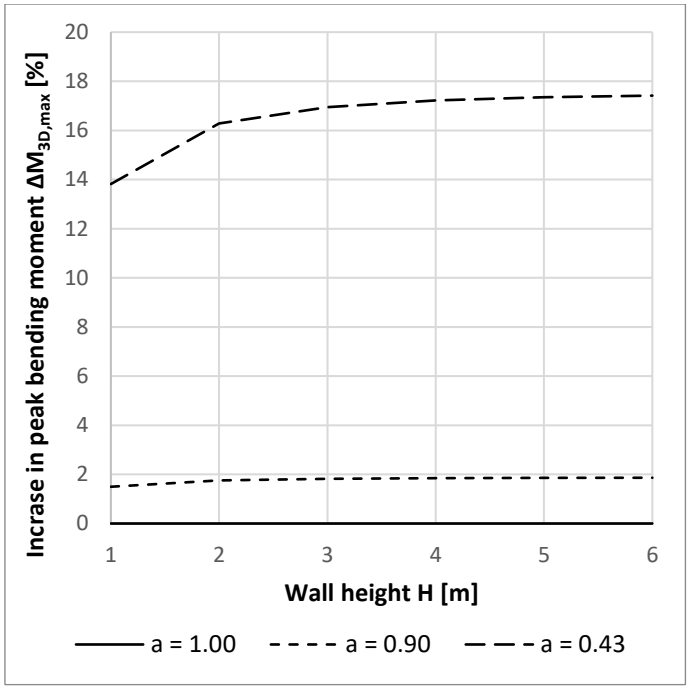

Figure 64: The dependence of the increase in bending moment ΔM_{3D} on wall height

For practical use, only the results obtained for flexural stiffness ratio *a* = 0.90 are relevant, as that corresponds to a wall with minimal horizontal reinforcement according to (EN 1992-1-1, 2004). The minimal horizontal reinforcement in this case is limited by at least 25% of the area of vertical reinforcement. Less reinforcement in horizontal direction is not allowed by the code, and therefore, the flexural stiffness ratio *a* should not drop below 0.90 in any wall structure.

The flexural stiffness ratio *a* is also not expected to rise above 1.00 in practice. Values of flexural stiffness ratio *a* over 1.00 would correspond to a situation, where the area of reinforcement is larger in horizontal than vertical direction, which is unlikely given the fact that the main load bearing direction is vertical for the structures studied in this thesis.

This study shows that in structures that are designed according to (EN 1992-1-1, 2004), the peak moment increase due to unequal reinforcement in horizontal and vertical direction should not exceed 1.9 %. Therefore, the peak moment can reach up to 101.9 % of its original value obtained on a three-dimensional model. Based on this finding, the correction coefficient k_9 is proposed, see Equation 68 for its value and Equation 69 for its use.

$$k_9 = 1.019 \qquad \textit{Equation 68}$$

$$M_{3D} = k_9 * M_{3D,max}\ (a = 1) \qquad \textit{Equation 69}$$

where $M_{3D,max}\ (a = 1)$ [kNm/m] is the maximum bending moment in vertical direction for equal reinforcement in both x- and y-directions

The correction coefficient k_9 is to be applied on the value of three-dimensional reference peak bending moment $M_{3D,max}$ *(a = 1)* that corresponds to a wall equally reinforced in both horizontal and vertical direction.

x. Wall edge restraints

Supports of structural models have generally major influence on the internal forces. Cantilever walls may have free ends on sides or can be attached to other structures. This section aims to study the difference between the behaviour of walls with free and fixed side edges.

A three-dimensional model of a 70 m long wall was prepared. C30/37 concrete class was used, and the wall was 300 mm thick. The wall was subjected to 160 kN of point load at the top wall edge. The horizontal position of the load *x* varied along one half of the wall length (due to wall symmetry), from 0.0 m to 35.0 m with 0.2 m step. Each individual loading was modelled as a single load case, creating 176 load cases in total. The model was prepared in two modifications – with free and fixed side edge.

The envelope of peak bending moments $M_{3D,max}$ for all 176 load cases was observed. The results are plotted as the dependence of peak bending moment $M_{3D,max}$ on horizontal load position *x* in Figure 65.

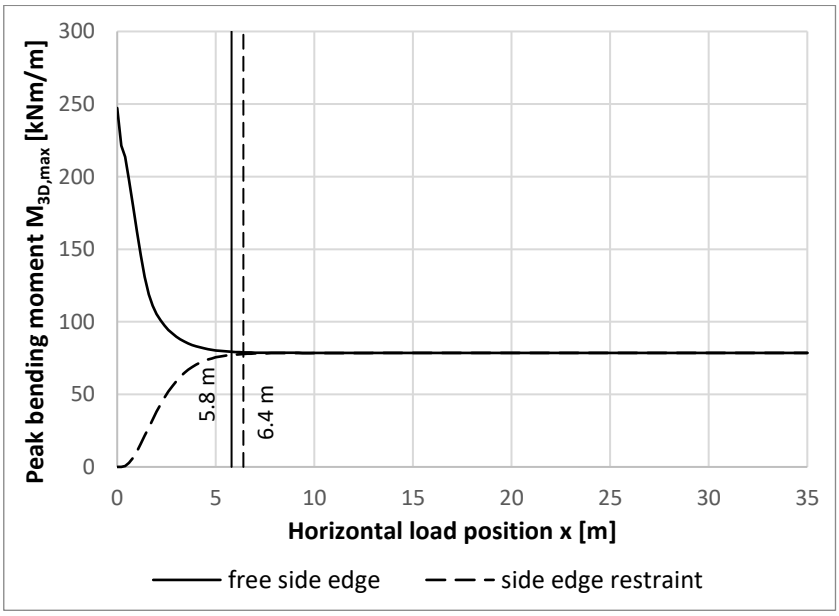

Figure 65: Peak bending moments in walls with free and fixed side ends

The majority of the two curves in Figure 65 is identical and constant. The two curves differ at the load positions near the wall end. The curve representing the wall with free edge shows increase in peak bending moment $M_{3D,max}$ as it reaches the wall end. That is caused by the fact that the bending moment is not provided with as much length for its distribution and concentrates into a smaller area, which increases its peak. Contrarily, the curve of the wall with fixed edge shows decrease in peak bending moment $M_{3D,max}$ and eventually reaches zero for the load position *x* at the very edge of the wall. The moment reduction near the wall end is caused

by the presence of the edge support. The edge support bears part of the bending moment as the force nears to the edge, decreasing the bending moment in the wall body. In case of the wall supported at its edge, the peak bending moment does not exceed the value obtained in the central area.

The load position x for which the peak bending moment $M_{3D,max}$ starts to noticeably increase/decrease when moving towards the wall end is marked by vertical lines in the graph for both curves. The exact stationary point of the curves is in fact further from the edge as the bending moments $M_{3D,max}$ changes very slowly in the near-constant region. For that, the border lines were plotted with 1% deviation from the exact stationary points to provide information more relevant for structural design. The margin marking the divergence point is not equal for the wall with free and fixed side end.

It can be concluded that a fixed side end of a wall causes decrease in vertical bending moment in the edge zone. In case of fixed side edge, it is safe to assume that peak bending moment in the edge area does not exceed the peak bending moment in the central area.

e. Wall-imp

The findings of Section 7.d were used to develop a calculation tool for convenient structural design of cantilever walls subjected to concentrated loads. Wall-imp was created in MS Excel environment, and for that, it brings transparent results.

The purpose of Wall-imp is to determine maximum vertical bending moment on a cantilever wall subjected to a point load. The point load simulates the equivalent static load of vehicle impact event or any other cause of load acting on a very small area. The assumed structural model is a straight RC wall with fixed support along the base, with or without fixed supports of side ends. The resulting bending moments include torsional effects according to Wood-Armer theory.

Wall-imp combines the simplicity of a two-dimensional model approach and precision of a three-dimensional modelling. It allows to quickly produce accurate results without any demands on FEM software.

i. Principles and use

Figure 66 shows that the user interface is organized into the input field, the zone information field, the applicability check field and the result field.

The input field contains following parameters to be set by the user:

L [m]	Wall length in horizontal direction
H [m]	Wall height
F [kN]	Point load applied perpendicular to wall plane
h [m]	Horizontal position of the load above the wall base
Side supports	Wall side ends can be fixed or free

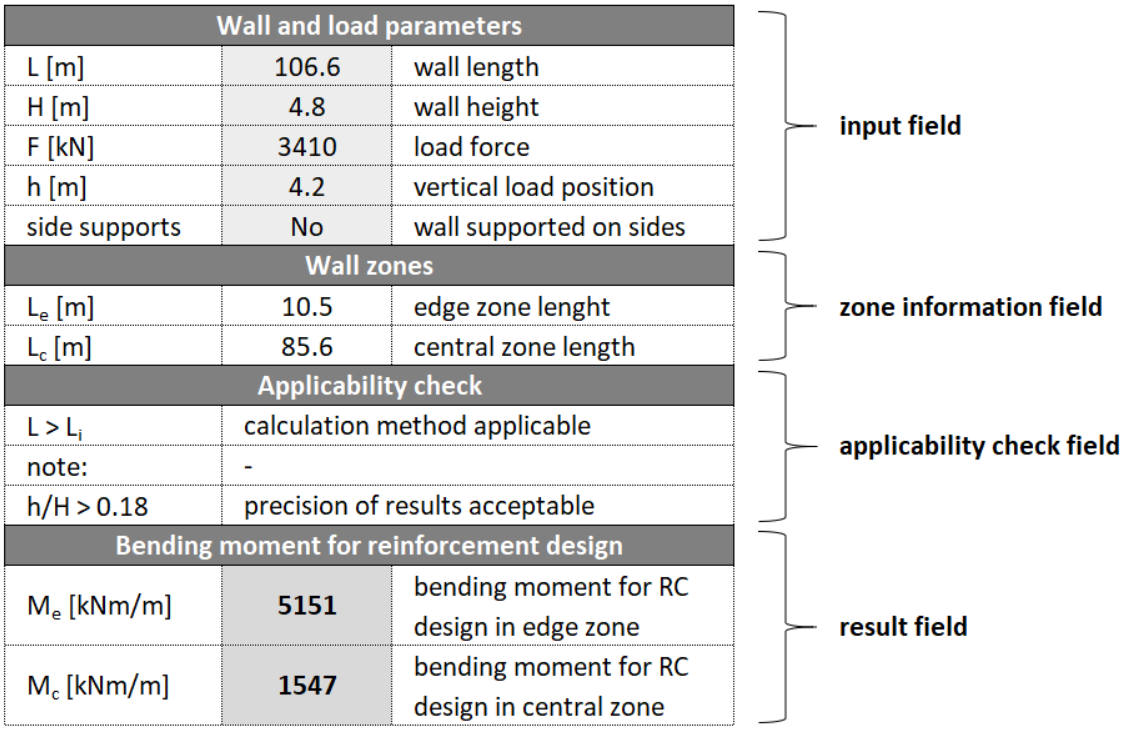

Figure 66: Wall-imp user interface

The effect of following parameters was analysed in Section 7.d, however, it was non-existent or negligible within the range of Wall-imp applicability, and therefore, the parameters are not used in Wall-imp:

t [mm]	Wall thickness
f_c [MPa]	Concrete strength
a [-]	Ratio of reinforcement used in horizontal to vertical direction

Section 7.d also presents study on the effect of load distribution over horizontal length *d*. This parameter was not included in Wall-imp since its interference with other parameters caused unclear conclusions, as it was proved during the first stage validation of Wall-imp.

The zone information field shows how the wall can be divided into zones, in which the results are applicable. The zones were defined according to Section 7.c.

Applicability check field provides information whether Wall-imp is suitable tool for the given geometry. There are two checked conditions:

1. Wall length is *L* is larger than influenced length L_i.

   If the first condition is not met, it means that the wall is too short to be divided into central and edge zone. Therefore, the results of are not applicable. In such situation, the note field presents a suggestion for the designer. If the wall length *L* is smaller than or equal to the influenced length L_i but still larger than 1 m, it is suggested to the designer to prepare individual three-dimensional model. If the wall length *L* is smaller than or equal to 1 m, it is suggested to the designer to perform calculation on two-

dimensional model, which is possible even without use of any software. See Figure 67 and Figure 68 for illustration.

Wall and load parameters		
L [m]	15.0	wall length
H [m]	4.8	wall height
F [kN]	3410	load force
h [m]	4.2	vertical load position
side supports	No	wall supported on sides
Wall zones		
L_e [m]	10.5	edge zone lenght
L_c [m]	-6.0	central zone length
Applicability check		
$L > L_i$	calculation method NOT applicable	
note:	suggested solution: 3D model	
h/H > 0.18	precision of results acceptable	
Bending moment for reinforcement design		
M_e [kNm/m]	**5151**	bending moment for RC design in edge zone
M_c [kNm/m]	**1547**	bending moment for RC design in central zone

Figure 67: Wall length check

Wall and load parameters		
L [m]	0.8	wall length
H [m]	4.8	wall height
F [kN]	3410	load force
h [m]	4.2	vertical load position
side supports	No	wall supported on sides
Wall zones		
L_e [m]	10.5	edge zone lenght
L_c [m]	-20.2	central zone length
Applicability check		
$L > L_i$	calculation method NOT applicable	
note:	suggested solution: 2D model	
h/H > 0.18	precision of results acceptable	
Bending moment for reinforcement design		
M_e [kNm/m]	**5151**	bending moment for RC design in edge zone
M_c [kNm/m]	**1547**	bending moment for RC design in central zone

Figure 68: Wall length check

2. The ratio of the vertical load position to the total wall height h/*H* is larger than 0.18.

   It was found and presented in Section 7.d.vi that the error of approximation is excessive for the walls where the load is placed very much below its top edge. The error of 5% was set to be the margin of acceptability, and that corresponds to *h/H* ratio equal to 0.18. Wall-imp notifies the designer that this margin has been crossed and the results might be highly distorted, see Figure 69 for illustration.

Wall and load parameters		
L [m]	106.6	wall length
H [m]	4.8	wall height
F [kN]	3410	load force
h [m]	0.8	vertical load position
side supports	No	wall supported on sides
Wall zones		
L_e [m]	10.5	edge zone lenght
L_c [m]	85.6	central zone length
Applicability check		
$L > L_i$	calculation method applicable	
note:	-	
h/H > 0.18	precision of results compromised	
Bending moment for reinforcement design		
M_e [kNm/m]	**3312**	bending moment for RC design in edge zone
M_c [kNm/m]	**1006**	bending moment for RC design in central zone

Figure 69: Vertical load position check

The result field provides two values of maximum bending moment in vertical direction at wall base:

1. Bending moment M_e applicable in the edge zone of the wall

   The value corresponds to the load being horizontally located at the very end of the wall. For practical use it is convenient for the designer to use this value for the reinforcement design in the whole edge zone. That is very conservative, but safe approach. Another, less conservative, but still safe option is to presume linear transition between the extreme edge moment value and the value applicable in the central zone, as it is described in detail in Section 7.d.vii.

2. Bending moment M_c applicable in the central zone of the wall

   The value corresponds to the load being horizontally located anywhere withing the central zone of the wall.

ii. Limits of application

The algorithms used in Wall-imp were determined by a study of the effects of all individual load and geometry parameters and their interaction. Each parameter was examined within a certain range of values. Wall-imp should not be used for input values outside these ranges, unless it was proven that it is safe to extrapolate the findings of each parameter study. Table 21 presents the limits of all parameters and related recommendations.

Parameter	Lower limit	Upper limit	Note
Wall length L	Influenced length L_i	-	More suitable approaches are suggested for lengths below the lower limit
Wall height H	0.6 m	-	Walls shorter than 0.6 m should not be analysed by using shell elements in models as their thickness/size ratio does is more suitable for solid elements. Since Wall-imp is based on study of shell element model, its results are not applicable for walls shorter than 0.6 m. The study was performed on walls up to 6.0 m of height, however, the precision of the results was generally increasing with increasing wall height, and so it is concluded that Wall-imp may be used for walls without any upper limit in height.
Wall thickness t	-	600 mm	Walls with thickness over 600 mm should not be analysed as Wall-imp was designed based on study of thickness range up to this value and the outcomes cannot be extrapolated.
Magnitude of load F	-	-	-
Load distribution d	-	-	Not applicable in Wall-imp
Load vertical position h	h/H = 0.18	H	Errors larger than 5% were detected for *h/H* ratio lower than 0.18
Load horizontal position x	0	L	-
Concrete strength f_c	-	-	-

Parameter	Lower limit	Upper limit	Note
Reinforcement ratio a	0.9	1.0	Horizontal/vertical reinforcement ratio smaller than 0.9 would not follow Eurocode requirements on minimum reinforcement cross-sectional area. It is expected horizontal/vertical reinforcement ratio to be less than or equal to 1.0 as the main load bearing direction is vertical.
Side edge restraint	No	Yes	-

Table 21: Limits of Wall-imp applicability

Wall-imp provides results approximating three-dimensional linear analysis on shell elements. Non-linear behaviour of reinforced concrete is usually not considered in common engineering practice. Linear analysis neglects heterogeneity of reinforced concrete, assumes constant value of Young elasticity modulus for all levels of stain, and does not consider local decrease in stiffness of cracked concrete. Although linear analysis is used in majority of design projects, non-linear analysis brings more realistic results. A non-linear model of a retaining wall was prepared in Atena (model setup consulted with Ing. Jan Kubát), see Figure 70, to be compared to a linear model prepared in Robot Structural Analysis software. Both models analysed an infinite wall.

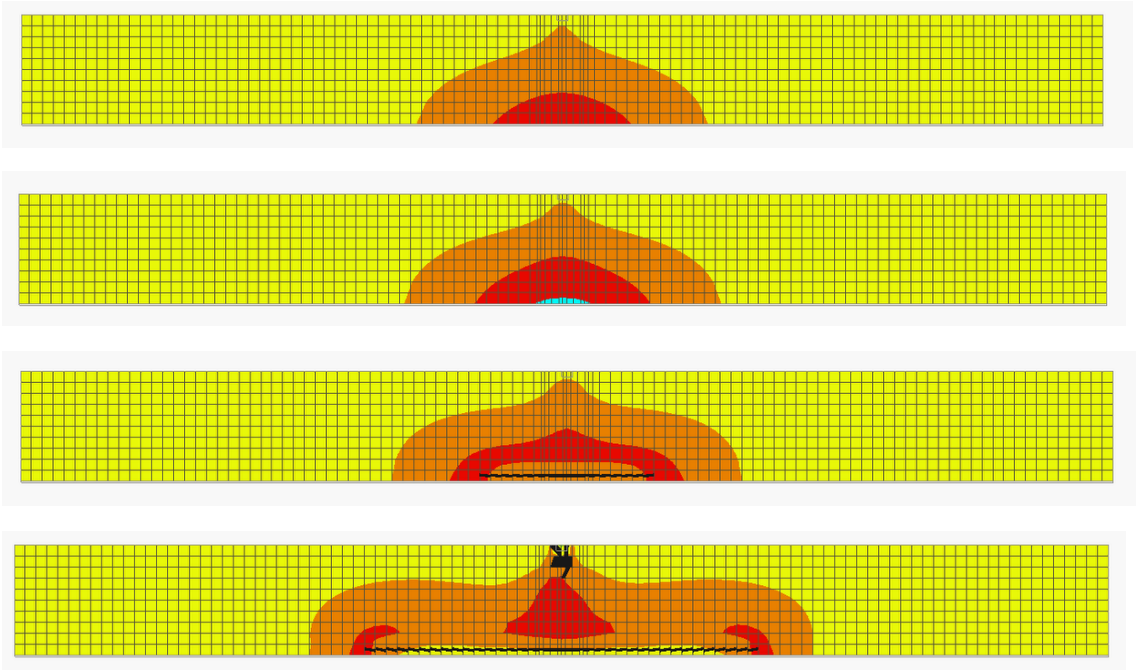

Figure 70: Non-linear wall model

The behaviour of the infinite wall length was simulated with a 70 m long wall in case of Robot Structural Analysis software and 20 m long in case of Atena software;

both models met the conditions from Section 7.c to properly simulate an infinite wall. In both models, the wall height was set to 3 m, wall thickness to 300 mm, concrete class to C30/37 and the loading force of 160 kN was placed at the top of the wall. Both wall models were fixed at the bottom. Non-linear model was reinforced with B500B bars of 12 mm diameter with 150 mm spacing in both vertical and horizontal direction. The linear model does not require reinforcements specification.

Table 22 provides comparison of results of both models. The maximum deformation *w* is larger in case of the non-linear model, as the cracking of the material locally decreases bending stiffness of the wall. The peak bending moment $M_{3D,max}$ obtained from the linear model was transformed to a stress in the tensile concrete face to be compared to the stress obtained from the non-linear model. The tensile stress lower in case of the non-linear model, as the cracking of the material causes stress redistribution. It can be concluded that in this case, the linear model provides more conservative results of the peak bending moment at the wall base in vertical direction, while the deflection is underestimated when using linear model. Computational time of the linear model is approximately 40x shorter than the non-linear. That explains why linear models are much more common in engineering practice.

	Linear model	Non-linear model
Tensile stress σ [MPa]	5.2	2.0
Maximum deformation w_{max} [mm]	3.1	5.1
Computational time [s]	6	~240

Table 22: Comparison of linear and non-linear analysis

The non-linear model also revealed that not only the peak bending moment at the wall base, but also the peak bending moment at the area of force application is decisive for the proper wall design. The stresses caused by the loading force at the area of its application are causing the initial cracking of the wall; the horizontal crack at the wall base follows.

Wall-imp is a calculation tool created for determining peak bending moments $M_{3D,max}$ on cantilever walls at their base, and for that it provides results, that are not as accurate as those provided by non-linear analysis, but are safe to use in structural design.

iii. Validation of results

A set of ten validation models was prepared to check correctness of Wall-imp results. The parameter values were chosen by a random number generator within reasonable limits presented in Table 23.

Parameter	Min.	Max.
L [m]	0.5	150
H [m]	0.24	6
F [kN]	0	5000
h [m]	0.5	2.7
t [m]	0.1	0.6
a [-]	0.9	1
side supports	No	Yes
concrete class	C16/20	C50/60

Table 23: Parameter limits for validation

Table 24 contains all ten validation parameter combinations.

Case	1	2	3	4	5
L [m]	35.8	22.9	136.2	34.0	42.3
H [m]	4	2.4	2.6	4.8	3.3
F [kN]	2288	1929	4463	4341	224
h [m]	1.7	1.6	1.6	4.2	2.4
t [m]	0.40	0.51	0.60	0.4	0.36
a [-]	0.99	0.91	0.96	0.94	0.98
side supports	No	No	Yes	No	No
concrete class	C30/37	C30/37	C16/20	C35/45	C25/30

Case	6	7	8	9	10
L [m]	23.7	96.1	39.0	108.3	106.6
H [m]	4.2	1.8	5.1	3.4	4.8
F [kN]	4496	3924	998	4935	3410
h [m]	3.9	1.3	1.5	2.3	4.2
t [m]	0.26	0.3	0.45	0.58	0.22
a [-]	0.93	0.92	0.9	0.99	0.95
side supports	No	Yes	Yes	No	No
concrete class	C16/20	C30/37	C20/25	C25/30	C30/37

Table 24: Parameters of validation

All ten validation cases were analysed by FEM using three-dimensional models were subjected to two load cases; in the first the load was horizontally placed in the mid-length (to validate results of the central zone), in the second load case the load was horizontally placed at the side end of the wall (to validate results of the edge zone). For both load cases, the peak bending moments were evaluated. The ten validation cases were also approximated by Wall-imp. Table 25 contains comparison of FEM and Wall-imp results, including the error of approximation.

Case		1	2	3	4	5
FEM	Central zone	790	758	1657	1988	92
	Edge zone	2192	2350	-	6774	310
Wall-imp	Central zone	754	768	1724	1969	93
	Edge zone	2719	2466	-	6558	304
Error	Central zone	-4.6	1.3	4.0	-1.0	1.1
	Edge zone	0.7	4.9	-	-3.2	-1.9

Case		6	7	8	9	10
FEM	Central zone	2141	1616	328	1941	1561
	Edge zone	6819	-	-	6457	4932
Wall-imp	Central zone	2104	1613	322	1982	1547
	Edge zone	6860	-	-	6569	5151
Error	Central zone	-1.7	-0.2	-1.8	2.1	-0.9
	Edge zone	0.6	-	-	1.7	4.4

Table 25: Wall-imp validation

The error of 5% was determined to be acceptable. The errors of all validation cases are below this margin. Thus, it is concluded that Wall-imp provides satisfactory results.

8. Summary and conclusions

The objective of this thesis was to investigate the behaviour of RC elements under impact loading, and based on the findings, to develop a calculation tool for convenient analysis of RC cantilever walls subjected to concentrated loads. The objective was achieved.

While Section A provided general theoretical background on concrete structures under impact loading, Section B deeply investigated the problem of cantilever RC wall under concentrated loads. Specifically, the issue of idealisation by using two-dimensional models for structural analysis was in the focus. It was proved that the simplification of a three-dimensional problem to a two-dimensional model gives very inaccurate results and may lead to both over- and underestimation of the design.

The differences between two- and three-dimensional models were deeply investigated, and the effect of various wall geometry and load parameters were quantified. The influence of 10 parameters on the peak bending moment in vertical direction was examined – wall length, wall height, wall thickness, load magnitude, load distribution, load vertical and horizontal position, concrete strength, reinforcement, and presence of side supports of the wall. Three-dimensional FEM models were prepared to obtain results for further examination. Following observations and conclusions were made:

- Wall length affects the distribution of vertical bending moment over horizontal axis of the wall, and thus, significantly influences the peak value of the moment. For walls short in length, an individual analysis approach needs to be taken in order to obtain accurate results. The length requiring such approach was determined. For longer walls, zones were defined, distinguishing between behaviour of edge and central parts of the wall. In the edge zones, the proximity of wall end affects the value of peak bending moment. In the central zones, the peak bending moments are intact by wall ends and the moment values are equal to values that would be obtained of infinitely long wall.
- The influence of wall height on the peak bending moment dramatically differs in two- and three-dimensional models. In two-dimensional models, the peak bending moment is proportional to the wall height. In three-dimensional models, the dependence is non-linear. The ratio of results on three- and two-dimensional approach was evaluated for varying wall heights. Since the ratio defines the relationship between the results from three- and two-dimensional models, it was proclaimed a correction coefficient. When the correction coefficient is applied to the results from the two-dimensional model, the value equal to the result from a three-dimensional model is obtained. The correction coefficient is not constant; the dependence of the correction coefficient on the wall height was expressed by a power function. The correction coefficient and its dependence on wall height differs for central and edge zone of the wall. It was quantified for both cases.
- The effect of wall thickness on the peak bending moment was found to be negligible in the cases where the thickness is small enough to be suitable for modelling by plate elements. From a certain thickness to size ratio, the

wall should not be modelled as a plate element and if it is modelled in such way, even the results of three-dimensional analysis are not reliable.

- Load magnitude directly influences the peak value of vertical bending moment. However, it was found that the ratio of the moments from three- and two-dimensional models remains intact by the load magnitude. This means that the correction coefficient proposed above is universally applicable for loads of arbitrary magnitude.
- The effect load distribution in horizontal direction was quantified for the case where the load is situated at the top edge of the wall. The quantification was based on discretization of the distributed load to a series of point loads, evaluating their individual contribution to the peak bending moment, and summarizing their effect. An equation was proposed to determine the peak bending moment with the wall height and load distribution length being the variable factors. Walls subjected to distributed load placed below the top wall edge were examined as well. However, due to mutual interference of individual parameters, no equation expressing dependence of the peak bending moment on wall height, load distribution length and vertical load position was found.
- Horizontal position of the load affects the value of peak vertical bending moment in the edge zones of the wall. It was observed that the value of the moment increases with increasing proximity of the end of the wall. The extreme value of peak bending moment is achieved when the load force is placed at the very end of the wall. For such position of the load, the effect of variable wall height was analysed and a correction coefficient expressing the relationship between results of three- and two-dimensional models was determined.
- The results of three- and two-dimensional analysis differ remarkably for walls subjected to a load placed below their top edge. The part of the wall above the load (free height) does not influence the results of two-dimensional models at all. In three-dimensional approach, the free height provides space for the bending moment to distribute, thus decreasing the peak value. The effect of the free height was evaluated and resulted in proposal of a new correction coefficient. This correction coefficient expresses the relationship between the peak bending moment of a walls with and without free height above the load.
- Concrete strength does not affect the internal forces in the wall in any investigated loading scenario.
- The ratio of reinforcement area in vertical and horizontal affects the stiffness of the wall in the two directions, and therefore, affects the distribution of bending moment and its peak value. However, the effect is negligible for elements reinforced in compliance with standards.
- For walls without side supports, the peak vertical bending moment increases with the load nearing the end of the wall. Contrarily, the peak bending moment decreases with the load nearing the end of a side-supported wall. This means that the wall area most sensitive to the load differs for the two cases.

Based on the findings from the investigation of the wall and load parameter effects, Wall-imp design tool was developed. Commonly used idealisations of the

problem (except for the two-dimensional simplification) were adopted in Wall-imp – plate elements fixed at the base to simulate the embedment of the wall, ESF to replace the dynamic aspect of the load, point load to neglect the real application area of the load, etc. Based on the wall geometry, load magnitude and load position, Wall-imp computes the peak bending moment in vertical direction, which can be further used for the design of the main loadbearing reinforcement. The value of Wall-imp lies in the fact that it provides results with the accuracy of three-dimensional modelling, while the simplicity of its use is equal to the two-dimensional approach. That significantly saves engineers' time and reduces demands on software, as the tool was developed in the widely spread MS Excel spreadsheet. The tool is suitable for long cantilever walls that are exposed to concentrated loads in their whole length.

References

AASHTO-LRFD. 2012. *American Association of State Highway and Transportation Officials - Bridge design specifications.* 2012.

Abbas, Ali A. and Cotsovos, Demetris M. 2015. Numerical investigation of the behaviour of RC wide beams under impact loads. *5th ECCOMAS Thematic Conference on Computational Methods in Structural Dynamics and Earthquake Engineering .* 2015, pp. 2904-2914.

Abdelkarim, O. I. and ElGawady, M. A. 2017. Performance of bridge piers under vehicle collision. *Engineering Structures.* 2017, Vol. 140, pp. 337-352.

Adhikary, Satadru Das, Li, Bing and Fujikake, Kazunori. 2012. Dynamic behavior of reinforced concrete beams under varying rates of concentrated loading. *International Journal of Impact Engineering.* 2012, Vol. 47, pp. 24-38.

Akin, E. J. 2015. *Impact Load Factors for Static Analysis.* Houston : Rice University, 2015.

Baera, Cornelia, et al. 2016. Concrete structures under impact loading: General aspects. *Urbanism. Arhitectura. Constructii.* 2016, Vol. 7, 3, pp. 239-250.

Bhatti, M. Asghar. 2006. Retaining Wall Design Optimization with MS Excel Solver. *7th Analysis and Computation Specialty Conference at Structures.* 2006.

Choi, W. S., Park, K. B. and Park, G. J. 2005. Calculation of Equivalent Static Loads and its Application. *Nuclear Engineering and Design.* 2005, Vol. 235, 22, pp. 2337-2348.

Daudeville, Laurent and Malécot, Yann. 2011. Concrete structures under impact. 2011, Vol. 15, pp. 101-140.

Do, T. V., Pham, T. M. and Hao, H. 2018. Dynamic responses and failure modes of bridge columns under vehicle collision. *Engineering Structures.* 2018, Vol. 156, pp. 243-259.

EN 1991-1-7. 2006. *Eurocode 1 - Accidental Actions.* : CEN, 2006.

EN 1992-1-1. 2004. *Eurocode 2 - Design of concrete structures - Part 1-1: General rules and rules for buildings.* s.l. : CEN, 2004.

fib Model Code. 2010. Lausane : International Federation for Structural Concrete (fib), 2010.

Fujikake, Kazunori, Li, Bing and Soeun, Sam. 2009. Impact response of reinforced concrete beam and its analytical evaluation. *Journal of Structural Engineering.* 2009, Vol. 135, 8, pp. 938-950.

Grote, D. L., Park, S. W. and Zhou, M. 2001. Dynamic behavior of concrete at high strain rates and pressures: I. experimental characterization. *International Journal of Impact Engineering .* 2001, Vol. 25, pp. 869-886.

Horská, Alena. 2020. Calculation Tool for Reinforced Concrete Wall Analysis and Assessment. *Proceedings of PhD Workshop.* 13 11 2020.

Horská, Alena, Jiříček, Pavel and Foglar, Marek. 2015. Impact performance of FRC slabs under various strain rates. *EPJ Web of Conferences.* 2015, Vol. 94.

Hu, B., et al. 2018. Efficient reliability-based design tool for reinforced earth retaining walls of heavy haul railway considering internal failure modes. *Joint Rail Conference 2018.* 2018.

Jiang, Wei, et al. 2018. Analysis of dynamic response of steel reinforced concrete bridge piers under impact. *Materials Science and Engineering .* 2018, Vol. 397.

JTG D60. 2004. *General code for design of highways bridges and culverts.* 2004.

Juhász, K. P., Schaul, P. and Nagy, L. 2017. Effect of the loading rate on fibre reinforced concrete beams. *Materials Science and Engineering.* 2017, Vol. 246.

Kaveh, Ali, Hamedani, Kiarash Biabani and Bakhshpoori, Taha. 2020. A spreadsheet-based tool for optimal design of reinforced concrete cantilever retaining walls. *Periodica Polytechnica Civil Engineering.* 2020, Vol. 64, 1, pp. 156-168.

Kennedy, Robert P. 1976. A review of procedures for the analysis and design of concrete structures to resist missile impact effects. *Nuclear Engineering and Design.* 1976, Vol. 37, 2, pp. 183-203.

Koechlin, Pierre and Potapov, Serguei. 2009. Classification of soft and hard impacts—Application to aircraft crash. *Nuclear Engineering and Design.* 2009, Vol. 239, pp. 613-618.

Koktan, Jiri, Cajka, Radim and Brozovsky, Jiri. 2019. Comparison of 2D and 3D finite element structural analysis of foundation slab on elastic half-space. *ARPN Journal of Engineering and Applied Sciences.* 2019, Vol. 14, 6, pp. 1112-1119.

Liu, B., et al. 2017. Experimental investigation and improved FE modeling of axially-loaded circular RC columns under lateral impact loading. *Engineering Structures.* 2017, Vol. 152, pp. 619-642.

Majeed, Zireen Z. A., et al. 2019. Contact force generated by impact of boulder on concrete surface. *International Journal of Impact Engineering.* 2019, Vol. 132.

Mavrouli, O. and Corominas, J. 2010. Vulnerability of simple reinforced concrete buildings to damage by rockfalls. *Lanslides.* 2010, Vol. 7, 2, pp. 169-180.

Mestrovic, D., Cizmar, D. and Miculinic, L. 2008. Reliability of concrete columns under vehicle impact. *WIT Transactions on the Built Environment.* 2008, Vol. 98, pp. 157-165.

Özel, H. F. and Arici, Y. 2013. Comparison of 2D vs. 3D Modeling Approaches for the Analyses of Concrete Faced Rockfill Dams. *Earthquake Engineering & Structural Dynamics.* 2013, Vol. 42, 15.

Pajak, Malgorzata. 2011. The influence of the strain rate on the strength of concrete taking into account the experimental techniques. *Architecture, Civil Engineering, Environment.* 2011, Vol. 3, pp. 77-86.

Pham, T. M. and Hao, H. 2016. Review of Concrete Structures Strengthened with FRP Against Impact Loading. *Structures.* 2016, Vol. 7, pp. 59-70.

Riisgaard, Benjamin, et al. 2007. Dynamic Increase Factors for High Performance Concrete in Compression using Split Hopkinson Pressure Bar. 2007.

RILEM TC 162-TDF. 2002. Test and design methods for steel fibre reinforced concrete. *Materials and Structures.* 2002, Vol. 35, pp. 579-582.

Sagar, Mamidi Sai Kumar and Ganta, Srinivas. 2016. Multi-objective Optimization of Reinforced Cement Concrete Retaining Wall. *Anvenshana's International Journal of Research in Enggineering and Applied Sciences.* 2016, Vol. 1, 10, pp. 304-316.

Salama, Magdy I. 2012. Analysis of slabs spanning in two directions under concentrated load. *HBRC Journal.* 2012, Vol. 8, 3, pp. 212-216.

Sangi, Abdul Jabbar. 2011. *Reinforced Concrete Structures under Impact Loads.* Edinburgh : Heriot-Watt University, 2011. PhD Thesis.

Sovják, Radoslav, et al. 2013. Experimental Investigation of Ultra-high Performance Fiber Reinforced Concrete Slabs Subjected to Deformable Projectile Impact. *Procedia Engineering.* 2013, Vol. 65, pp. 120-125.

Thai, Duc-Kien and Kim, Seung-Eock. 2014. Failure analysis of reinforced concrete walls under impact loading using the finite element approach. *Engineering Failure Analysis.* 2014, Vol. 45, pp. 252-277.

Visser, William. 2017. *High Strain Rate Deformation Mechanisms of Body Centered Cubic Material Subjected to Impact Loading.* Kingston : University of Rhode Island, 2017. PhD Thesis.

Wang, C. M, Reddy, J. N. and Lee, K. H. 2000. Theories of Plate Bending. *Shear Deformable Beams and Plates.* 2000, 6, pp. 89-109.

Wood, R. H. 1968. The Reinforcement of Slabs in Accordance with a Pre-Determined Field. *Concrete.* 1968, Vol. 2, 2, pp. 69-76.

Wright, Christopher. 2012. *Introduction to Structural Impact.* Fairfax : PDHonline.org, 2012. PDHonline Course S164.

Yong, Arnold C. Y., et al. 2020. Cantilevered RC Wall Subjected to Combined Static and Impact Actions. *International Journal of Impact Engineering.* 2020, Vol. 143.

—. 2020. Experimental and Analytical Assessment of the Flexural Behaviour of Cantilevered RC Walls Subjected to Impact Actions. *Journal of Structural Engineering.* 2020, Vol. 146.

Yoo, D. Y. and Banthia, N. 2017. Mechanical and structural behaviors of ultra-high-performance fiber-reinforced concrete subjected to impact and blast. *Construction and Building Materials.* 2017, Vol. 149, pp. 416-431.

Zhao, Wucaho, Qian, Jiang and Jia, Pengzhao. 2019. Peak Response Prediction for RC Beams under Impact Loading. *Shock and Vibration.* 2019, Vol. 2019.

Zhou, Deyuan, et al. 2017. Study on Impact Behavior and Impact Force of Bridge Pier Subjected to Vehicle Collision. *Shock and Vibration.* 2017, Vol. 2017.

List of symbols

a	[-]	ratio of reinforcement in horizontal/vertical direction
d	[m]	load distribution length
E	[Pa]	elasticity modulus
EI_x	[Nm^2]	bending stiffness of a 1 m wide wall section in horizontal direction
EI_x	[Nm^2]	bending stiffness of a 1 m wide wall section in vertical direction
F	[N]	point load
f	[N/m]	discretized uniformly distributed load acting on length of Δd
F/d	[N/m]	uniformly distributed load
f_c	[Pa]	compressive strength
f_d	[Pa]	material strength under dynamic loading
f_s	[Pa]	material strength under quasi-static loading
f_t	[Pa]	tensile strength
H	[m]	wall height
h	[m]	vertical load position from wall base
h'	[m]	free height; the height of the wall above load
k_2	[-]	correction coefficient, rectifies the error of two-dimensional modelling for walls subjected to a point load at their wall top in central zone
k_5	[-]	correction coefficient, rectifies the error of two-dimensional modelling and using point load instead of distributed load for walls loaded at their wall top in central zone
k_7	[-]	correction coefficient, rectifies the error of two-dimensional modelling for walls subjected to a point load at their wall top at the wall side edge
k_9	[-]	correction coefficient, rectifies the possible error given by reinforcement orthotropy
L	[m]	wall length
l	[m]	horizontal position at the wall base
L_c	[m]	central zone length

L_e	[m]	edge zone length
L_{ex}	[m]	length of the wall exposed to impact
L_i	[m]	influenced length
$L_{i/2}$	[m]	influenced half length
l_p	[m]	horizontal distance from the peak bending moment
M_{2D}	[Nm/m]	bending moment obtained from a two-dimensional model (representing 1 m of wall length)
$M_{2D,f}$	[Nm/m]	bending moment caused by discretized load f from two-dimensional model
$M_{2D,max}$	[Nm/m]	maximum bending moment obtained from a two-dimensional model (representing 1 m of wall length)
M_{3D}	[Nm/m]	bending moment obtained from a three-dimensional model
$M_{3D,f}$	[Nm/m]	bending moment caused by discretized load f from three-dimensional model
$M_{3D,max}$	[Nm/m]	maximum (peak) bending moment obtained from a three-dimensional model
$M_{3D,max,F}$	[-]	maximum (peak) bending moment from a point load equivalent to distributed load
M_c	[Nm/m]	peak bending moment in the central zone of the wall, computed by Wall-imp
M_e	[Nm/m]	peak bending moment in the edge zone of the wall, computed by Wall-imp
M_{rel}	[-]	relative bending moment; ratio of three-dimensional bending moment to a reference bending moment
$M_{rel,max}$	[-]	relative maximum (peak) bending moment; ratio of maximum three-dimensional bending moment to a reference bending moment
$M_{rel,max,2}$	[-]	relative maximum (peak) bending moment; ratio of maximum three-dimensional bending moment to maximum two-dimensional bending moment
$M_{rel,max,5}$	[-]	relative maximum (peak) bending moment; ratio of maximum three-dimensional bending moment from distributed load to maximum (peak) bending moment from equivalent point load

$M_{rel,max,6}$	[-]	relative maximum (peak) bending moment; ratio of maximum three-dimensional bending moment for vertical load position h ≠ H to maximum three-dimensional bending moment for vertical load position h = H
$M_{rel,max,7a}$	[-]	relative maximum (peak) bending moment; ratio of maximum three-dimensional bending moment for horizontal load position x on a wall of finite length to maximum three-dimensional bending moment on wall of infinite length
$M_{rel,max,7b}$	[-]	relative maximum (peak) bending moment; ratio of maximum three-dimensional bending moment to maximum two-dimensional bending moment
n	[pcs]	number of division elements
t	[mm]	wall thickness
x	[m]	horizontal load position from wall end
x_{min}	[m]	distance between the wall end and the closest impact load position
Δd	[m]	distribution length division element
$\dot{\varepsilon}$	[s^{-1}]	strain rate

List of abbreviations

CC	Consequence class
CMOD	Crack mouth opening displacement
DIF	Dynamic increase factor
ESF	Equivalent static force
ESL	Equivalent static load
FEM	Finite element method
FRC	Fibre reinforced concrete
RC	Reinforced concrete
UHPC	Ultra-high performance concrete
UHPFRC	Ultra-high performance fibre reinforced concrete
ULS	Ultimate limit state

List of tables

List of figures